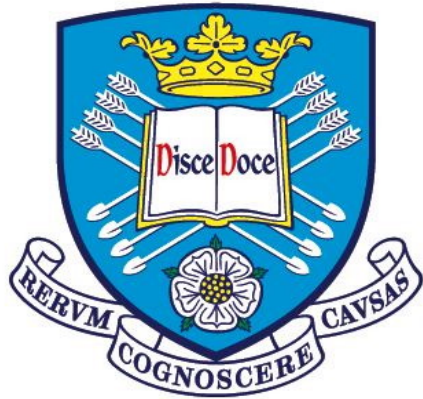# DEVELOPMENT OF A FLUIDIC OSCILLATOR-DRIVEN FLOTATION SYSTEM

A Thesis submitted for the degree of Doctor of Philosophy (PhD) in the Department of Chemical and Biological Engineering at the University of Sheffield, UK.

by

JAMES O. HANOTU

January 2013

Dedication

To my family, who dedicated and offered unconditional love throughout my study and to the wonderful memories of my loving grandmothers: Augusta Chiorlu and Ihunwo Hanotu whose support and advice inspired commitment and focus till this day.

ABSTRACT

Treatment of liquid effluents is a serious challenge owing to the high stability and colloidal nature of the particles. In many applications, microbubbles (< 150 μm) are employed for separation purposes due to their buoyancy and increased surface area to volume ratio. This property has been exploited in the water treatment industry for separation in a process known as dissolved air flotation (DAF). Though practically efficient, the process is energy intensive operating at >5 bars and consequently consuming ~90% of the total energy required in water purification plants. Other approaches in generating microbubbles for separation are not without challenges. One example is dispersed air flotation, which generates bubbles several orders of magnitude larger than the bubble exit pore and consequently unsuitable for flotation of these colloidal particles.

These two concerns have been addressed in this research with the designing and development of a microbubble diffuser driven by a fluidic oscillator to facilitate microbubble generation suitable for flotation as well as investigating its performance for flotation applications. This fluidic oscillator converts continuous air supply into oscillatory flow with a regular frequency to generate bubbles of the scale of the exit pore. Bubble characterisation results showed that average bubble size generated under oscillatory air flow state from a 50 μm pore membrane was 86 μm, ~ twice the size of the diffuser pore size of 38 μm. In contrast, continuous airflow at the same rate through the same diffusers yielded an average bubble size of 1059 μm, 28 times larger than the pore size.

In the first application, fluidic oscillator generated microbubbles were investigated for the separation of emulsified oil using Aluminium sulphate as the coagulant. The effect of surfactant concentration on oil droplet size was investigated. It was found that oil droplet size varied inversely proportional to surfactant concentration. In addition, it was found that the oil removal efficiency also depends on the surfactant concentration. The maximum oil removal efficiency by Microflotation was found to be 91% under lowest surfactant concentration tested (0.3 wt%) whilst at highest surfactant concentration used (10 wt%); lowest recovery efficiency (19.4%) was recorded.

In the second application, the separation of algal cells under fluidic oscillator generated microbubbles was investigated by varying metallic coagulant types, concentration and pH. Best performances were recorded at the highest coagulant dose (150 mg/L) applied under acidic conditions (pH 5). Amongst the three metallic coagulants studied, ferric chloride yielded the overall best result of 99.2% under the optimum conditions followed closely by ferric sulphate (98.1%) and aluminium sulphate with 95.2%.

The third application investigated the performance of Microflotation for the recovery of yeast cells from their growth medium at different pH levels, flocculant dose and varying bubble sizes. In this study, the food-grade-constituent- Chitosan was used as the flocculant. Results reaching 99% cell recovery were obtained under various conditions examined. Bubble size profiling showed an increase in average bubble size with diffuser pore size. Also, cell recovery efficiency was a function of both bubble size and particle size (cell size). For smaller particles (<50 μm), relatively smaller bubbles (<80 μm) were found to be more effective for recovery, otherwise, relatively larger bubbles (80-150 μm) proved to be efficient in recovering larger particles (particle size: ~250 μm). Acidic and neutral pHs were effective in separation as hydrophobic particles were formed. As pH tends towards alkalinity, flocs become more hydrophilic, leading to low recovery from the aqueous solution. In addition, separation efficiency was dependent on flocculant dose as increase in concentration improved flocculation and consequently, yeast recovery. However, above a critical concentration, overdosing occurred and inadvertently, recovery efficiency decreased.

The results compare well with conventional dissolved air flotation (DAF) benchmarks, but has a highly turbulent flow, whereas Microflotation is laminar with several orders of magnitude lower energy density.

ACKNOWLEDGEMENTS

CONTENTS

Contents

LIST OF FIGURES

Appendix I

Design of the Distributor-Vane microbubble diffuser

Appendix II

Instrument used for Assay Samples

LIST OF TABLES

Chapter 1

INTRODUCTION

This chapter introduces the research study, starting with a general background to put the work into perspective before narrowing down to the problem the research aims to address and the already available solutions. A detailed description of the research hypothesis is presented followed by the research aims and objectives. Next, the scope of the investigation is highlighted, as is the limitation. In the final section, the significance of the study is explained before describing the work structure.

1.1   Background

Pollutants have always been present in water bodies. Ages before the advent of industrialisation, contaminants eventually gained entry into watercourses from the air, land surfaces via erosion or leaching from soil. However, the natural self-purification capability of water bodies meant that many of these contaminants were readily reduced and or removed. Unarguably, it is this natural self-cleaning ability of water that made the water-dependant life on earth possible. With the birth of civilisation, concentration and nature of contaminants in water bodies were severely altered due to anthropogenic activities. As population increased, cities became larger from mere settlements to towns and then to states, so did the amount of pollutants increase until the natural self-cleaning ability of local water bodies was overwhelmed. Effects were first apparent in minor streams, then major streams and lakes following suite.

1.2   Problem Statement

Efficient supply of portable water for human consumption is very important but so also is the recovery of valuable materials (oil or particles) found in aqueous solutions. By focusing on particle removal from aqueous solution, both the liquid and particles can be obtained simultaneously as separate useful products. A large body of experimental evidence show the reclamation of products such as oil (Al-Shamrani et al., 2002b, Al-Shamrani et al., 2002a, Hosny, 1996, Zouboulis and Avranas, 2000), minerals (Englert et al., 2009), algae (Teixeira and Rosa, 2007, Teixeira et al., 2010) and in cases where water scarcity is the challenge, potable water (Kitchener and

Gochin, 1981, Edzwald, 1995) can be achieved by separation. Occasionally given the effluent volume and complex chemical composition, treatment becomes uneconomical even in instances where potentially recoverable valuable products are involved. Current separation techniques where efficient in recovery are either energy intensive or only suited to batch small-scale operations.

1.3   Separation Methods

Many separation techniques have been developed to address this concern. The earliest are the non-bubble based techniques, which include: Centrifugation, filtration and sedimentation. Centrifugation as a separation technique is one of the most widely employed recovery systems particularly for cells. The concerns with centrifugation however have been widely reported. Applying centripetal force to cells can have detrimental outcomes. Cell lysing due to centrifugation is a huge problem as is the cost associated with equipment purchase and maintenance. Although relatively efficient (compared to other non-bubble based recovery techniques) (Molina Grima et *al*., 2003), centrifugation is still marred and limited to batch small-scale production, not to mention its high-energy consumption.

Filtration and sedimentation share a common difficulty of long processing time. However, filtration differs significantly as a multi-stage production process, often requiring the arrangement of filters in series. Fine membranes are first set to screen out larger particles followed by ultra-fine mesh sizes. The other common problem with filtration is the high-pressure build up at the membrane interface, requiring substantial energy use to overcome the resultant pressure. Also, because membranes are highly susceptible to clogging, regular maintenance is required which could become cost ineffective. Nonetheless, another ineffectiveness of filtration lies in the low separation efficiency with sub-micron particles (Mohn 1980).

Sedimentation by contrast exploits the density differential between colloidal particle and their containing fluid along with gravity effect to achieve result. Thus larger and denser particles will readily settle out of solution. Other finer, less dense particles however, may remain in suspension indefinitely. In addition to the typically low recovery efficiency, other shortcomings of sedimentation are obvious: Long retention

time and large space requirements are some of the main examples. But another equally important but less reported disadvantage with this recovery approach is the high moisture content of the recovered end-products (Molina Grima et *al*. 2003). Moisture content reduction is essential if dry products are required for subsequent use. Rarely, recovered co-product may be required in cream forms (e.g. cream yeast, for resale or repitching into a fresh batch), but usually at low moisture content. Owing to the high cost of heating, it is therefore important to reduce the water constituent of any sludge.

1.4   Microbubble Application

Flotation was developed to solve the problems associated with non-bubble based separation techniques. Basically, it is a rate enhancing approach over sedimentation and has been widely explored in various industries. In essence, the key sub-process is the generation of microbubbles that attach to hydrophobic particles, resulting in buoyant aggregates which then rise to the surface of the flotation cell, where following bubble rupture, the particles are recovered (Dai et al., 2000).

Given that the suspended/dispersed oil or particles are colloidal in nature, flotation especially for portable water treatment requires the application of substantially small bubbles (20-100 μm). Application of gas bubbles in liquid is gaining widespread interest across many fields. Generally, the processes entail efficient ways of facilitating bubble-particle interaction in the liquid rather than merely passing the bubbles through the liquid without it actually adhering and lifting the particles out of solution. Best practices however, require that the particles in the aqueous solution attain optimum collision, attachment and stability efficiencies respectively (Derjaguin and Dukhin, 1993) with the gas bubble for complete capture prior to reaching the liquid surface. As such, one of the most efficient ways of achieving this is miniaturising the bubbles. Due largely to their high surface area to volume ratio, particle flotation by small bubbles occur more rapidly and efficiently. Ahmed and Jameson (1985) estimate a 100-fold enhancement in separation performance for fine particles with bubble size reduction from approximately 700 to 70 μm. Further, small bubbles have gentle convective force relative to large bubbles by reason of their low rise velocity (Schulze, 1992), resulting in tender contact with fragile flocs.

The major hurdle in flotation however lies in the generation of the sub-100 µm bubbles. This is so because in order to overcome the wetting force binding them to the exit pores, bubbles tend to grow substantially beyond their exit pores before detachment. For this reason, attempting to generate sub-100 µm bubbles by steady continuous gas supply is futile. Several other conventional approach developed to offset this challenge have been well explored. Essentially, these techniques entail the combination of air and water in a vessel either by the dissolution of one (usually air) into the other or by the application of a shear force to induce partial dissolution. Popular examples are dissolved air flotation (DAF) and induced air flotation (IAF). DAF is the most widely employed flotation separation system for water treatment. As an energy intensive system, DAF succeeds on the initial high-pressure application for the dissolution of air in water and ultimately its release from a nozzle at a reduced pressure downstream a saturator. Whilst these techniques are widely successful in meeting the bubble size requirements and consequently optimum separation efficiency, their handicap is found in the energy consumption. Apart from their complexities (usually involving different stages and equipment), conventional flotation systems are also intrusive, pumping in large volume of unwanted water into a flotation unit. Furthermore, high moisture content may result from the excess water, incurring additional costs in dewatering. The challenge therefore is to develop a robust, effective and energy efficient flotation separation/recovery technique that can handle continuous large-scale production.

1.5   Bubbles by Oscillation

A low-pressure offset system with the promise of cheap microbubble generation has been designed by Zimmerman et *al*., (2008), and already applied for the generation of 600 µm (Zimmerman et *al*., 2008) and 400 µm (Al-Mashhadani et *al*., 2011; Zimmerman et *al*., 2011) from a 20 µm pore diffuser but yet fully explored for sub-100 µm bubble production. Unlike conventional dispersed air mechanisms that depend to no avail on diffuser structure for the generation of microbubbles, fluidic oscillation by contrast pinches off the bubble at the infant stage, generating relatively uniformly sized, largely non-coalescent microbubbles of the scale of the exit apertures

using only gas. It is a self-excited, bistable and robust device with no-moving part. Thus nothing is at risk of breakage and therefore requires low maintenance.

1.6   Research Hypothesis and Aims

Thus this research seeks to explore the potential of the fluidic oscillator in generating sub-100 µm bubbles and ultimately the application in separation. Throughout this thesis, the term ''Microflotation'' is used to refer to the application of bubbles generated by fluidic oscillation for the removal of colloidally dispersed oil or particles from the liquid continuous phase. Essentially, it is a type of flotation unit powered by the fluidic oscillator. This research hypothesizes that microflotation can alleviate the problems common to both types of separation options - non-bubble and bubble based - particularly by its low energy use, high recovery efficiency and scalability to industrial requirements, provided it can achieve the desired bubble size range (sub-100 µm sized bubbles).

Therefore, the aims of this research are:

1) To design and develop a system that can achieve microbubble generation 20 – 150 µm and test its effectiveness and efficiency by applying the generated microbubbles in the separation of colloidal dispersed oil or particles.

2) To improve the understanding of the operational and design factors related to the microflotation system.

The objectives are to:

i.   Measure and quantify using the fluidic oscillator, the bubble size distribution under the following conditions: varying pore size, diffuser type, flowrate and feedback loop length and provide information on their effect on recovery efficiency.

ii. Compare the performance of microflotation with another known separation techniques with key information on recovery efficiency, bubble size distribution as well as moisture content of the sludge produced.

iii. Investigate the effect of varying parameters such as pH, coagulant type, coagulant concentration and particle size on particle recovery efficiency.

1.7   Study Scope and Limitations

The scope of this study is to design and implement a microflotation system for colloidal particle/oil separation from aqueous medium recovery thus information such as bubble and particle size distribution and diffuser design can be found in the chapters ahead. Nonetheless, there are some limitations worth mentioning. Firstly, the designed microflotation system was only applied in the separation of oil, recovery of algae and yeast cells respectively, however, some other examples such as the application of microflotation for mineral recovery, bacterial harvest e.t.c. have not been investigated owing mainly to time and budget constraints. Another limitation relates to the absence of a computational fluid model to aid in predicting and optimizing particle-particle as well as particle-bubble behavior respectively in a separation unit. Nonetheless, these limitations do not affect the overall result quality and ultimately, the significance of the study.

1.8   Significance of Research

Given the high energy consumption and associated costs in microbubble generation, the results from this work can significantly influence not just the water and wastewater treatment industries but also the mineral and metallurgical industry where recovery of valuable minerals is sought. Furthermore, harvesting represents an important unit operation in the production of biofuel from microorganisms. If the generation of sub-100 μm bubbles can be achieved with the energy efficient fluidic oscillator and microflotation successfully applied in these and other related sectors for particle/oil recovery, substantial savings in energy could be achieved leading to increase in production and a huge step towards energy independence.

1.9   Study Structure

This work is structured into eight chapters. The first chapter introduces the research work. In this chapter, background information of the problem is provided with detailed information on the available conventional approach in providing solution. Further, the research hypothesis is established, as are the aim and objectives. Chapter two reviews the relevant works done in the area of separation. The potential application sectors are first outlined followed by a comprehensive literature review of

the different separation techniques both bubble and non-bubble based systems. Under the bubble-based systems, critical information on the dynamics of microbubbles rising in a liquid continuous phase is provided. Another significant review, relates to the science governing flotation. Here, the different relevant models underlying the concept of flotation are drawn up. Then, detailed review of the various methods of bubble generation is presented, leading to a review of microbubble generation with the fluidic oscillator. In chapter three the methodologies and materials used to accomplish this study are detailed. These include the experimental procedures employed in the design of a microbubble diffuser, bubble and particle size characterization and the investigation of microflotation performance for oil, algae and yeast recovery. The first set of result - bubble size distribution- is presented in chapter four under varying operating parameters such as flow rate, diffuser type and flow type (oscillatory and steady flow). Also important is the result of the frequency of oscillation. Based on the performance of the different diffusers in microbubble generation, a choice is made on the appropriate diffuser and operating conditions for application in separation. Chapter five presents results of the first application of the microflotation system in separation. Here, separation results of emulsified oil droplets investigated under different experimental conditions are analyzed and discussed with important interest on the effect of surfactant concentration on the size distribution of oil droplet and the overall influence on separation of the droplets. Next, the result of algal harvest and dewatering, another application with microflotation is given in chapter six. Again results for recovery efficiency are reported using different coagulant types and concentrations. Also presented is the effect of pH on the recovery efficiency of algae. In chapter seven, the performance of microflotation on the harvest of yeast cell is outlined. Information on the effect of varying microbubble sizes on recovery efficiency is also provided. In addition to the effect of pH and flocculant concentration on recovery efficiency, the effect of particle charge measured by zeta potential on the recovery efficiency is also presented. Nonetheless, moisture content results of cells harvested under flotation and sedimentation (i.e. with and without bubbles) is also shown. Finally, the main findings are summarized and the drawn conclusions presented in chapter eight followed with recommendations for future works.

Chapter 2

LITERATURE REVIEW

2.1   Introduction

This chapter provides a critical assessment of relevant literature on the separation of colloidal particles. Firstly, a general description of colloids and their typical properties is presented. Next, the concept and importance of particle aggregation is considered, as is the role of chemical pretreatment in colloidal particle recovery. Then the various separation/recovery techniques are critically evaluated starting with non-bubble based techniques such as filtration, centrifugation and sedimentation and then moving on to highlight the benefits and ultimately the application of microbubbles as a flotation technique. In the section following on from that, microbubble general behavior is discussed with emphasis on their terminal rise velocity. Further, a significant part of the literature review considers the fundamentals of flotation. The last section however, presents an overview of the main bubble-based separation techniques, classifying them by the modes of bubble generation. Finally, the chapter concludes with the generation of microbubbles with the fluidic oscillator and gives an overview of the working mechanism of the novel device, on which principles the core of this research work is centered.

2.2   Properties of Particles in Aqueous Solution

A good understanding of particles and their behaviour is essential for their separation from an aqueous medium. The important features of colloidal particles are their sizes, concentration and distribution, shape and the interactions between other particles and the host solvent. Naturally, particle sizes encountered in water treatment range between 0.001-100 μm; suspended particles are generally larger than 1 μm while the colloidal particles will vary from 0.001-1 μm (Bach, 2004; Armenante, 2012). Constituents classified as dissolved are typically smaller than 0.001μm, again depending on the quantification method. The size distribution of particles in natural waters may be defined on the basis of particle number, particle mass, particle diameter, particle surface area, or particle volume.

Particles in an aqueous solution can have a wide range of shapes. Typically, the shape of the particles found in water are spherical, ellipsoid, semi-spherical, disk and disk-like, coiled among others (Pileni, 2003). Many microorganisms such as algae and yeast are semi-spherical or ellipsoidal in shape while oil droplets in an emulsion are spherically shaped. Nonetheless, large organic molecules are usually found to be in form of a coil which may either be compressed or fairly linear. The shape of particles however, will vary depending on the features of the source water. Furthermore, particle shape has an effect on the electrical attributes and the particle-solvent interactions.

Generally, there are two classifications of colloidal particles found in water with respect to their affinity for the containing liquid medium- hydrophobic (water repelling) and hydrophilic (water attracting). Hydrophobic particles usually possess a well-defined interface between the water and the solid phases and have a low attraction for water molecules (Vinogradova, 1995). Their stability results from the presence of a surface charge, which attract other ionic species resident in the liquid medium, leading to the formation of charged electrical layer surrounding the colloidal particle (Lu and Song, 1991; Zangi and Berne, 2006). Also, they are thermodynamically unstable and as such will agglomerate irreversibly with time in the presence of an agglomerating agent. By contrast, hydrophilic particles such as clay, humic acid, metal oxides or proteins are thermodynamically stable in the aqueous solution and have polar or ionized surface functional groups; their reactions after agglomeration are thus usually reversible.

2.2.1 *Particle Electrical Charge*

Knowledge of the charge type and magnitude of colloidal particles is valuable as it provides insight to the limits of chemical pretreatment during flotation. The main electrical charge of low-density particles in water is the surface charge, Surface charge adds to the relative stability of the particles, which prevents particles from agglomerating. Thermodynamically unstable particles in water can flocculate and settle but will require sufficient period of time. To aid the removal of low-density particles in water therefore, a study of the cause of particle stability would facilitate

our understanding and eventually aid in designing and optimizing processes to destabilize and ultimately recover particles from solution.

Usually, the surface charge on particles may develop from several sources as most particles have complex surface chemistry, nevertheless, studies have shown that the electrical charges found on the surface of particles develops from four main ways namely: isomorphous replacement (also known as crystal imperfection), structural imperfection, preferential adsorption of specific ions and ionization of inorganic groups on particulate surfaces (Stumm and Morgan, 1996).

2.2.1.1 Zeta Potential

Regardless of the mode of development of electrical charges on colloidal particles, distribution of these charges on the surface of particles affects the dispersion of ions in the surrounding interfacial region, leading to a rise in the concentration of counter ions (oppositely charged ions) near the surface of the particle to satisfy electro-neutrality (Fig 2.1) (Williams and Williams, 1978). These ions are strongly held to the colloidal particle by electrostatic forces, forming the initial thin inner shield of charges known as the Stern layer (Kirby and Hasselbrink, 2004a; Kirby and Hasselbrink, 2004a). Adjacent this first layer, ions are less strongly held together and are attached to oppositely charged ions, leading to the formation of an electric double layer. Close to the Stern layer, more oppositely charged ions to that on the colloidal particle gather, forming the diffuser layer. Around this layer, is the shear plane, which is loosely attached to the particle relative to the Stern layer but is unsusceptible to external velocity gradient in the liquid and therefore bound to the particle as particle move within the liquid continuous phase (Hunter, 1981).
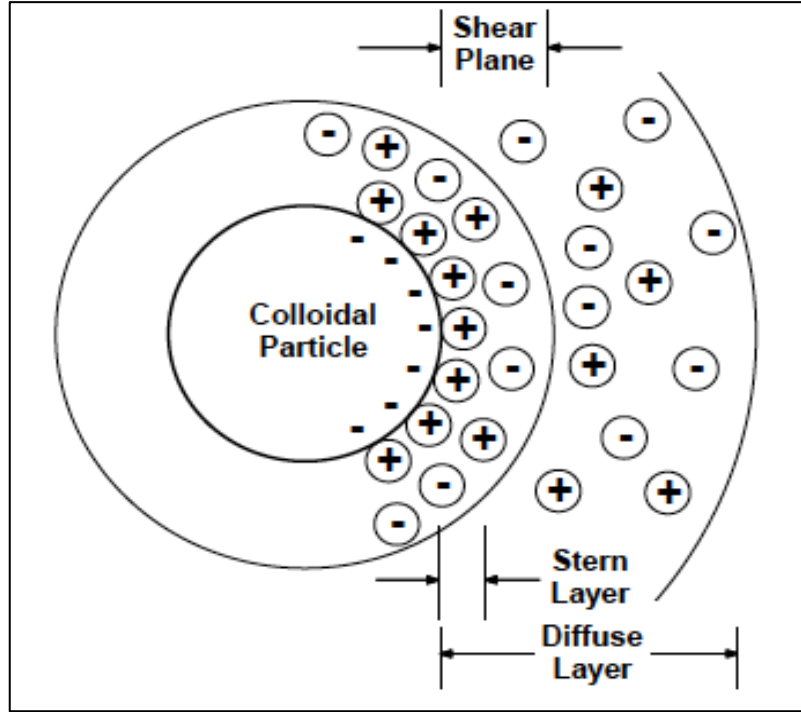
Fig 2.1: Distribution of charges around a particle showing the different layers. Closely and firmly packed opposite ions surround the particle surface followed by the stern layer where relatively less strongly held ions are found just away from the particle surface. These two arrangements of charges are referred to as the double layer. Further away from the double layer exists loose ions that result in the formation of the diffuse layer. The shear plane extends from the mid Stern layer to the diffuse layer. Source: (Armenante, 2012).

The electrical potential difference between the colloidal particle in the shear plane and the liquid bulk is known as the zeta potential and decreases away from the particle (Fig 2.2). In essence, the zeta potential is a measure of the electrical charge of a colloidal particle. A denotation of the potential stability of the colloidal system can be given by the magnitude of the zeta potential and it can be mathematically expressed as:

$$Z = \frac{v^0 K_z \mu}{\varepsilon \varepsilon_0} \qquad \text{(Eq. 2.1)}$$

Where,

v_0 = electrophoretic mobility, (μm/s)/(V/cm) = $\frac{v_E}{E}$

v_E = electrophoretic velocity of migrating particle, μm/s (also reported as nm/s and mm/s)

E = electrical field at particle, V/cm

K_z = constant that is 4π or 6π

11

μ = Dynamic viscosity of water, N.s/m^2

ϵ = permittivity relative to a vacuum (ϵ for water 78.54)

ϵ_0 = permittivity in a vacuum, 8.854188×10^{-12}, C^2/J.m or N/V^2

The dispersion of a solid in a continuous fluid results in a colloidal system. In separation, the main interest is the dispersion of solids in a liquid medium. The higher the magnitude of the zeta potential, the higher the repulsion between particles and consequently, lower particle-particle agglomeration. However, if the zeta potential of the particles is low then there is no force preventing them from agglomerating and flocculating.
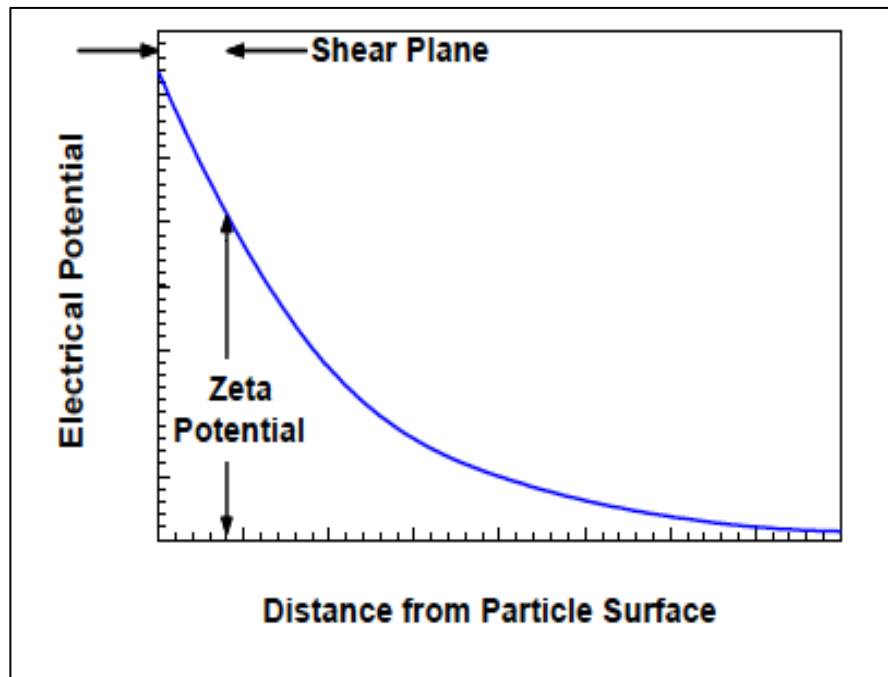
Figure 2.2: Typical electric potential around a charged particle. The electrical potential of a particle decreases away from the particle, as does the zeta potential. Source: (Armenante, 2012).

In general, the differentiating factor between a stable and an unstable suspension can be taken as +30 mV or -30 mV. Mean zeta potential for colloidal particles in wastewater ranges from -12 to 40 mV (Crittendon and Harza 2005). A crucial factor influencing the particle zeta potential however is the medium pH. Usually, under alkaline pH, the magnitude of the zeta potential increases as pH increases (see fig 2.3). Conversely, as pH tends towards acidity, this magnitude reduces until a point is reached where neutrality is attained (zeta potential = zero). This point is referred to as the isoelectric point (IEP) and often results in the presence of enough counter ions.

Naturally, particles have the highest potential for agglomeration at the isoelectric point. Beyond this point towards acidity, the net charge becomes positive.
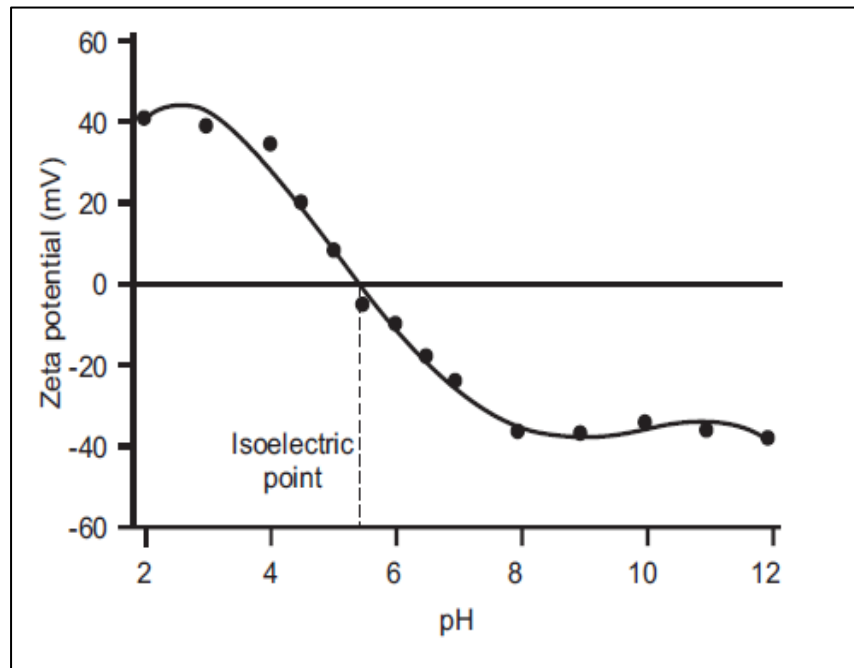
Figure 2.3: A typical plot of zeta potential as a function of medium pH. The magnitude of the zeta potential increases towards the negative under alkaline pH and towards the positive under acidic pH. The point where the curve intersects the origin is known as the isoelectric point. Source: Crittendon and Harza, 2005

2.2.2   Improving Particle Size

One of the rate limiting factors in separation by flotation is the agglomeration of particles. Until the repulsive force existing between particles is neutralized, particle agglomeration will not occur. Several methods for enhancing particle size have been explored and reported. In general, the similarity of these techniques is to induce particle-particle attraction by overcoming the repulsive force. The known agglomeration processes are: selective flocculation, hydrophobic agglomeration and coagulation

2.2.2.1 Selective Flocculation

The process of selective flocculation involves the formation of flocs by bridging on the target particles. Long chain polymers are added which adsorb onto the surfaces of mineral particles by electrostatic forces before bridging with other particles to form loose flocs (Gregory, 1998). This technique however is widely used in the mineral

industry were selective mineral separation is required but as yet fully explored in other fields such as portable water treatment, waste water treatment e.t.c.

2.2.2.2 Hydrophobic Aggregation

Hydrophobic aggregation is similar to froth flotation (Miettinen et *al*., 2010) where particles are held in close proximity to be selectively hydrophobised. The particles undergo strong agitation (Koh and Warren, 1980; Warren, 1982). Miettinen et *al*. (2010) reported that non-polar oil could be an additive to improve aggregate strength. The other types of hydrophobic aggregation include: emulsion flotation, shear flotation, oil extended flotation, spherical agglomeration, carrier flotation and two liquid extraction (Hoover and Malhotra, 1976; Fuerstenau, 1980; Subrahmanyam and Forssberg, 1990).

2.2.2.3 Coagulation

Coagulation differs from selective flocculation in that the addition of an electrolyte causes a decrease in electrostatic repulsion between particles. The energy barrier between particles that prevents agglomeration is overcome by coagulant addition. The disadvantage associated with this method of particle agglomeration is that it produces heterocoagulation and so mainly employed in fields other than the mineral industry (Miettinen et *al*., 2010). Nonetheless, aggregation by coagulation is still the most widely applied technique of the three sorts but choice of technique ultimately depends on the recovery process as well as the desired end product.

Particle destabilization by the addition of a coagulating or flocculating agent occurs by four (4) known mechanisms viz: the compression of the electrical double layer, adsorption and charge neutralization, adsorption and inter-particle bridging and the enmeshment in a precipitate. Broadly, there are two main categories of coagulant and flocculants viz: Organic and inorganic coagulants and Organic flocculants (see Table 2.1).

Table 2.1: List showing major classes of coagulant and flocculants. The different types are grouped into organic and inorganic coagulant as well as organic flocculants. Adapted from: Renault et *al.*, 2009).

Coagulants and Flocculants		
Organic and Inorganic Coagulants	Mineral additives	Calcium salts Lime
	Hydrolysing Metal Salts	Aluminium Sulphate Ferric Chloride Ferric Sulphate
	Pre-hydrolysed Metals	Polyaluminium chloride Polyaluminosilicate sulphate
	Polyelectrolytes	Coagulant aids
Organic Flocculants	Cationic and anionic polyelectrolytes	
	Non-ionic polymers	
	Amphoteric and Hydrophobically modified polymers	
	Natural Flocculants	starch derivatives Guar gums Tannins Alginates

2.2.2.3.1   *Organic and Inorganic Coagulants*

Metal salts are the most common coagulants available and are still widely employed in water purification with aluminium salts being the most commonly used. These cations hydrolyse rapidly in the liquid medium and interact with particles, neutralising their net surface charge. When aluminium salts are added to an aqueous solution a rapid hydrolysis reaction occurs to form other dissolved Al ions (Eq. 2.2 and 2.3). The main Al-hydroxide precipitates that result following dissolution of the metal salts are: Al^{3+}; $Al(OH)^{2+}$; $Al(OH)^{1/2+}$, $Al(OH)^{1/4-}$ and the amorphous $Al(OH)_{3(am)}$ (Pernitsky and Edzwald, 2006). Al species distribution in an aqueous solution is however pH dependent (see fig 2.4). Figure 2.4 shows a plot of Al species distribution under varying temperatures. In acidic pH, Al^{3+} is the predominant species present. But with increase in pH, Al ions with lower positive charge become dominant. As pH exceeds 6.5, the most active species are the $Al(OH)^{1/4-}$. Similarly, the presence and concentration of Fe^{3+} species increases under acidic pH when ferric salts undergo dissolution but the concentration decreases with a shift in pH towards neutrality with

the formation of more $Fe(OH)^{2+}$ and $Fe(OH)_2^+$ species (Fig 2.5). Other species formed are $Fe(OH)^{4-}$ under basic pH.

The addition of hydrated aluminium sulphate results in the hydrolysis of the trivalent metal salt and then the formation of insoluble aluminium hydroxide species, which precipitate out of solution as in the reaction below:

$$Al_2(SO_4)_3 \leftrightarrow 2Al^{3+} + 3SO_4^{2-} \qquad \text{(Eq. 2.2)}$$

$$Al(SO_4)_3.18H_2O + 6H_2O \Leftrightarrow 2Al(OH)_3 \downarrow + 6H^+ + 3SO_4^{2-} + 18H_2O \qquad \text{(Eq. 2.3)}$$
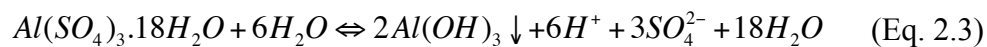
The addition of ferric salt to an aqueous solution results in the hydrolysis of ferric chloride and then the formation of insoluble ferric hydroxide, which precipitate out of solution as in the reaction below:

$$FeCl_3 \Leftrightarrow Fe^{3+} + 3Cl^- \qquad \text{(Eq. 2.4)}$$

$$FeCl_3 + 3H_2O \Leftrightarrow Fe(OH)_3 \downarrow + 3H^+ + 3Cl^- \qquad \text{(Eq. 2.5)}$$
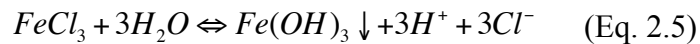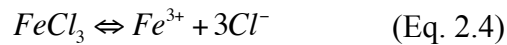
Speciation of coagulants can also be temperature dependent (fig 2.4). Pernitsky and Edzwald (2006) reported on the influence of temperature on the speciation of Al. Under cold temperature water, positively charged Al species dominate. However, aside the effect of temperature and pH, the distribution and performance of a coagulant is also a function of other Al-complexing species: NOM, F⁻, $PO^{3/4-}$, $SO^{2/4-}$ (Pernitsky and Edzwald, 2006).
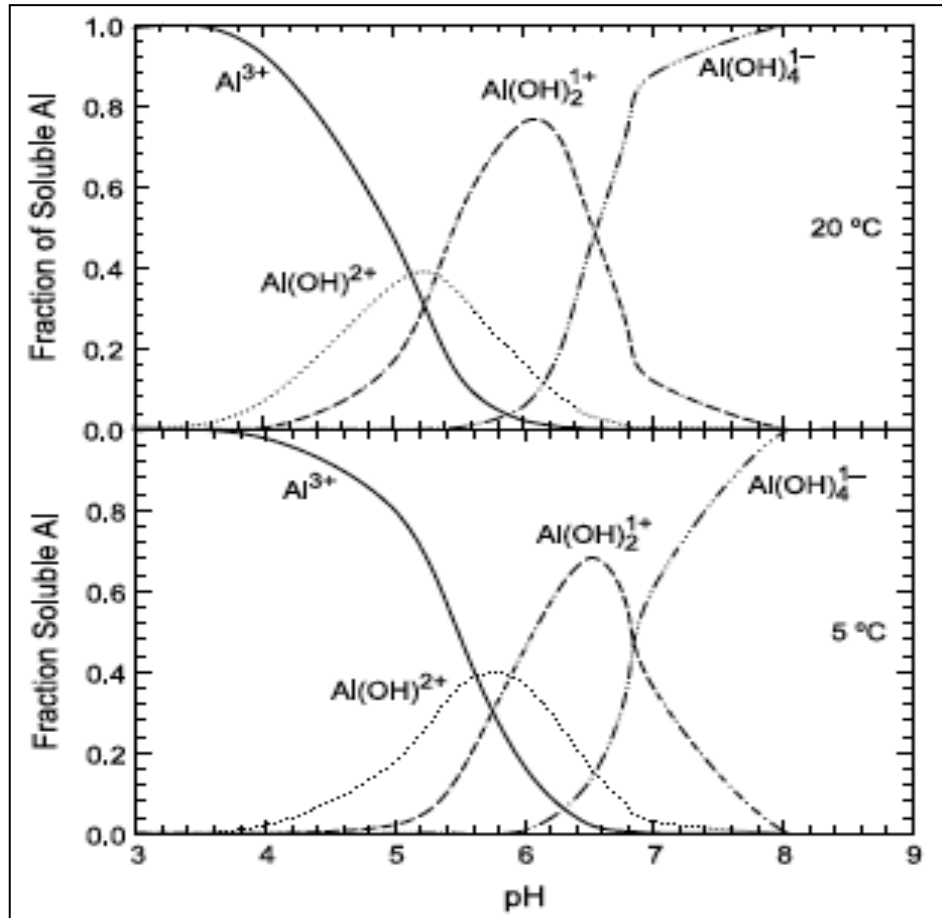
Figure 2.4: Theoretical distribution of Al species as a function of solution pH under 5°C and 20°C. The curves are theoretical solubility curves for aluminium salt dissolved in deionized water at 20°C and 5°C and based on the thermodynamic results for Al hydrolysis reaction. Source: Pernitsky and Edzwald (2006).
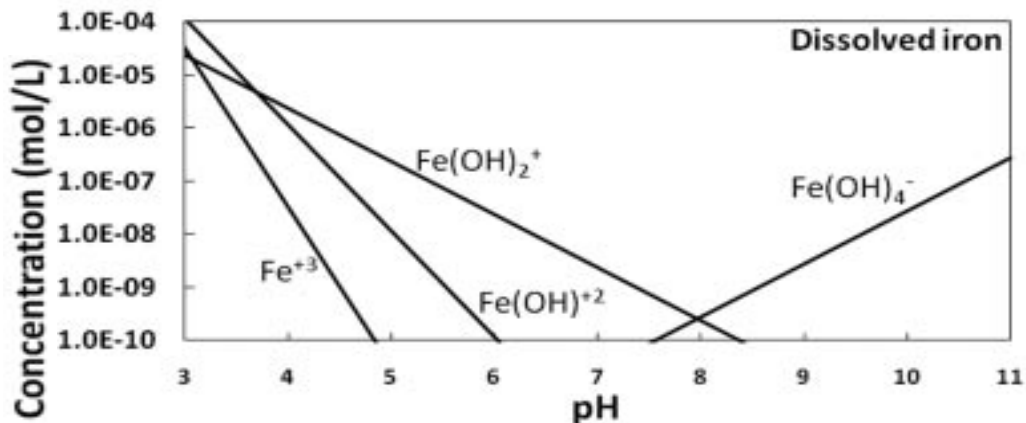
Figure 2.5: Dissolved Fe^+ distribution as a function of pH. Ferric salts express a similar behaviour as do Alum. Trivalent ions are formed and are dominant under acidic conditions. As condition tend towards neutrality however, $Fe(OH)^{2+}$ ions become numerous. $Fe(OH)^{4-}$ species are the dominant species under basic condition (> pH 8). Source: Wyatt et al., (2012).

17

Apart from their abundance, metal salts are easy to use and more importantly, cost effective and as such remain the most widely used in water and wastewater treatment facilities (Renault et *al*. 2009). One main disadvantage however, is the high sludge content they generate. Its also been reported that the dewatering of sludge generated with metal salts are more energy consuming (Renault et *al*., 2009) possibly due to the high sludge moisture content. In addition, the use of metal salts are a source of environmental and health concern given their possible toxic nature. High dosage of aluminium in water may have health implications to humans (Renault et *al*., 2009).

Table 2.2: Characteristics of common Inorganic Coagulants. The sulphate-based coagulants have higher molecular weight than their chloride counterparts. Source: (Armenante, 2012).

Name	Formula	Mol. Weight	Density (kg/m^3)
	$Al_2(SO_4)_3$	342.1	
Alum	$Al_2(SO_4).14H_2O$	594.3	2710
	$Al_2(SO_4).18H_2O$	666.7	
Ferric chloride	$FeCl_3$	162.1	2800
Ferric sulphate	$Fe_2(SO4)_3$	400	1899
Ferrous sulphate	$Fe_2(SO_4)_3.7H_2O$	278	3097
Lime	$Ca(OH)_2$	74.1	2200

2.2.2.3.2   *Synthetic Polymers*

Due to the disadvantages linked with metal coagulants, the use of coagulants synthesised from organic polymers have increased. Their advantages over metal salts in general include: high efficiency at low temperatures, lower dosage requirement, higher separation efficiency, reduced sludge volume, relatively less pH dependent and increase in floc strength (Renault et *al*., 2009). The major concerns linked with polyelectrolytes however are comparatively high cost, non-biodegradability and toxicity. Bolto and Gregory (2007) reported that in water and wastewater treatment, the contaminations arising from the use of synthetic polymers are as a result of residual unreacted monomers- ethyleneimine, acrymalid and trimethyllolmelamine and by-products of the polymer reactions.

2.2.2.3.3 *Organic Flocculants (Natural Polymers)*

Natural flocculants are the alternatives to synthetic polyelectrolytes. Bioflocculants include biopolymers such as alginates, starches and chitosan. Other bioflocculants are microbial products obtained from microorganisms (yeast, bacteria and fungi). These natural polymers are an interesting alternative mainly from an environmental friendly perspective but also, given their abundant occurrence in nature. Several authors (Crini, 2005) report that bioflocculants are safe to use, biodegradable and produce no secondary pollution and as a consequence suitable for food and fermentation purposes. Their classification are according to their origin, chemical characteristics or application. Chitosan is the most widely investigated of this group.

2.2.2.3.3.1 Chitosan

Chitosan is a bioflocculant and copolymer of *D-glucosamine* and *N acetyl-D-glucosamine* made from the deacetylation of chitin a naturally occurring product in crustaceans (Fig 2.6). Chitin is one of the most abundant natural polymers and is widely used in various industries for different applications. Unlike other coagulant and flocculants, chitosan has been approved as a food grade constituent in many countries such as the US, Japan, Germany, France e.t.c.
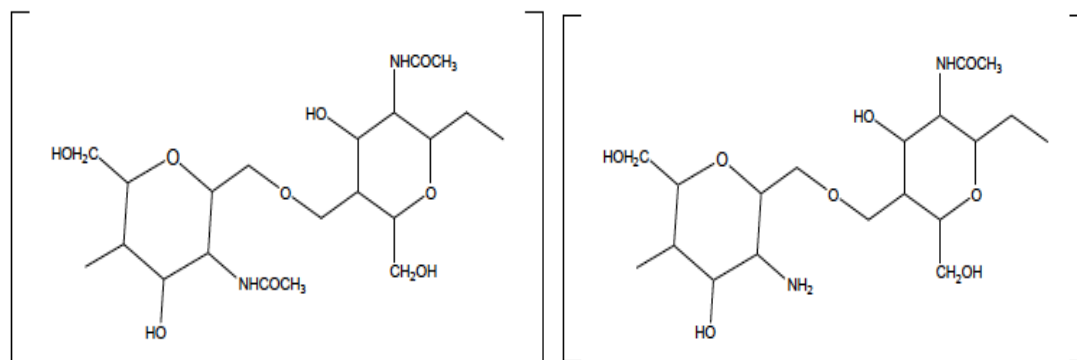
Figure 2.6: Molecular Structure (a) Chitin (b) Chitosan. Chitosan is a polysaccharide with a molecular weight a function of the degree of deacetylation. Chitosan is insoluble in water but dissolves in most acids. Source: Chen (2008).

Apart from its non-toxicity, and biodegradability, chitosan is renewable and has high chelation behaviour (Crini and Badot, 2008; Guibal 2004; Varma et al., 2004). Renault et *al.* (2009) reported that sludge of increased density and low volume is generated with chitosan relative to sludge from metal salts and also, because of the high density of the sludge produced, other downstream operations such as drying are facilitated. Moreover, it is also non-corrosive and therefore safe to handle without causing irritation to the eyes and skin. Chi and Cheng, (2006) reported that sludge from milk processing plant raw water was not toxic and are suitable for use to facilitate plant growth. Table 2.3 provides a summary of the benefits of chitosan as an agglomerating agent in separation.

Table 2.3: Advantages of chitosan and potential application in water and wastewater treatment. Source: Renault et *al.*, 2009).

Advantages	Potential Applications
Non toxic	Flocculant to clarify water (drinking water, pools)
Biodegradable	Reduction of turbidity in food processing effluents
Renewable resource	Coagulation of suspended solids, mineral and organic suspensions
Ecologically acceptable polymer (eliminating synthetic polymers, environmentally friendly)	Flocculation of bacterial suspensions
Efficient against bacteria, viruses, fungi	Interactions with negatively charged molecules
Formation of salts with organic and inorganic acids	Recovery of valuable products (proteins)
Ability to form hydrogen bonds intermolecularly	Chelation of metal ions
Ability to encapsulate	Removal of dye molecules by adsorption processes
Removal of pollutants with outstanding pollutant-binding capacities	Reduction of odours
	Sludge treatment
	Filtration and separation
	Polymer assisted ultrafiltration

2.3 Separation Systems

Colloidal separation systems are based on two classifications: Non-bubble and bubble-based systems. Non-bubble based systems are so called as their application excludes the use of bubbles. The reverse is the case for the other separation systems.

In the next sections, both systems for separation are reviewed; firstly the non-bubble based systems and then the bubble-based systems.

2.3.1   Non-Bubble Based Techniques

Separation has long been practiced without the use of microbubbles. Infact, in many industries currently non-bubble based systems are still the preferred colloidal particle recovery techniques regardless of the fact that these methods are time consuming, expensive and relatively inefficient, preventing their application for continuous large scale production in industries (Hatti-Kaul and Mattiasson 2001). Some of the traditional techniques employed include filtration, sedimentation and centrifugation. Many of the literatures reviewed in section 2.3.1 are of particular importance to both recovery of algal and yeast cells found later in this research work.

2.3.1.1 Filtration

Although, well advanced, filtration and sedimentation share a common difficulty of long operating time and low particle recovery (Molina Grima et *al*. 2003; Hanotu et *al*., 2013). However, filtration differs significantly as a multi-stage production process, often requiring the arrangement of filters in series. Fine membranes are first set to screen out larger particles followed by ultra-fine mesh sizes. The other common problem with filtration is the high-pressure build up at the membrane interface, requiring substantial energy use to overcome the resultant pressure. Also, because membranes are highly susceptible to clogging, regular maintenance is required which could become cost ineffective. Nonetheless, another ineffectiveness of filtration lies in the low separation efficiency with sub-micron particles. Some examples of filtration techniques include: Rotary drums (Gudin and Therpenier, 1986; Gudin and Chaumont, 1991), Sand filters (Ben-Amotz and Avron, 1987), continuous rotary vacuum filters (Shuler and Kargi, 2002).

2.3.1.2 Centrifugation

Cell separation from culture media by centrifugation has also been explored using industrial centrifuges-tabular bowl and disc stack centrifuges (Shuler and Kargi 2002). The concerns with centrifugation however have been widely reported. Applying centripetal force to cells can have detrimental outcomes. Cell lysing due to centrifugation is a huge problem as is the cost associated with equipment purchase

and maintenance. Several investigators have also reported the associated negative impacts as a result of sheared cells. Cells exposed to centrifugation have shown to exhibit low viability. Chlup et *al* (2008) reported that centrifugation results in a reduction in intracellular trehalose and glycogen yeast levels. Apart from the increase in proteinase *A* activity which lowers beer foam stability, centrifugation can also cause the release of yeast cell wall mannan (which induces beer haze). Furthermore, separation by centrifugation involves high capital investments, maintenance and high-energy consumption (Xu et *al* 2005) and these prohibit their application in the production of bio-ethanol from yeast (Xu et *al*., 2005). Although relatively efficient (compared to other non-bubble based recovery techniques) (Molina Grima et *al*., 2003), centrifugation is still marred and limited to small-scale batch production. This section is of particular importance to both recovery of algae and yeast cells found in later in this research work.

2.3.1.3 Sedimentation

Occasionally, cells are allowed to settle out of medium by the addition of an agglomerating agent or flocculent cells, as is the practice in the fermentation industry. Sedimentation exploits the density differential between colloidal particle and their containing fluid along with gravity effect to achieve result. Thus larger and denser particles readily settle out of solution. Other finer, less dense microbial cells may remain however in suspension indefinitely or in extreme cases, infinitely. In addition to the typically low recovery efficiency, other shortcomings of sedimentation are obvious. Long retention time and large space requirements are some of the main examples. But another equally important but less reported disadvantage with this recovery approach is the high moisture content of the recovered end-products (Molina Grima et *al*. 2003). Moisture content reduction is essential if dry products are required for subsequent use. Rarely, recovered co-product may be required in cream forms (e.g. cream yeast) for resale or repitching into a fresh batch, but usually at low moisture content. Owing to the high cost of heating, it is therefore important to reduce the water constituent of any sludge. Hanotu et *al*., (2012) reported increased moisture content in harvested yeast cells using sedimentation as a recovery alternative.

2.3.1.4 Flocculation

This method of recovery is mainly applied in the yeast industries. Flocculation is another mode of cell separation from their containing medium. The ability of yeast cells to naturally flocculate has been largely exploited particularly by the brewery industry. Currently, recovery of cells by self-flocculation is one of the most widely employed techniques in the industry. The phenomenon of yeast flocculation can be explained by three mechanisms namely: Lectin-model theory, the colloidal theory and the Ca^{2+} bridge theory. The lectin model has been widely accepted as the prevalent mechanism governing flocculation but it has also been suggested that all three mechanism may play contributory roles (Speers et *al*., 2006). Cations play an important role in yeast flocculation but their impart is quantity and yeast strain dependent. Stratford (1989) reported that Ca^{2+} released from the cells are the possible reason for the flocculation of yeast cells at reduced salt concentration. In a different study by Mill (1964), the authors reported that flocculation in yeast cells was due to the Ca^{2+} ions linking two carboxyl, phosphate and sulphate groups at cell surfaces. Hydrogen bonds between hydroxyl groups promote the aggregate stability (Mill, 1964). Amri et *al*., (1979) observed however that the flocculation of yeast cells was associated with carboxyl groups but also, confirmed the influence of Ca^{2+} bridges in yeast flocculation.

Another essential factor is the type of medium (Dengis et *al*, 1995) and concentration of free and labile Ca^{2+}. This amount is necessary to induce the lection conformation. However, the available Ca^{2+} is dependent on both pH and the presence of complexing compounds in the solution (Soares and Seynaeve 2000b). Apart from Ca^{2+}, several other divalent metal ions are known flocculant promoters. Nishihara et *al* (1982) reported that Mg^{2+} plays a crucial role in the flocculation of cells. Stewart and Goring (1976) reported that Mg^{2+} and Mn^{2+} could play the exact role Ca^{2+} plays as a flocculant. The authors also reported that concentration of other metal ions such as potassium and sodium (1-10 mg/L) induced flocculation. These metal salts lower the surface charge of cells and as a consequence, alter their modifying effect on surface proteins (Stratford, 1992). Other salts reported to inhibit yeast cell flocculation include the alkaline-earth metal ions Sr^{2} and Ba^{2+}(Nishihara et *al*., 1982; Stratford,

1989; Kuriyama et al., 1991), Na^+(Mill, 1964; Nishihara et al., 1982; Stratford 1989), K^+ (Stratford, 1989; Amri et al., 1979), citrate ions (Stratford, 1989), Ca^{2+}(Stratford and Brundish, 1990), Mg^{2+}(Stratford and Brundish, 1990), Mn^{2+}(Kuriyama et al., 1991) Cs salts (Stratford and Brundish, 1990), Al^{3+}(Kuriyama et al., 1991), La^{3+}(Kuriyama et al., 1991) and Li^+(Stratford, 1989). Like salt, sugar is an essential medium constituent that could influence the yeast cell flocculation but its effect is strain dependent. The different varieties of sugars have their respective effects on flocculation. Kihn et al., (1988) reported that while S $cerevisiae$ was inhibited by mannose, $S.$ $uvarum$ was inhibited by mannose, maltose and glucose. When cells flocculate, the densities of the aggregate increases to the sum of the respective individual cell densities and results in cell settling out of culture medium. One of the main problems with this approach is its ineffectiveness to separate colloidal yeast cells. In addition to the significant time consumption, separation of yeast cells by flocculation is unsuitable when continuous large-scale production is needed.

2.3.1.5 Others

Some other recovery methods include adsorption to an inert support, gel entrapment and entrapment within a porous matrix (Kourkoutas et al. 2004). A known problem with cell immobilization is cost and the differences in the metabolic pathway between free cells and immobilized microorganisms. The change in the cell physiology caused by immobilization or the change in the chemical and physical environment of immobilized cells is probably the cause of these differences in metabolic pathways (Shen et al. 2003). Strehaiano et al (2006) reported that cell entrapment can have deleterious effects such as diffusional limitation and mass transfer problems, causing development of substrate, oxygen and product gradients in the culture environment. Recovery of cells by precipitation is also a common practice. The addition of coagulants such as cationic or anionic polymers has been explored by several authors. Weeks et $al.,$ (1983) investigated the precipitation of yeast cells with inert powder from nickel particle. Whilst Stratford and Bond (1992) used lectin Concanavalin A, Dauer and Dunlop (1991) used magnetic particles prior to using magnetic separation. Co-flocculation with flocculent yeast cells is also a common practice in yeast recovery. Mortier and Soares (2007) used $S.cerevisiae$ cells as flocculents to flocculate other cells. Other coagulants such as polyelectrolytes and polymeric

particles that reduce cell surface charge have been used to induce yeast settling. Unfortunately, the use of these materials in yeast separation has not gained food grade constituent approval.

The next section will analyse bubble-based separation systems (i.e flotation systems). But before reviewing the methods for bubble generation for flotation separation, it is expedient to provide an insight into microbubbles; their benefits, and general behaviour in varying liquid media: contaminated and uncontaminated media leading to the science and fundamentals of flotation.

2.4   Benefits of Microbubbles

The main advantage of microbubbles is the surface area to volume ratio. Almost all physical transport processes- mass, heat and momentum- hugely rely on the surface area of the interface between the phases (Zimmerman et *al.*, 2009). Mathematically, it is clear that the surface area to volume ratio of a gas bubble increases inversely proportionate to its diameter:

$$\frac{S}{V} = \frac{4\pi r^2}{\frac{4}{3}\pi r^3} \qquad \text{(Eq. 2.6)}$$

For a constant volume of the bubble phase the equation becomes

$$S = \frac{3}{r}V_0 \qquad \text{(Eq. 2.7)}$$

Where S is the surface area and r the bubble radius. When a litre of air is distributed in 100-micron size bubbles, the total interfacial area obtained is 10 m^2. In addition to that, due to the constant rise of the bubbles, there is an increased mass transfer coefficient (Desphande and Zimmerman, 2005a,b). So in general, microbubbles are more efficient in mass or heat exchange. This is clearly supported by the equation for the description of interphase mass transfer flux J (moles/s):

$$J = K_l S(c_g - c_l) \qquad \text{(Eq. 2.8)}$$

Where S, K_l, c_g and c_l, are the interfacial area, mass transfer coefficient and molar concentrations respectively. The mass flux J varies directly proportionate to S and thus varies inversely proportionate to the bubble size (d).

Likewise, the effect of microbubble on heat and mass transfer propagation is also true for momentum transfer, with some adjustment. Stokes law is a clear illustration of a microbubbles residence time in a viscous liquid:

$$U_{stokes} = \frac{2g\Delta\rho d^2}{9\mu} \qquad \text{(Eq. 2.9)}$$

Where r, μ, g and ρ are the radius of the sphere, fluid viscosity, acceleration due to gravity and the difference between the gas density and the surrounding fluid respectively.

From the Equation (2.9) microbubbles reside longer for the same liquid height than do coarse bubbles. It follows therefore that microbubbles have much longer time for momentum transfer from bubble to liquid dragged along with them, though their momentum is relatively small. However, (Zimmerman et al., 2009) argues that the overall momentum flux of microbubbles in significantly higher with decreasing bubble size since momentum is also transported by shear stress across the surface area of the bubble. By direct implication, microbubbles provide a higher ability to drag when in motion than coarse bubbles for the same volume of fluid holdup.

2.4.1 Microbubble Behaviour

In flotation, ~150 µm bubbles represent the upper bubble size threshold for colloidal particle recovery from an aqueous medium. The reason is mainly that their behaviour in a liquid continuous phase is governed essentially by hydrodynamic forces, making inertia less significant in analysing their behaviour. Furthermore, their terminal rise velocities, having a Reynolds number less than 1 (one) are an accurate parameter in the prediction or assessment of boundary layer conditions existing at the liquid-vapour interface before bubble-particle interaction. Given their high surface tension and very small inertial effects, microbubbles are more spherical as they move at their terminal velocities. Another peculiar behaviour of microbubbles over large bubbles is their ability to shrink when their diameter is below a threshold value due to an increase in internal pressure. The pressure differential existing between the inside and outside of the bubble can be illustrated by the Young-Laplace equation:

$$\Delta P = \frac{2\gamma}{r} \qquad \text{(Eq. 2.10)}$$

The ΔP, γ and r are the pressure difference, the surface tension, and bubble radius respectively. Parkinson et *al*., (2008) studied the pressure difference between microbubbles of varying sizes in water and showed that the microbubble internal pressure increases sharply as their size decreases below 50 μm with pressures of 19.4 and 3kPa recorded for microbubbles of 15 and 100 μm sizes respectively. Compared to the pressure of a disjoining thin film (~15-20 nm) (A disjoining pressure is a supplementary pressure arising when a hydrostatic pressure of a thin layer differs from the pressure of the liquid bulk phase), the internal pressure of microbubble was also significantly higher. Owing to the pressure differential, diffusion of entrapped gases occurs from a higher-pressure inside the bubble to a lower pressure zone in the surrounding aqueous solution. Thus, a decrease in microbubble size and an increase in the internal pressure results, causing microbubbles to further lessen and possibly, eventually collapse. This behaviour of microbubbles is crucial in cases where high mass and momentum transfer is sought. One popular example is in the dissolution of gaseous nutrient in a microbial culture. Some authors (Al-Mashhadani et *al*., 2011; Zimmerman et *al*., 2011) have reported on the increased efficiency with microbubbles over coarse bubbles. Also important and worthy of mention is their buoyancy force. As their sizes decrease, so do their associated buoyancy forces. Parkinson et *al.*, (2008) measured the buoyancy force and reported results between ¬10^{-11} and 10^{-8} N for 15 and 100 μm-sized bubbles respectively. The high internal pressure of a microbubble combined with its low buoyancy force and insignificant inertial effect, leads to widespread application in many bioprocesses.

2.4.2 *Terminal Rise Velocity*

Microbubble movement and dynamics have vital implications in gas-liquid systems. After emerging and necking of from its exit pore, microbubble rises and then accelerates to a maximum level where its buoyancy force- a function of its density and size - is equalized by the drag force impeding its motion. Viscous and inertial energy dissipation inside the liquid medium is responsible for the drag force and fluctuates significantly, depending on medium hydrodynamics around the gas bubble. Likewise, this is affected by the size and velocity, as well as by the bubble surface condition– mobile (uncontaminated), immobile (contaminated) or at an intermediate condition (Parkinson et *al.*, 2008; Manor and Chan, 2009). Estimating bubble terminal

velocity (U_t) therefore requires an understanding of the drag force experienced by the rising bubble. Several literature (Bozzano and Dente, 2001 Alves et al., 2004; Manor and Chan 2009) regarding bubbles report numerous empirical relationships for the coefficient of drag (C_d), especially relating the Reynolds number to C_d. Coefficient of drag was calculated by Stokes for a solid particle, which was later further developed by Hadamard and Rybczynski in 1911, ignoring the shear stress drag component at the boundary for a fluid drop or bubble. As such, the inertial component of the Navier-Stokes equation is ignored, leading to the resultant equations for C_d, 24/Re and 16/Re respectively, which holds only where $Re \ll 1$. Other attempts at modifying the coefficient of drag basically entailed empirical corrections to account for non-sphericity. A well attempted summary however of C_d and U_t values across a wide range of Re was done by Clift et *al*., (1978) and Harper (1973) (Figure 2.2). Their studies hinged on the terminal rise velocities of microbubbles, under scenarios of Re tending towards zero ($Re \to 0$).

2.4.2.1 Terminal Rise Velocity in Clean Medium

The terminal velocity of immobile surfaces (solid spheres) when in motion in a viscous liquid was described sufficiently by the Stokes Law (equation 2.2:see benefit of bubbles for equation) at low Re. It is worth noting that Equation 2.2 is not applicable to turbulent regime (higher Reynolds number) as inertia is excluded in its derivation (Clift et *al*., 1978). As Re tends towards unity, this discrepancy becomes considerable which is the case for microbubbles (~100 μm-sized) rising in water. Hadamard and Rybczynski (1911) described the terminal velocity for a fluid by solving the Navier-Stoke equation with the boundary parameters modified to account for the internal viscosity as

$$U_t(H - R) = \frac{2\Delta\rho g r^2}{3\mu} \frac{\mu + \mu'}{2\mu + 3\mu'} \qquad \text{(Eq. 2.11)}$$

The internal viscosity of the fluid drop is represented by μ'. The adjustment of Stokes's law in Equation 2.9 to Hadamard-Rybczynski equation in Equation 2.11 signifies the reduced capability of the microbubble surface to sustain tangential stress. Frumkin and Bagotskaya (1947) conducted experiments with mercury droplets falling in liquid glycerin while Kelsall et *al*., (1996) studied oxygen bubbles (30-110 μm) rising in solutions to justify the modification (*H-R* equation) made to Stokes's law.

28

For cases with a fully mobile surface and negligible internal viscosity (i.e. $\mu' < \mu$) the shear stress becomes zero at the boundary given the inability of the mobile bubble surface to support tangential stress. Thus, the terminal rise velocity U_t (H-R) (Equation 2.11) yields:

$$U_t(H-R) = \frac{\Delta \rho g r^2}{3\mu} = \frac{3}{2} U_t(ST) \qquad \text{(Eq. 2.12)}$$

From Equation 2.12 and from works of several investigators (Moore, 1959; Levich 1962; Duineveld, 1995; Kelsall et al., 1996; Sam et al., 1996; Takahashi 2005; Manor et al., 2008; Parkinson et al., 2008; Manor and Chan 2009) a microbubble having a clean mobile surface, rising in a liquid medium exceeds the terminal rise velocity by a factor of 1.5 more than that estimated by Stokes' law (see Fig 2.7). Therefore, the terminal rise velocity can serve as an essential indicator in estimating the purity of water (Parkinson et al., 2008) as well as the amount of surfactant or contaminants at the bubble surface and consequently a measure of the mobility of microbubbles.
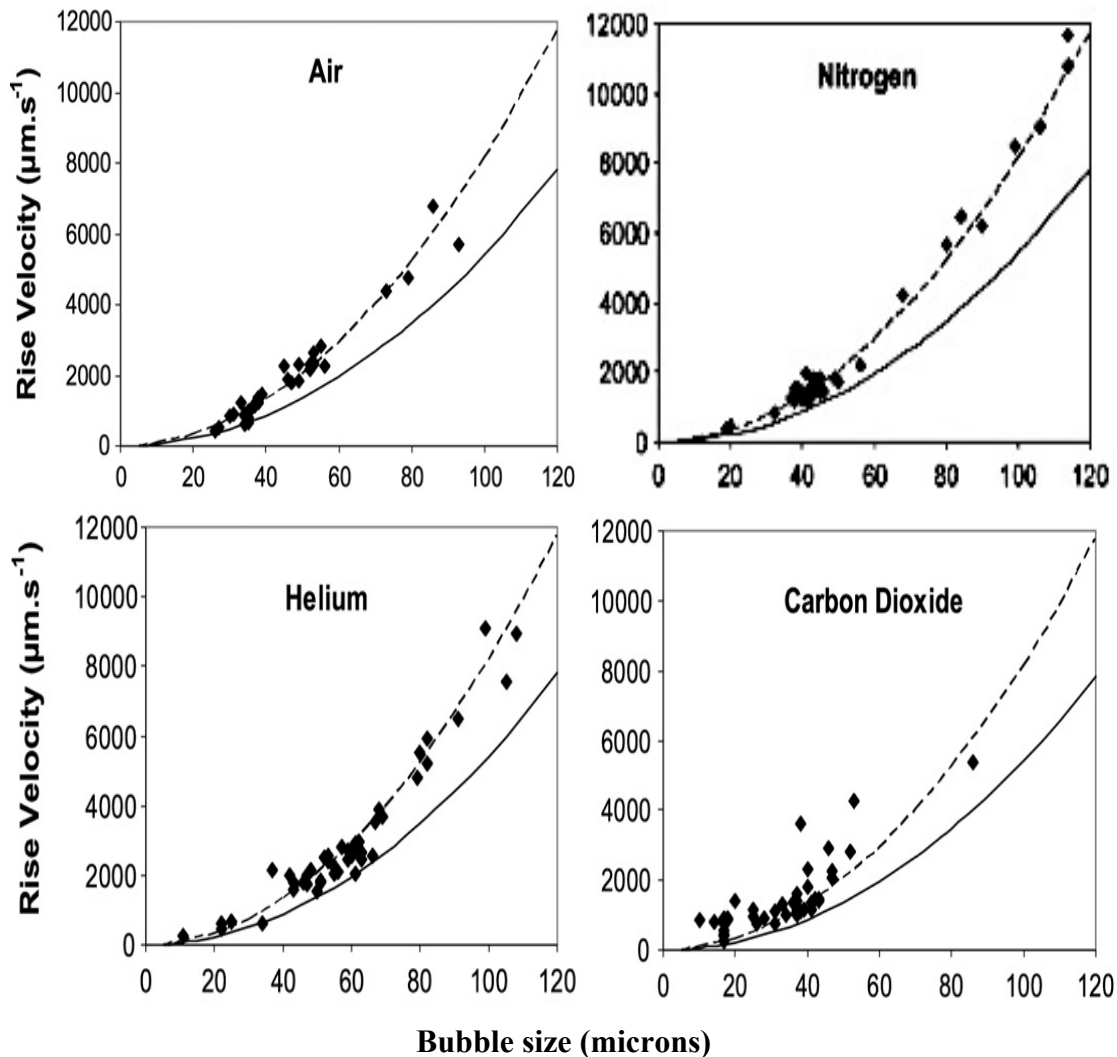
Figure 2.7: Terminal rise velocity versus bubble diameter plots for air bubbles in water. Comparisons with Stokes' (solid lines, —) and Hadamard–Rybczynski (broken lines, - - -) terminal velocity predictions are shown. Data points represent single bubbles. Source: Parkinson et *al*. (2008).

2.4.2.2 Terminal Rise Velocity in Contaminated Medium

In a liquid medium with surface-active molecules (even small traces), microbubble velocity is retarded as a result of the decrease in the bubble's surface mobility (Kelsall et *al*., 1996; Manor et *al*., 2008; Manor et *al*., 2008 Parkinson et *al*., 2008) and internal circulation as surfactants molecules are adsorbed to the gas-water interface (Fuerstenau and Wayman 1958; Nguyen, 1998). The tangential hydrodynamic shear stress acting on the bubble forces movement of the adsorbed surfactant molecules towards the bubble's lower hemisphere as it rises through a liquid column, thus creating a 'Marangoni' surface tension gradient that prevents liquid movement along the interface as studies by (Harper, 1973 and Levich, 1962) reveal. In a different

30

study, Sam et *al.*, (1996) also observed that after release in a liquid medium during the stress-free state of the bubble surface, microbubbles were observed to accelerate to the highest velocity before adsorption of surfactant resulted in deceleration following surfactant introduction. Given this condition, the terminal velocity of the rising microbubble therefore approaches that of a solid sphere. This effect is known as 'surface viscosity' and was first described by Boussinesq (1885).

Furthermore as bubble size decreases, other forms of impurities can even induce the tangential shear stress like colloidal particles or droplets as in the case of oil-emulsion. While investigating the performance of the microflotation system for colloidal particle separation, Hanotu *et al.,* (2013) observed that particles given the same particle size, smaller bubbles were less efficient in the recovery of particles from medium.

2.4.2.3 Effect of Gas Type

The influence of gas type on microbubbles rise velocity has been limited to hydrogen and oxygen bubbles. Parkinson et *al.*, (2008) studied rise velocity of freshly generated single bubbles of varying gases with diameters < 100 μm (Re < 1). Their results (Fig 2.7) showed that the terminal rise velocity of N_2, O_2 and H_2 microbubbles corresponded with the rise velocity predicted by Hadamard-Rybczynski equation (Eq 2.12), which showed that surfaces of these bubbles were to be fully mobile. A rather different outcome (Fig 2.7d) was observed with CO_2 microbubbles however as microbubbles larger than 60 μm exhibited velocities beyond those predicted by the Hadamard-Rybczynski equation. The authors attributed this behaviour to the high solubility of CO_2, which is possibly due to the high partial pressure of the gas (Fig 2.8). Another explanation for the rise in terminal velocity of CO_2 microbubbles was linked to its exothermic nature when released thus decreasing the local viscosity of the water and increasing rise velocity.
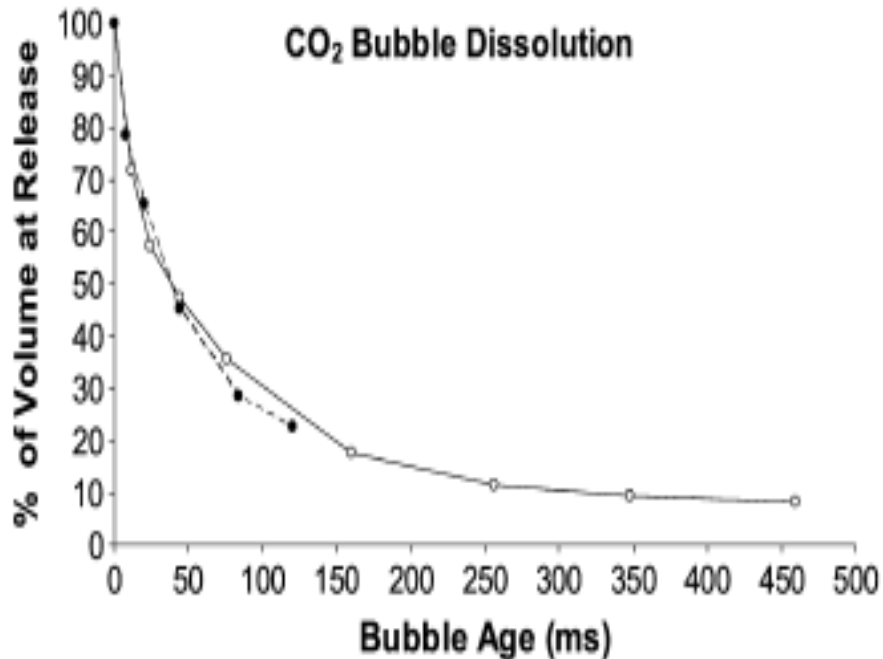
Figure 2.8: Graph of CO_2 bubbles as a function of resident time after release in pure water. The gas bubble gradually but continuously decreased in size with time. The terminal rise velocity as a result of the gas dissolution is significantly affected, exceeding values predicted by both Stoke and Hadamard-Rybczynski equation for immobile and mobile surfaces. Source: Parkinson et *al.*, (2008).

2.4.3 *Interaction with solids*

Bubbles in a liquid medium are often interacting with solid particles either in the form of microorganisms or other colloidal particles. The approach and interaction of two bodies in a fluid is a measure of the balance between their respective driving forces as well as the forces that oppose their contact. Several authors (Manica et *al.*, 2010; Parkinson and Ralston 2010) stated that viscous hydrodynamic drag resists the intervening liquid and enhances as the distance between both bodies becomes smaller and the fluid more confined. Depending on the nature of the hydrodynamic boundary conditions at the surface of the approaching bodies, this drag force changes significantly especially at small separations. Under the influence of a tangential shear, surface tension gradient obstructs movement of liquid at the liquid-vapour interface (Pallas and Pethica 1983), resulting in the bubble exhibiting tendencies of a solid. Measurements of surface tension are commonly used as a proof of the presence of contamination by surfactant in a liquid. Parkinson and Ralston (2010) have shown from measuring microbubble terminal rise velocity, that the trace contamination can alter the boundary condition at the L-V interface from full slip as illustrated by

Hadamard-Rybczynski rise velocity equations to 'no slip' as demonstrated by Stokes' rise velocity equation at contaminant concentration levels insufficient to cause any observable change in surface tension (< 0.1 mN.m^{-1}). Owing to this change in behaviour caused by changes in surface tension, contamination has become very sensitive issue in studies involving fluid-fluid interface boundary conditions.

2.5   Flotation Fundamentals

2.5.1   Overview

Separation of fine particles and our knowledge of the fundamental science governing its practice owes a lot to the efforts of many researchers in the past decades. In the mid-1900s, Gaudin et *al*. (1942) revealed that particles of varying sizes exhibit different separation tendencies. In order words, larger particles behave differently from finer particles. The author suggested thereafter that flotation rate was independent of particles of size up to 4 μm but varied proportionately to particles of diameter range 4-20 μm. A couple of years afterwards Sutherland (1948) developed the first theoretical particle-bubble collision model. To determine the rate of flotation, the model assumed that the flow field around the microbubble was the uniform motion of an inviscid fluid. Based on this assumption, the streamline around a bubble could be estimated from the potential flow theory.

Following that, Derjaguin and Dukhin (1961) studied the flotation of fine particles with the inclusion of hydrodynamics forces, diffusiophoresis and surface forces. The authors eventually proposed a mathematical expression to explain how the relationship between three efficiencies (see Eq. 2.16) affects the overall flotation rate. In their theory of flotation of small particles, Derjaguin and Dukhin characterized the particle-bubble interaction process into three distinct zones (Fig 2.9). In zone 1, the particle is relatively far from the bubble and the dominant force is the hydrodynamic force. The hydrodynamic force acts to move the particle around the bubble, whilst gravity and inertial forces propel the particle towards the bubbles, viscous forces however retard the particle movement. Zone 2 describes an occurrence where due to the liquid flow around the surface of the bubble, a tangential stream develops which transports the adsorbed surfactants or ions in the liquid to the lower hemisphere from the upper hemisphere of the bubble. Thus, a strong electric field is generated between

the upper surface and the particle due to the varying motilities and concentration of ions at the lower hemisphere of the bubble. Zone 2 is largely controlled by two forces - diffusional and electrophoretic forces, hence the term - diffusiophoretic zone. The particle-bubble interaction in this zone is similar to collision sub-process. As particle approach bubble and distance between both become a few hundred nanometers apart, surface forces dictate interactions in Zone 3. The rate of liquid film thinning is a function of the net surface charge. Therefore Zone 3 is considered an attachment sub-process because particle attachment to bubble is influenced by this process.
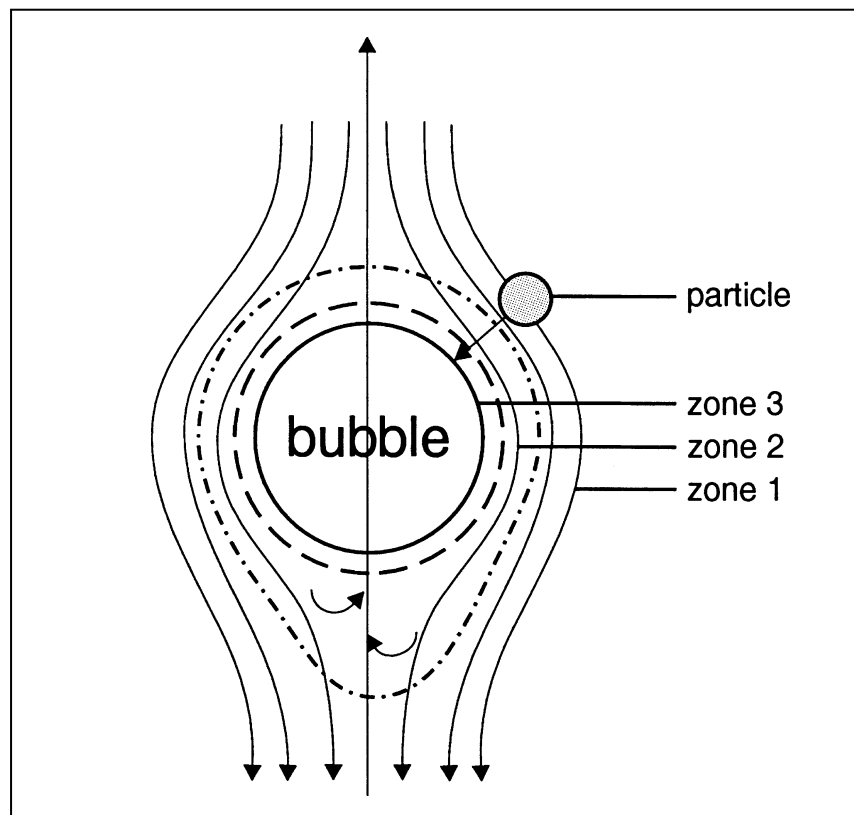
Figure 2.9: Schematic representation of the three particle-bubble interaction zones. Zone1: is characterized by hydrodynamic forces; in Zone 2, Diffusiophoretic forces dominate and Zone 3, Surface force influence interaction. Source Derjaguin and Dukhin (1961).

The works of Reay and Ratcliff (1973) (see model below: Eq. 2.27-2.29) revealed the possibility of two flotation regimes. Whilst the first suggested regime relates to particles >3 μm, the second occurs for particles approaching the nano-scale (< 3 μm). Obviously, as the particles tend towards the nano regime, they become prone to Brownian diffusion and the flotation process (collision mechanism) here is dictated by Brownian diffusion but otherwise, for micro-particles, the particle-bubble collision efficiency is a function of particles size and increases with particle size. Because

Brownian diffusion is the collision mechanism as particles approach the nano-regime, particle-bubble collision efficiency increases with decrease in size of particles (Reay and Ratcliff, 1973). The first estimation of the particle-bubble collection efficiency under potential flow condition was reported by Anfruns and Kitchener (1977). Nguyen et *al*., (2006) further demonstrated that collection efficiency was lowest for particle diameters ranging from 10 nm to 0.1µm. However, beyond this particle size range, two mechanisms are known to dominate: collision and interception mechanisms.

2.5.2 *Flotation Kinetics*

Particle removal or recovery from a continuous medium is a time dependent process as well as dependent on particle concentration (Sutherland, 1948; Jameson et *al*., 1977). Mathematically, we can represent the flotation process as:

$$\frac{dN}{dt} = -kN \qquad \text{(Eq. 2.13)}$$

Where *N*, *k* and *t* are the particle concentration, flotation rate constant and time respectively. Therefore, the recovery of particle (*R*) can be defined as:

$$R = \frac{N_o - N}{N_o} \qquad \text{(Eq. 2.14)}$$

N_o denotes the initial particle concentration. The flotation rate constant (*k*), considering a batch flotation process without mixing (Jameson et al., 1977; Yoon and Mao, 1996) becomes:

$$k = \frac{3J_d}{2d_b} E_{col} \qquad \text{(Eq. 2.15)}$$

The bubble – particle collection efficiency, bubble diameter and the superficial gas velocity (which is the volumetric gas flowrate divided by the flotation column cross-sectional area) are denoted by E_{col}, d_b and J_d respectively.

Derjaguin and Dukhin (1961) first defined the collection efficiency (*Ecol*) (Eq 2.16) as the product of three (3) distinct processes. These independent processes are: the collision efficiency (E_c), attachment efficiency (E_a), and the stability efficiency (E_s).

$$E_{col} = E_c * E_A * E_S \qquad \text{(Eq 2.16)}$$

Prior to approaching the bubble, the particle in the suspended medium is initially under the influence of hydrodynamic forces. These forces influence the particle away from and around the bubble surface. On the other hand, viscous forces act to slow the

particle down. The gravity and inertial forces, by contrast accelerate the particle towards the bubble surface to initiate the first process - particle-bubble collision. Following that, the forces acting on both the particle and bubble surfaces have to be balanced to support the rupture of the intervening thin liquid film and subsequently, the formation of the three-phase contact (tpc) between bubble and particle for the second process - particle-bubble attachment. The last process concerns the agglomeration stability - particle-bubble stability. The attachment forces have to supersede the detachment forces for particle-bubble stability to be achieved at any point in the flotation cell. Conditions that meet these requirements give rise to particle recovery by bubbles from the system. The next sub-sections will discuss these efficiencies, their theories and respective models.

2.5.3 Particle-bubble collision

The first of the efficiencies or probabilities is the collision probability, which occurs prior to particle-bubble attachment and stability of the agglomeration. The particle approaches a bubble until a critical distance before the surface forces begin to influence the relationship (Derjaguin and Dukhin, 1961). Several investigators have studied and developed many collision mechanism theories. The following section, reviews briefly the widely accepted and applied mechanisms.

2.5.3.1 Collision mechanisms

In order to analyse the bubble-particle collision, knowledge of the forces acting on both the gas bubble and solid particle, particularly the forces responsible for particle deviation from fluid streamlines around the surface of the bubble and as such prevent collision. Inertial, hydrodynamic drag and gravitational forces are the main forces influencing particle movement. Apart from shear-induced collision mechanism (Abrahamson, 1975), which usually occurs between particle and bubble of similar sizes (Miettinen et al., 2010), other types of collision mechanisms are largely considered in flotation separation. Another form of collision mechanism: collision by diffusion (Reay and Ratcliff, 1973; Yang et al., 1995; Nguyen et al., 2006) has been defined. In addition, Brownian, gravity, inertia and interception are the other particle-bubble collision mechanisms (see Fig 2.10). Their characterization is primarily based on the particle size, as this is central to the forces acting on the particle. For instance,

the Brownian diffusion is suited for particles in the submicron regime, which display random motion in a continuous fluid. The interception collision mechanism however, is as a result of liquid flow, which drives particles along the liquid streamlines. Contact with bubbles given this condition is due to particle's finite size. The collision of particles by the inertial mechanism is relevant to larger and denser particles given their inability to travel along specific liquid streamlines but rather move along a straight path. In other words, their movement is mainly due to their size and density been greater than that of the containing liquid. Thus, particles possess a settling velocity causing their travel path to deviate from the liquid streamlines. This deviation however may eventually result in the particle colliding with the bubble surface. Particle collision with bubble can result from one or a combination of these collision mechanisms (Miettinen et *al.*, 2010).
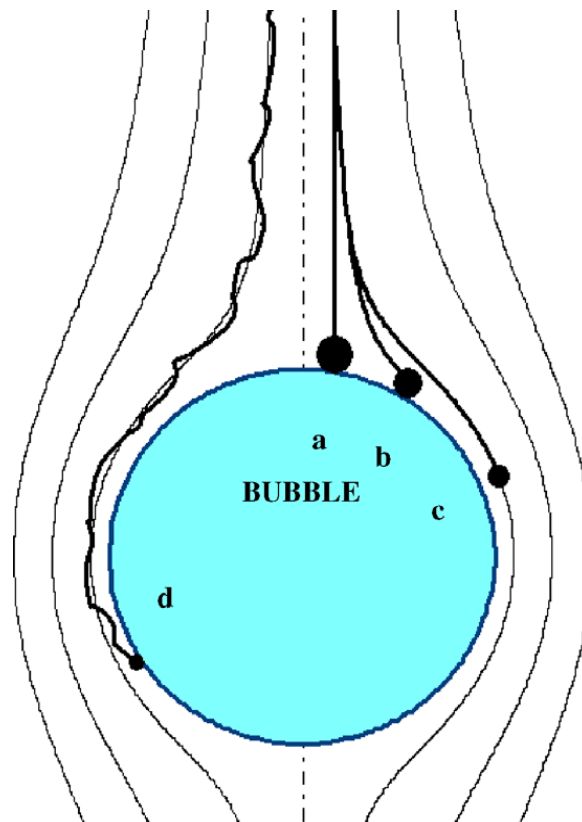
Figure 2.10: Diagram of the four particle-bubble collision mechanisms. The black and blue circles represent the particle and bubble respectively while the thin and thick lines are used to show the liquid streamlines and the particle trajectories respectively. (a) Collision by inertia. (b) Collision by gravity (c) Collision by interception (d) Collision by Brownian diffusion. Source: Miettinen et *al.*, (2010).

Two forces govern the collision mechanisms described above: Inertial and Long-range hydrodynamic interaction forces (LRHI) (Derjaguin et *al.*, 1993). For relatively large particles, the inertial forces are dominant whereas the LRHI influence the collision mechanism as the particle size decreases. The LRHI acts to influence particle movement to follow the liquid streamlines. Stokes number (Eq. 2.17) is dimensionless property employed to describe the relationship between a particle under the LRHI and within a specific distance to the bubble. In addition, it can be used to predict the particle motion pathway in the liquid as well as the interactions between bubble and particle (Ralston et *al.*, 2002).

$$\text{St} = \frac{\rho_p U_b d_p^2}{9 d_b \mu_f} \qquad \text{(Eq. 2.17)}$$

The bubble velocity, fluid dynamic viscosity, liquid density, bubble and particle diameter are represented by U_b, μ_f ρ_p, d_b, d_p respectively.

Reynolds number (Re_b) is also a dimensionless number employed to characterise the flow conditions of a fluid. It is the ratio of inertial forces to the fluid viscous forces. Mathematically it can be represented as:

$$Re_f = \frac{U_b \rho_f d_b}{\mu_f} \qquad \text{(Eq. 2.18)}$$

Here the fluid density ρ_f is considered. Estimating the liquid streamlines around the bubbles can be achieved with the analytical solutions of the continuity equations at two flow conditions - Stokes and potential flow. The stokes flow condition is used for bubble Reynolds number less than unity and the potential flow conditions employed at $80 < Re_b < 500$ (Schulze, 1992).

2.5.3.1.1 Collision models

Particles within a specified distance from the bubble's trajectory are bound to collide with the bubble. Thus, the particle-bubble collision efficiency (E_c) can be taken as the ratio of the cross-sectional area πR_{cr}^2 and the projected area of the bubble and the particle.

$$E_c = \frac{\pi R_{cr}^2}{\pi (R_p + R_b)^2} \qquad \text{(Eq. 2.19)}$$

Gaudin et *al*. (1942) and Gaudin (1957) developed the particle-bubble collision model using the Stokes flow stream function above (Eq. 2.17). In other words, they assumed a Stokes flow condition around the bubble, which considers the bubble's Reynolds number to be below unity (Schulze, 1992).

$$E_{c-st} = \frac{3}{2} \left(\frac{d_p}{d_b}\right)^2 \qquad \text{(Eq. 2.20)}$$

2.5.3.1.1.1   *Potential flow model- Sutherland*

Another collision model developed was by Sutherland (1948) when the author considered the collision mechanism to be by interception. The potential flow model (for large Reynolds numbers) was used to estimate the streamlines within the area of the rising bubbles and consequently the particle-bubble collision efficiency (E_{col}). Sutherland's model also considered the effect of Brownian motion and concluded that either the particle or bubble must be of size > 0.1 µm.

$$E_{c-pot} = \frac{3d_p}{d_b} \qquad \text{(Eq. 2.21)}$$

2.5.3.1.1.2   *Yoon and Luttrell Flow Model*

The collision model by Yoon and Luttrell (1989) assumed the interception mechanism of particle bubble collision as well as a stream function. The model is relevant for cases when the Reynolds number of bubble is between 1 and 100 (intermediate Reynolds numbers) (Yoon and Luttrell, 1989).

$$E_{C-YL} = \left(\frac{3}{2} + \frac{4Re_b^{0.72}}{15}\right)\left(\frac{d_p}{d_b}\right)^2 \qquad \text{(Eq. 2.22)}$$

From the collision efficiency equation above, the collision efficiency increases as the square of the particle diameter to bubble diameter.

2.5.3.1.1.3   *Rulyov Model*

The Rulyov (1989, 2001) model is based on the interception collision mechanism for bubble sizes <600 µm. The author assumed a surfactant concentration layer adsorbed to the surface of the bubble and based on the resulting retardation experience by the bubble, the author developed the bubble-particle collision efficiency:

$$E_{C-R} = C\,(Re_b)\left(\frac{d_p}{d_b}\right)^2 \qquad \text{(Eq. 2.23)}$$

The bubble Reynolds number is denoted by Re_b, while d_b and d_p are the diameters of the bubble and particle respectively. Given that the model is suited to intermediate flow, the above equation (Eq. 2.23) can be employed for a range of bubble Reynolds number from 1- 40 (Miettinen et *al.*, 2010).

2.5.3.1.1.4   Reay and Ratcliff Model

By assuming Stokes flow conditions around the bubble, the authors developed two bubble-particle collision models for particles below 0.2µm and the other for particles ranging from 3 µm to 20 µm diameter. The authors defined the concentration of particles and the concentration of unadsorbed particles in the zone close to the bubble surface as C_B and C_S respectively in the bulk liquid for 0.2 µm particles (particles affected by Brownian diffusion). In cases where C_s is zero, the particles are adsorbing strongly but if C_S is equal to C_B (i.e. C_B is unchanged) then the particles are adsorbing slowly. Therefore the diffusivity of particles (D_p) was expressed using the Stokes-Einstein equation below:

$$D_p = \frac{k_B T}{6\pi \mu_{fR_p}}$$
(Eq. 2.24)

The particle diffusivity is represented as D_p, whereas k_B denotes the Bolzman constant. μ_f and R_p are the fluidic dynamic viscosity and particle radius respectively. Lastly, T is the absolute temperature. In their derivation, they considered the net flow of particles around the bubble vicinity per unit time using Fick's law (Eq. 2.25) and expressed the concentration of particles collected by the bubble per time in Eq 2.26).

$$N_1^t = 4\pi Rb2kp(C_B - C_S)$$
(Eq. 2.25)

$$N_2^t = \pi R_b^2 U_b C_B$$
(Eq. 2.26)

The collection efficiency model by Reay and Ratcliff was obtained by taking the ratio of (Eq. 2.25) and (Eq. 2.26) and using Stokes equation, the authors derived the bubble rise velocity at 25°C in (Eq. 2.27).

$$E_{Col-RR} = 1.17 \text{ x } 10^{-11} \frac{C_B - C_S}{R_b^2 R_P^{2/3} C_B}$$
(Eq. 2.27)

Equation (2.27) shows that collection efficiency increases with smaller particle and bubbles size. It is worth mentioning that their collection model is appropriate for

particle size < 0.2 µm and a concentration boundary layer thickness of approximately 1.6 µm.

In relation to the particle-bubble collision model for particles range 3-20 µm, the authors assumed gravity to be the only influence, causing particle deviation from the liquid streamlines. The two models developed are for cases where the particle and liquid densities are the same (Eq. 2.28) and the other for particle density 2.5 times greater than liquid density (Eq. 2.29). Both models showed collision efficiency to be proportional to the particle and bubble sizes as well as the densities of the particle and surrounding liquid.

$$E_{C-RR} = 1.25 \left(\frac{R_p}{R_b}\right)^{1.9} \quad \text{(Eq. 2.28)}$$

$$E_{C-RR} = 3.6 \left(\frac{R_p}{R_b}\right)^{2.05} \quad \text{(Eq. 2.29)}$$

It is noteworthy, however to mention that Reay and Ratcliff's collision model was effective only for electrically uncharged particles.

2.5.3.1.1.5   Collins Model

By considering the population of particles adjacent the bubble, Collins (1975) developed a particle-bubble collision efficiency model. Essentially, the model took into account the particle flux next to bubble. By integrating the flux around the bubble surface, the particle-bubble collision efficiency was obtained as:

$$E_{C-C} \alpha \frac{1}{R_b^2 R_p^{2/3}} \quad \text{(Eq. 2.30)}$$

2.5.3.1.1.5   Yang et al. Model

The works of Yang et al. (1995) was basically for particles influenced by Brownian diffusion in the liquid medium. The authors used the Stokes and potential flow conditions for their models. In addition, the model considered the Marangoni effects. As a result of this effect, the bubble has interfacial tension gradients along its surface. The Marangoni number (Ma) is given by:

$$\text{Ma} = \frac{E_0}{\alpha R_b \eta_f} \quad \text{(Eq. 2.31)}$$

41

The E_0 is the Gibbs elasticity for the surface-active particles, α is the adsorption parameter of particles at equilibrium state. When the Ma $\to \infty$ the bubble surface is fully retarded and the bubble decelerated but mobile when finite.

$$E_{Col-Y} = \frac{1.842}{\sqrt{(1+\frac{2}{3}Ma)Pe}} + \frac{R_p}{R_b P_e} \qquad \text{(Eq. 2.32)}$$

$$E_{Col-Y} = 2.498 P_e^{\frac{-2}{3}} + \frac{R_p}{R_b P_e} \qquad \text{(Eq. 2.33)}$$

For the interception regime, the collection efficiency derived is given as:

$$E_{Col-Y} = \frac{1}{1+\frac{2}{3}Ma}\left[\left(\frac{R_p}{R_b} + (1+Ma)(\frac{R_p}{R_b})^2 + (\frac{R_p}{R_b})^3\right)\right] \qquad \text{(Eq. 2.34)}$$

$$E_{Col-Y} = \frac{3}{2}\left(\frac{R_p}{R_b}\right)^2 + \left(\frac{R_p}{R_b}\right)^3 \qquad \text{(Eq. 2.35)}$$

For potential flow conditions, the collection efficiency is given as:

$$E_{Col-Y} = 3\left[\left(\frac{R_p}{R_b}\right) + (\frac{R_p}{R_b})^3\right] \qquad \text{(Eq. 2.36)}$$

They finally developed several collision models (Eq. 2.32-2.36). In summary the authors concluded that the particle-bubble collection efficiency is the addition of the interception and diffusion contributions. Also, the collision efficiency varied indirectly with particle size for the diffusion regime but varied directly with particle size for the interception regime. For the case of an uncontaminated bubble surface (mobile surface), they authors concluded that the collection efficiency increases as the bubble surface became more mobile and with decreased in bubble size.

2.5.4 Particle-bubble Attachment

Particle-bubble attachment is the next probability after collision. Generally, modelling particle-bubble attachment is based on the induction time and contact time. The particle will attach to bubble when the contact time between bubble and particle is longer than the induction time (Sutherland, 1948; Schulze, 1992). Miettinen et al., (2010) reported another approach to modelling the attachment of particle and bubble is via the energy barrier approach.

2.5.4.1 Induction time

Attachment does not necessarily occur with every particle-bubble collision. An amount of time is necessary for the intervening liquid film between particle and bubble to thin and rupture followed by the development of a three-point contact (Fig

2.12). As a result of this, not all particle collision with the bubble yields attachment. Liquid thinning prior to particle-bubble attachment is one of the main factors during induction. However the induction time is a function of particle size and particle charge or hydrophobicity. Results from Glembotskii (1953) and Ye and Miller (1988) show that as particle size increases and particle hydrophobicity decreases, induction time increases consequently. The measurement of the induction times have been reported to be < 1ms to 100 ms for coal particles of varying surface hydrophobicities (Ye and Miller, 1988). In a different study, Hewitt et *al*., (1994) estimated the thinning of the intervening liquid film using different concentrations of electrolytes on hydrophobic quartz plates and reported an increase in rate of liquid thinning as electrolyte increases. The authors concluded that attachment efficiency increases medium ionic strength. Furthermore, Hewitt et *al*., (1994) showed that the attachment efficiency (E_a) decreased with decreasing contact angle (hydrophobicity) and also with increasing particle size. Moreover, smallest bubble size investigated (0.75 mm) yielded the highest attachment efficiency followed by the 1 mm and 2 mm sized bubbles respectively given the same contact angle and particle sizes.
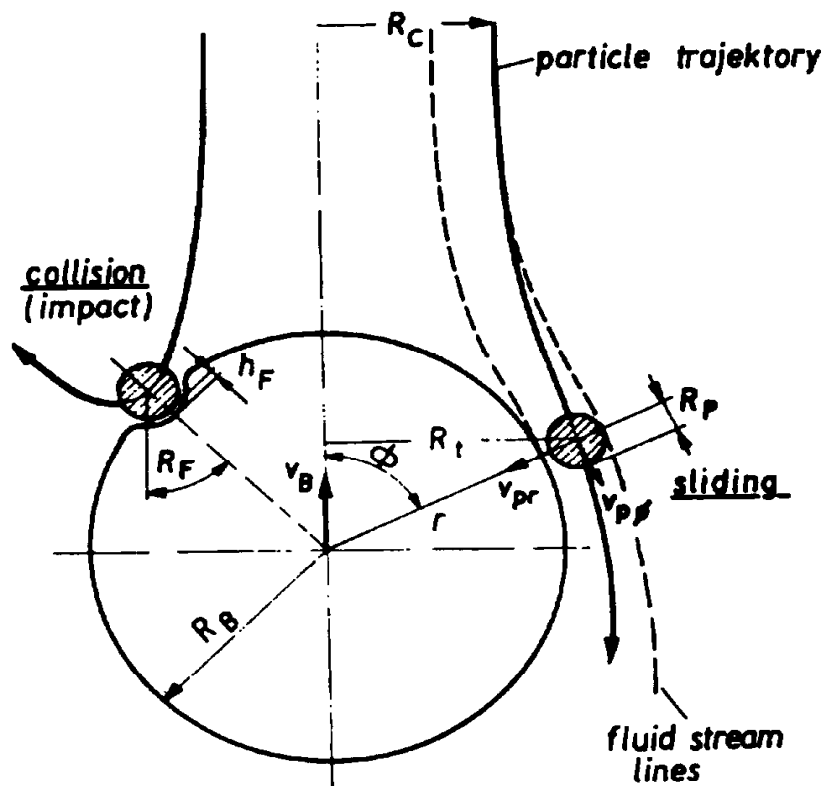
Figure 2.11: Schematic diagram of the particle-bubble interaction (contact) by impact and sliding. Source: Schulze (1992).

2.5.4.2 Contact time

After collision with bubbles, particles are in contact with the bubbles for a given period. Fig 2.11 shows a diagrammatic representation of bubble-particle interaction. The time a particle is in connection with a bubble is called the contact time or interaction time. After collision, rebound or sliding by particles occurs. If a particle only rebounds after collision, then the only component in the contact time is the impact time. For conditions when sliding takes place after the particle-bubble impact however, the contact time component then becomes the sum of the sliding and impact time. At collision angles less than 30°, Schulze and Gottschalk (1981) showed that the contact time component is the impact time and the contact time is about 1-4 ms but when the angle exceeds 30°, the contact time component becomes the sliding time and exceeds the impact time by 10-20 times.

Given their low collision kinetic energy, which is too small to cause any damage to the bubble surface, particles with diameters <100 μm only impact and slide on the surface of the bubble (Dobby and Finch, 1987). By contrast, bubble surface deformations are as a result of particle rebound but the contact times are very short (~10 ms) (Schulze, 1981).

A sliding time model (Eq. 2.37) developed by Dobby and Finch (1987) considered the potential fluid flow condition around a mobile bubble surface. The authors defined the sliding time as the time required for a particle to move from the collision point, at a specific angle θ_C, to the point where it exits the bubble surface (angle $\theta = 90$) (see Fig 2.11).

$$t_{sl} = -\frac{d_p+d_b}{2(U_p+U_b)+U_b(\frac{d_b}{d_p+d_b})^3} In\left(\tan\frac{\theta_c}{2}\right) \qquad \text{(Eq. 2.37)}$$

where the particle sedimentation velocity is denoted by u_p.

2.5.4.3 Attachment Models

2.5.4.3.1   Dobby and Finch Model

A critical collision angle (θ_{cA}) exists where the sliding time is equivalent to the induction time. Attachment angle is used to refer to this condition. Any condition where a particle with lower collision angle than the attachment angle will yield

particle-bubble attachment. Thus, projected area can be used to characterise particles attached to bubbles defined by the attachment angle. By converse, the maximum possible collision angle ($\theta_{c\ max}$) can be used to define the number of particles that undergo collision with bubble which are related to the projected area. Dobby and Finch (1987) suggested that the particle-bubble attachment efficiency is the ratio of both projected areas.

$$E_{A-DF} = \frac{\frac{\pi(d_p \sin \theta_{CA})^2}{4}}{\frac{\pi(d_p \sin \theta_{C,max})}{4}} \qquad \text{(Eq. 2.38)}$$

or

$$E_{A-DF} = \frac{sin^2\theta_{CA}}{sin^2\theta_{C,max}} \qquad \text{(Eq. 2.39)}$$

2.5.4.3.2   Yoon and Mao Model

The Yoon and Mao (1996) model of the particle-bubble attachment efficiency is the ratio of the potential energy barrier, E_1, and the kinetic energy of a settling particle. Yoon and Mao estimated the average kinetic energy of particles from the radial velocity of a dropping particle employing the empirical stream function of Yoon and Luttrell (1989).

$$E_{A-YM} = \exp\left(-\frac{E_1}{E_k}\right) \qquad \text{(Eq. 2.40)}$$

From their model, the particle-bubble attachment efficiency increases as E_1 decreases. Decreasing E_1 values can be obtained by increasing particle hydrophobicity or decreasing the electrostatic repulsion between negatively charged particles and bubbles. Their model also shows that attachment efficiency increases with increase in particle kinetic energy (E_k) values. In other words, the higher the kinetic energy of approaching particle, the greater the thinning and rupture rate of the intervening liquid film to allow the formation of a three-phase contact between particle and bubble.

2.5.4.3.3   Scheludko Model

Scheludko (1976) produced the attachment model using thermodynamic approach for the fine particles. The basis of the model was on the differential energy levels between the particle kinetic energy and the energy required to distort the interrupting liquid film. The author demonstrated that the particle kinetic energy must supersede the energy required to thin the intervening liquid film in order to form a three-phase

contact between particle and bubble. The minimum particle size $d_{p(min)}$ when the energies are in equilibrium can be obtained for a particular receding contact angle θ_r as:

$$d_{p(min)} = 2\left[\frac{3L^2}{U_b^2 \gamma_{LV}(\rho_p - \rho_f)(1 - \cos\theta_r)}\right]^{\frac{1}{3}} \qquad \text{(Eq. 2.41)}$$

where L and γ_{LV} are the solid-liquid-vapour three-phase contact line and the liquid-vapour interfacial tension respectively.

2.5.5 *Particle-Bubble Stability*

After particle collision with bubble the aggregate must attach and following that, remain stable for successful collection. To be able to remain stable through as it rises, the aggregate must resist strong detachment forces. These forces include, gravity, inertia and viscous forces and increase as the particle size increases because the particle area exposed to the detachment forces increases (Miettinen et al., 2010). The detachment forces scale-up 10^6 times more for 100 μm particles than when the particles are 1 μm in size (Derjaguin et al., 1982). Therefore, particle-bubble stability efficiency is approximately unity for highly hydrophobic 1μm particles (Miettinen et al., 2010).

2.5.5.1 Stability Models

Particle-bubble aggregate under quiescent conditions is influenced by forces such as: gravity of the particle, F_g, capillary force F_{ca}, the static buoyancy of the immersed part of the particle by the liquid, F_b and the hydrostatic liquid pressure, F_{hyd} (Sutherland and Wark, 1995). Schulze (1984) developed a model for particle-bubble stability under turbulent conditions presented below.

2.5.5.1.2   *Schulze model*

The particle-bubble stability efficiency (E_s) can be expressed as:

$$E_S = 1 - \exp\left(1 - \frac{1}{Bo'}\right) \qquad \text{(Eq. 2.42)}$$

where *Bo'* is the Bond number which is defined as the ratio of the detachment forces F_{det} to the attachment forces F_{att} (Eq. 2.43). The Bond number –a dimensionless parameter- is used to describe the aggregate stability.

$$Bo' = \frac{F_g - F_b + F_d + F_\gamma}{F_{ca} + F_{hyd}} \qquad\qquad \text{(Eq. 2.43)}$$

where F_τ is the capillary pressure in the gas bubble and F_d is the additional detaching forces.

The forces above can be expressed differently as:

$$F_g = \frac{4}{3}\pi R_p^3 \rho_p g \qquad\qquad \text{(Eq. 2.44)}$$

where gravitational acceleration is g. For the immersed part of the liquid, the static buoyancy is given as:

$$F_b = \frac{\pi}{3} R_p^3 \rho_f g [(1 - \cos \omega)^2 (2 + \cos \omega)] \qquad\qquad \text{(Eq. 2.45)}$$

where ω is the centre-angle between the rear part of the attached sphere and the projected three-point contact line (Fig 2.12).
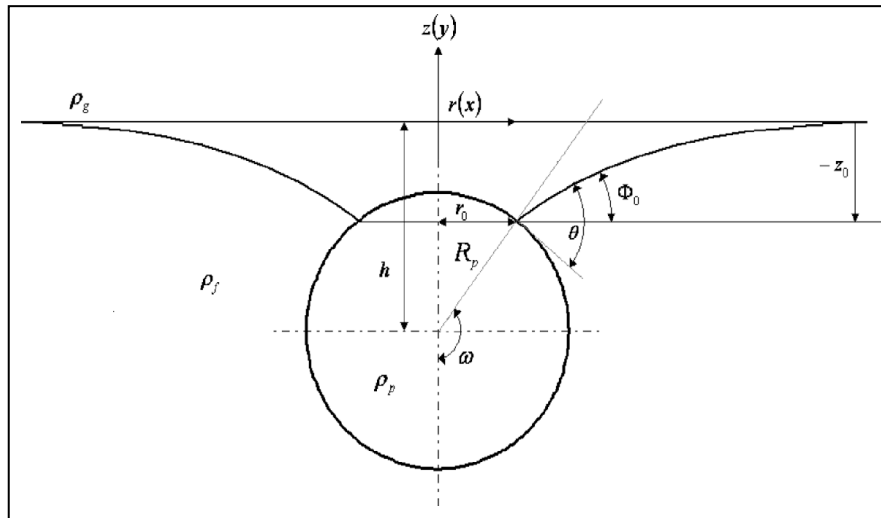
Figure 2.12: Schematic representation of an attached particle to bubble. The diagram illustrates the three-phase contact of a smooth spherical particle on a bubble. The stability of a bubble–particle aggregate is a function of the contact angle. Source: Schulze 1984.
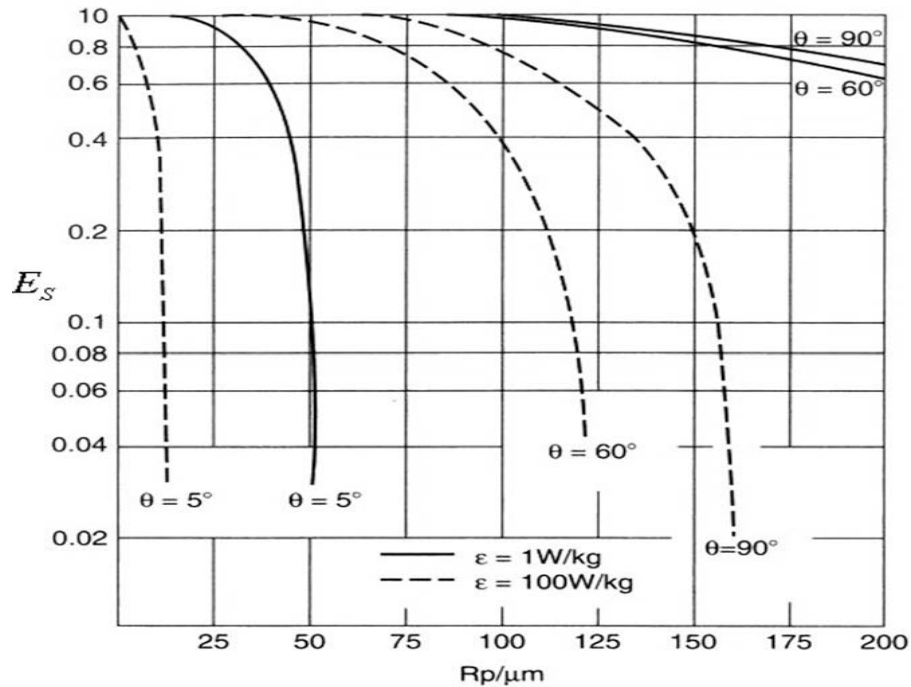
Figure 2.13: Graph of particle-bubble stability efficiency, E_s versus particle size at varying energy dissipation ε. R_p and contact angle, θ. Bubble radius $R_b = 0.5$ mm; $\rho_\rho = 2500$ kg/m^3; $\rho_f = 1000$ kg/m^3; $\gamma_{LV} = 70$ mN/m. Source: Schulze 1984.

Although recovery efficiency (Anfruns and Kitchener, 1977; Yoon and Luttrell, 1986; Hewitt et *al*., 1994; Dai et *al*., 1998a,b; 1999) and rate of flotation increases (Bennett et *al*., 1958; Reay and Ratcliff, 1975; Ahmed and Jameson, 1985) with smaller bubbles, there are limitations associated with microbubbles in flotation. One such hurdle is their low-rise velocity, which consequently results in high residence time and ultimately, prolonged flotation time (Miettenen et *al*., 2010). The other factor is regarding microbubbles low lifting force due to their low buoyancy, which renders them unsuitable for some flotation applications. Some authors (Schwarz *et al.,* 2002) have also reported high water recovery by microbubbles as another con with microbubbles. This high water is believed to cause high gangue mineral entrainment (Trahar and Warren, 1976; Liu and Wannas, 2004). But it is important to state that the latter factor also vary depending on the microbubble generation method, bubble size and stability. Nonetheless, the most important issue lies in the economic and efficient production of microbubbles. In the next sections, the bubble-based techniques are reviewed, first with a classification of the different methods of bubble generation then a critical assessment of their respective applications in flotation separation.

2.6   Bubble based Techniques

Generally, generating microbubbles can be broadly classified into three main ways. Firstly, the most readily available class basically involves the pressurization of air for its dissolution in a given liquid, and then after its release via a uniquely designed system of nozzles where the pressure drops to usher small bubbles based on the principle of cavitation. In the second class, ultrasound is used to produce local cavitation at different points in the ultrasonic wave. A low-pressure air stream is simply delivered through a porous medium to form small bubbles in the third class of bubble generation so that bubbles are necked-off with the aid of a supplementary element such as flow focusing, mechanical vibration or fluidic oscillation. The following sections will review major examples in each class of microbubble generation and their application in separation flotation.

2.6.1   The First Class: High Pressure

2.6.1.1 Dissolved Air Flotation

Dissolved air flotation is the most efficient and widely employed flotation option. According to Henry's law, the process essentially requires dissolving air in water at very high pressure. By so doing, the solution becomes supersaturated; leading to nucleation of microbubbles with size range 30-100 μm (generally < 100 μm) (Edzwald, 2010) as soon as pressure is reduces at the nozzle (see Fig. 2.14). DAF has been successfully applied in a wide range of industries for the recovery of valuable materials. Al-Shamrani et al., (2002 a,b) investigated the application of DAF in oil-emulsion treatment and reported oil recovery efficiency of 99%. Zouboulis and Avranas (2000) and Moosai and Dawe (2003) also applied DAF for oily wastewater clean up and recorded high performance with the DAF. Englert et al., (2009) applied DAF for the recovery of quartz particles using varying amine collector concentration and reported 6-53% by mass of quartz particles and concluded that DAF was efficient in the recovery of small particles. Teixeira and Rosa (2007) compared the performance of DAF and conventional sedimentation in the removal of cyanobacterial cells of *Microcystis aeruginosa* and revealed higher separation efficiency with DAF. Other applications with DAF include: Kitchener and Gochin, (1981) for portable water treatment, Waters (2008), Tessele et al., (1998) for metal removal.
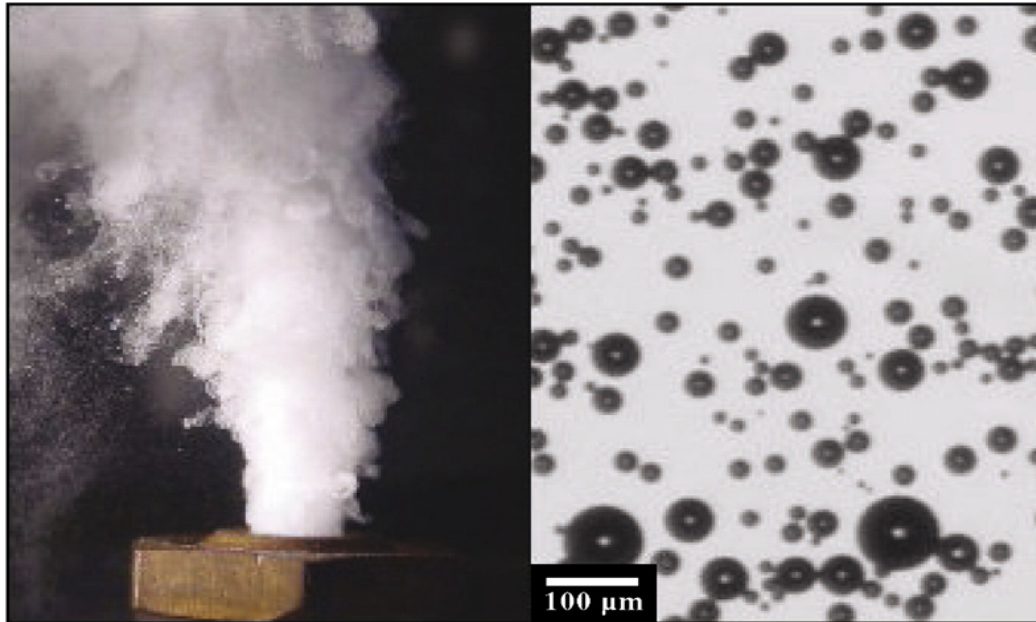
Figure 2.14: Microbubble generation from a DAF nozzle and the size characterization. Bubble less than 100 microns are generated but at a high-energy cost. Source: Rodrigues, (2003).

Unfortunately, this process is energy intensive, due to the high pressure required for air dissolution in water (Edzwald, 2010) as well as the work done by the pump in feeding the saturator with clarified water (Hanotu et *al*., 2011). Nonetheless, Zouboulis and Avranas (2000) and Al-Shamrani et *al*., (2002) all reported the existence of three basic configurations for the operation of DAF, namely:

Full-flow Pressure Flotation*:* Here the wastewater flowing into the flotation tank (influent) is first subjected to high pressure and then released in the tank to form the bubbles. This configuration is mainly employed when the particles in the wastewater do not require flocculation, hence the need for large volumes of air bubbles (Al-Shamrani et *al*., 2002).

Split-flow (partial) Pressure Flotaton: In this configuration, part of the influent wastewater is pressurized, and introduced into the flotation tank to form fine bubbles. Al-Shamrani et *al*., (2002) reported that this configuration is used in situations where particles are affected by the shearing effects of pressure pumps and also where the concentration of the particles in the water is low.

Recycle-flow Pressure Flotation*:* Here, a fraction (about 20-50%) (Zouboulis and Avranas, 2000) of the treated influent is pressurized, saturated with air and recycled back to the flotation tank, where it is released through specially designed needle valves to produce microbubbles less than 100 μm. This configuration is mainly considered for systems that require coagulation and flocculation, with the formation of mechanically weak flocs (Al-Shamrani et *al*., 2002). Hence, it is the preferred configuration in oily wastewater treatment (Zouboulis and Avranas, 2000).
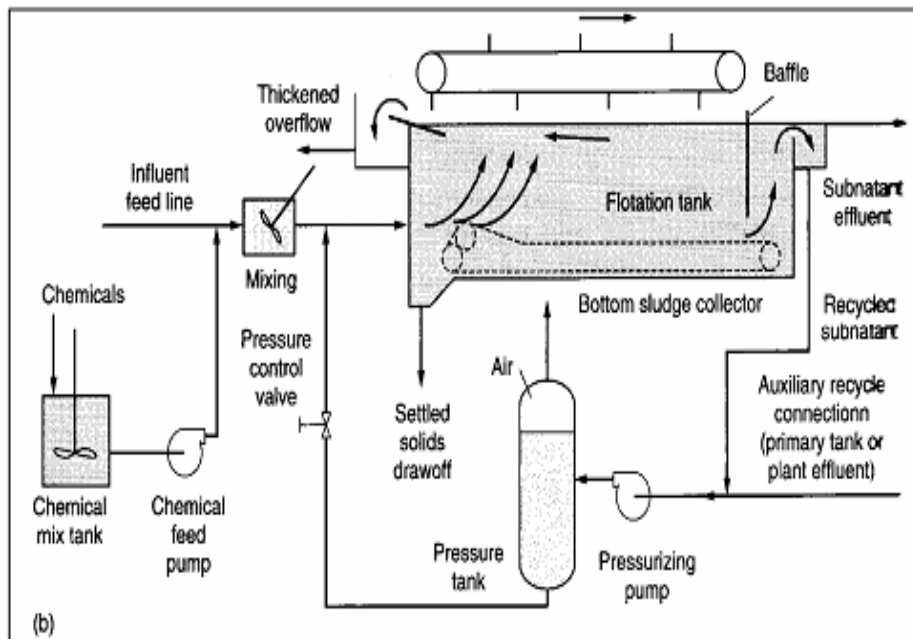
Figure 2.15: Schematic representation of a typical DAF unit for the recycle flow configuration. A fraction of treated effluent is pressurized and recycled back to mix with flocculated influent wastewater. (Source: Rubio et *al*., 2002).

Generally, for the DAF system to yeild optimum wastewater treatment (clarification), the particles in the effluent must first be pretreated - coagulated and flocculated, in order to enhance bubble-particle collision (Al-Shamrani et *al*., 2002). Bubble-particle interaction have been known to occur as a result of adhesion and hydrophobic forces.

However, Rodrigues and Rubio (2007) and Rubio et *al*. (2002) reported three basic mechanisms of their interaction in a DAF unit, illustrated diagramatically in Figure 2.16. These mechanisms are:

Nucleation at Solid Surfaces: A fraction of the compressed air which does not convert into microbubbles, stays dissolved in the water and "nucleates" at the surface of the particles.

Bubble Entrapment: This phenomenon occurs when rising bubbles are physically trapped inside flocs. This causes a significant reduction in the density of the resultant bubble-particle aggregate, thus enhancing flotation.

Aggregates Entrainment: This phenomenon depends mainly on hydrodynamics and bubble size distribution. This is the physical attachment of rising bubbles to flocs as they rise.
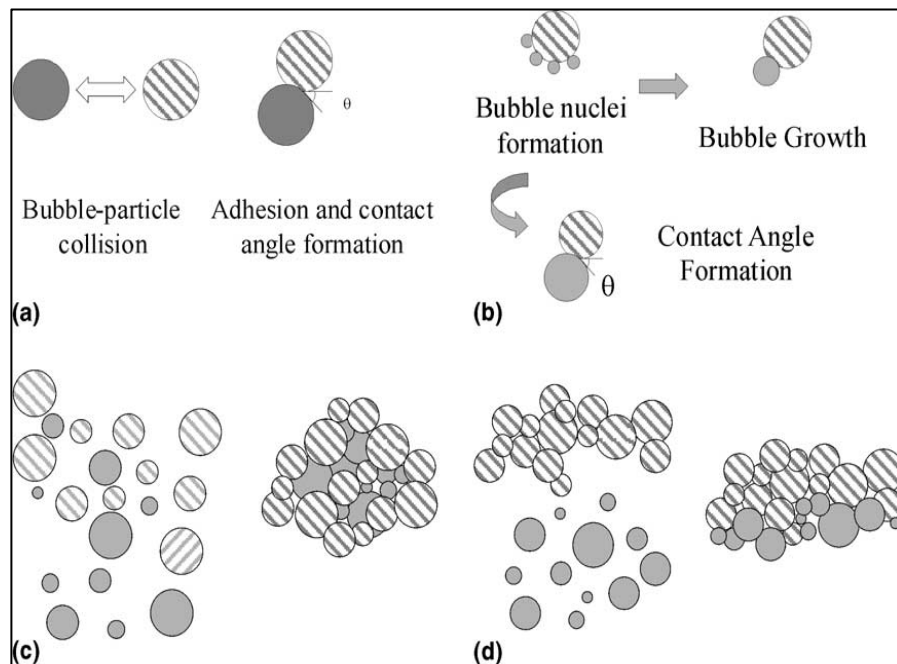
Figure 2.16: Bubble-particle mechanisms in DAF. (a) bubble-particle contact and adhesion; (b) bubble "nucleation" at particle surface; (c) entrapment of microbubble in aggregates; (d) entrainment of bubbles by aggregates (Source: Rubio et *al*., 2002).

While Rodrigues and Rubio (2007) opined that the first two mechanisms occur exclusively with microbubbles and that the last mechanism is the principal

mechanism in water treatment using DAF. Table 2.4 highlights some advantages and disadvantages of the DAF technique.

Table 2.4: Some advantages and limitations of the DAF technique. (Adapted from: Rubio et *al*., 2002; Rubio et *al*., 2007; Rodrigues and Rubio, 2007)

Advantages	Disadvantages
The system is compact - takes up less space than other Non-bubble based methods of separation.	Long retention times (20-60 min), resulting in inefficiency in the treatment of high volume of effluents and high flowrates.
Production of thicker sludge than other separation methods.	Poor handling of high density particles.
Flexibility in design and operating parameters.	Adverse weather effects on floating particles which could result in particle re-entrainment into treated effluent.
Ability to start-up rapidly in addition to being highly reliable in operation.	Expensive - the saturation (pressurization) process accounts for about 50% of the total operating energy costs. The other additional cost emanates from the use of pumps in lifting recycled water into saturators.
Produces high volume of treated effluent $(100 - 20{,}000 \text{ m}^3/\text{h})$	Low lifting power of microbubbles, limiting process to about 1-4% solids.

2.6.1.2 Turbulent Microflotation

Basically, turbulent microflotation (Fig 2.17) is a separation technique that is based on turbulent stream flow applied in a flotation channel. Microbubbles of approximately 40 μm (with the addition of surfactants to the liquid) in size are saturated in a liquid containing aggregated particles. Turbulent microflotation cells are usually long, narrow channels (Rulyov, 1989; Rulyov, 2001; Miettenen et *al*. 2010) where the treated effluent flows after saturation with microbubbles. The flow rate through the narrow channels is maintained to achieve turbulent stream flow conditions whilst also maintaining heterocoagulation of particles and bubbles and bubble-particle attachment. Not much literature exist on the application of turbulent microflotation in the separation of colloidal particles. Rulyov (2001) however

conducted experiments using turbulent microflotation and reported recovery efficiencies 10 times lower than results from dissolved air flotation.
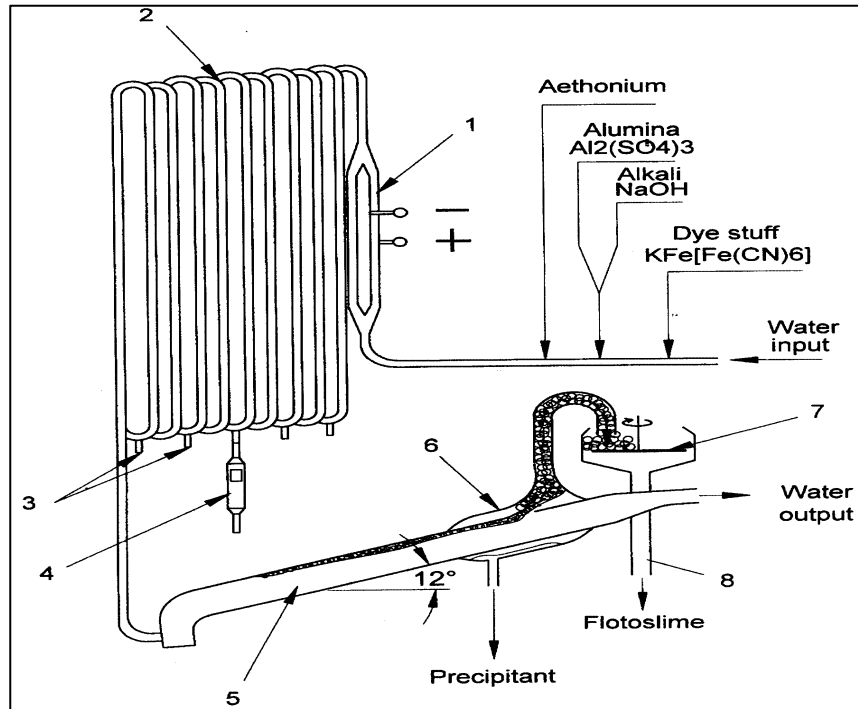
Figure 2.17: Schematic diagram of a turbulent microflotation system. (1) Electrolyser (Microbubble generator); (2) Tubular static mixer; (3) Samplers; (4) Microphotography cell; (5) Foam separator; (6) Flotosludge collector; (7) Disk foam beaker; (8) Flotosludge outlet. Source: Rulyov, 2001).

2.6.2   The Second Class: Ultrasound/Electrochemical

The application of an external field either ultrasound Makuta and Takemura (2006) or electricity to induce a chemical reaction and consequently the generation of microbubbles. The two main techniques in this class are the Ultrasound and Electroflotation techniques.

2.6.2.1 Ultrasound Technique

Ultrasound technique belongs to the second class of bubble generation. By oscillating a liquid under pressure in a highly viscous liquid by an ultrasonic wave, the gas liquid at the needle top oscillates and produces uniformly sized microbubbles (4-15 μm) at constant periodic rate. The viscosity of the liquid is a key parameter in this method of bubble generation as it not only influences the size range of bubbles but also the flux at each generation cycle. Makuta and Takemura (2006) reported that an increase in

bubble flux results because more daughter bubbles are formed from the parent (mother) bubble at reduced viscosity or surface tension effect relative to the inertial force. Otherwise, daughter bubbles remain undetached from mother bubbles.

2.6.2.2 Electroflotation

Electroflotation has long been employed for flotation in the mineral industry for mineral recovery particularly due to the uneconomic and inefficient capabilities of other techniques (Miettinen et *al.*, 2010). Basically, the technique entails the electrolysis of water (Eq. 2.46 and 2.47), where hydrogen and oxygen gas bubbles (22-50 μm) are produced in the process. While hydrogen (H_2) bubbles are formed at the cathode, oxygen (O_2) bubbles are formed at the anode.

$$H_2O \leftrightarrow 2H^+ + \frac{1}{2}O_2(g) + 2e^- \qquad \text{(Eq 2.46)}$$

$$2H_2O + 2e^- \leftrightarrow 2OH^- + H_2(g) \qquad \text{(Eq 2.47)}$$
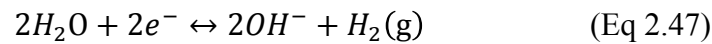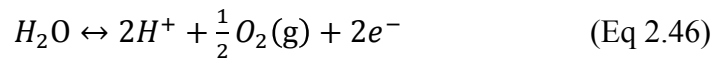
An advantage of this technique is the possibility to use air bubbles in conjunction with the hydrogen and oxygen bubbles (Miettinen et *al.*, 2010). The gas bubbles (microbubbles), formed on the surface of the electrodes attach to the particles and the aggregate ascend to the surface, where recovery is achieved by skimming (Mansour and Chalbi, 2006; Rubio et *al.*, 2002).
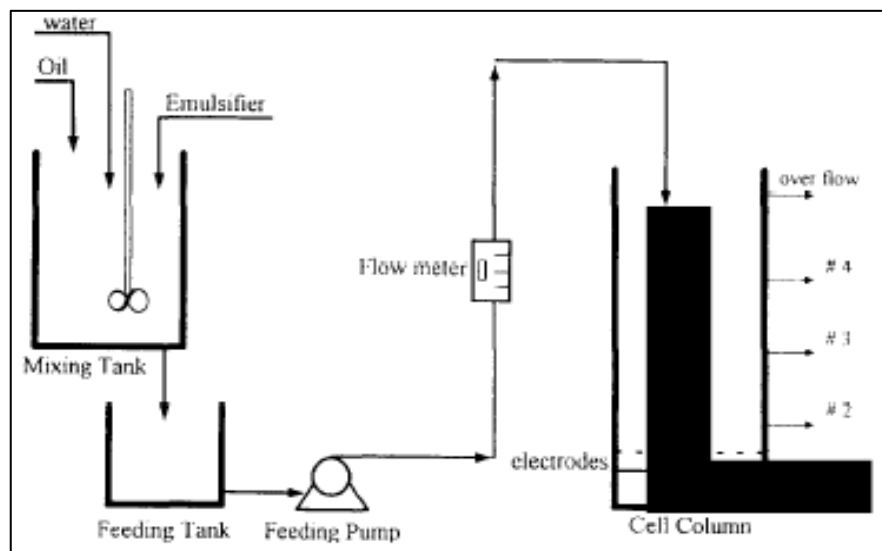
Figure 2.18: A schematic diagram of an Electroflotation unit. The system typically composes of an electrodes-anode and cathode in a flotation cell. Sub-100 μm bubbles are generated but at high-energy consumption. Source: Hosny, 1996.

Electroflotation has also been applied industrially for the removal of emulsified oil from water, as well as in the removal of pigments, ink and fibers from water (Rubio et al., 2002). Mansour et al., (2006) conducted experiments with an electroflotation cell and reported a purification level of 95% in the treatment of wasterwater from paper industry. In the treatment of tannery effluent, Murugananthan et al., (2004) demonstrated the effectiveness of an Electroflotation cell in removal of suspended solids, sulphides and COD. Electroflotation has also been effective in the removal of heavy metals - chromium from wastewater (Murugananthan et al., 2004) and in the treatment of restaurant wastewater. More importantly, the technology has been found to offer some level of disinfection and decontamination (Murugananthan et al., 2004) in the presence of chlorine ions. An investigation by Hernlem and Tsai (2000) showed that in the presence of certain levels of chlorine ions in solution, Electroflotation was effective in disinfecting water containing *Escherichia coli* by generating chlorine electrolytically. According to their report, sacrificial anodes of iron or aluminium can be used in wastewater treatment using this technology. This is because the alumunium or iron produces hydroxides which aid flocculation. On occasions, electrolytically generated hydrogen and oxygen bubbles may have detrimental effects on the surface properties of minerals, affecting their recovery from the liquid phase. Glembotskii et al., (1975) noted that sulphide minerals underwent physicochemical changes under electroflotation. Some advantages and disadvantages of this flotation technique are outlined in Table 2.5.

Table 2.5: Advantages and Disadvantages of the Electro-flotation Technique.

Advantages	Disadvantages
Production of uniform and finely dipersed gas bubbles. This increases the contact surface area between the oil drops and gas bubbles.	Low throughput. High electrode costs and maintenance. Voluminous sludge produced.
Possibility of selecting appropriate electrode surface and conditions in order to optimize separation.	High volume of produced sludge.
Production of clear effluent after separation i.e. high separation efficiency.	Production of hydrogen gas bubbles.

(Adapted from: Rubio et al., 2002; Mansour and Chalbi, 2006).

2.6.3   The Third Class: Low Pressure

While the first two groups of generating microbubbles are often related to high energy consumptions either by ultrasonic or air compression, the third method demonstrates the lowest energy utilization, provided it meets the application goal of bubble size distribution, bubble dispersion and gas phase holdup. The main techniques in this group include Induced Air Flotation (IAF) and Dispersed Air Flotation.

2.6.3.1 Induced Air Flotation (IAF)

This is a technique in which bubbles are formed by mechanical means through the combination of a high-speed mechanical agitator and an air injection system (Rubio et *al.*, 2002). According to Rubio et *al.*, (2002); Rodrigues and Rubio (2003) and Rodrigues and Rubio (2007), coarse bubbles (600 – 2000 µm) are produced by inducing air around the blades of a rotating impeller. Further, Zheng and Zhao (1993) reported that it uses the centrifugal force generated by a high-speed backspin impeller which produces gas, introduced into the separation column from the top of the liquid. In addition, the authors stated that the flotation separation process is completed by the thorough mixing of the gas and liquid after passing through a disperser located outside the impeller. The high-speed impeller acts as a pump which forces the fluid through disperser openings and creates a vacuum in the standpipe (see fig 2.19). This technique is mainly used in mineral processing industries as well as petrochemical industries for separation of oily sewage (Rubio et *al.*, 2002). Another area include waste water treatnent (Li and Tsuge, 2006).
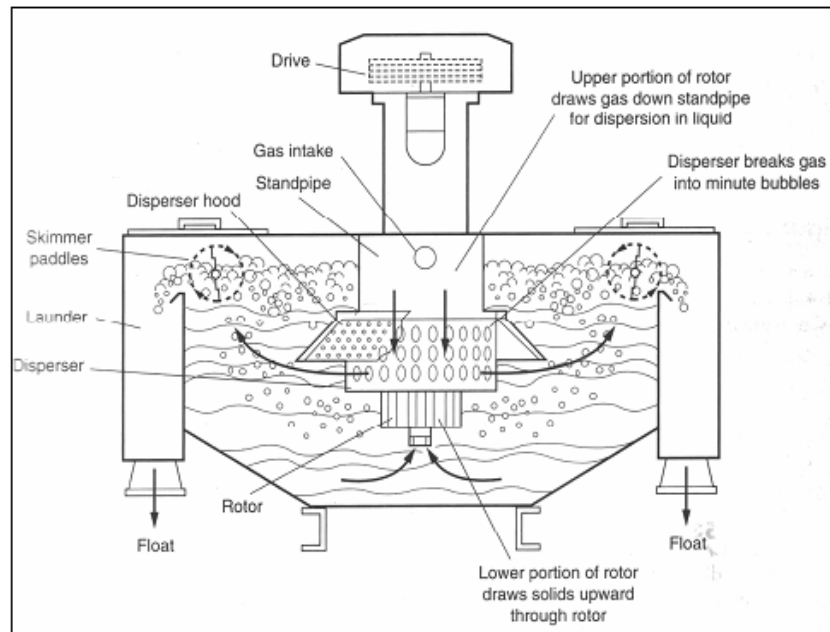
Figure 2.19: Induced –air flotation unit. Air is induced and dispersed into the liquid through the pumping action of the impellers. (Source: Chow, 2007)

2.6.3.2 Dispersed Air Flotation

Dispersed air flotation, basically involves the supply of continuous air stream directly into a porous material (usually a nozzle or a diffuser) from where bubbles are generated. By comparison with other microbubble generation methods, this technique is less energy consumptive. However, one main problem associated with this method is the difficulty in small bubble production (~500-3000 μm) produced as opposed to sub-100 μm) which therefore makes it ineffective in flotation separation. Though it may seem that microbubble production from porous surfaces only entails reduction in pore size of the surfaces, but even producing smaller apertures requires absolute care and precision. Reducing diffuser pore size is obviously expensive and demands more expertise compared to larger size production. Also, because more friction arises with fine apertures and through the passages leading to these apertures, more pressure drop is needed.

Logically, one would expect that by blowing small bubbles through a pore, reducing the pore size to the smallest size possible would result to the smallest bubble possible. Nevertheless, a number of reasons prevent this from holding true. For example, during bubble growth from a single pore, the liquid clings to the walls of the pore, serving as an anchor, which allows the wetting force to attach the growing bubble to

the surface of the pore. Until this anchoring force is disturbed, the growth of the bubble continues to a point when the force due to bubble buoyancy supersedes the anchoring hold on the bubble, before the bubble is released. This force nonetheless varies directly proportionate to the contact perimeter. In this method of bubble generation, the bubble eventually releases due to the force difference between the anchoring and buoyant force and unfortunately does so when the bubble size is several order of magnitude more than the size of its exit pore. Also important is the wetting properties of the solid surface. The more contact the bubble makes with the pore surface and material, the gas phase of the bubble, if pore material is hydrophobic, will form another anchoring force with the solid surface of its exit pore over a wider area, increasing the buoyant force and thus bubble size needed to surmount it. In the case of a hydrophilic surface, this additional anchoring force is non-existent.

Another reason for generating coarse bubbles from small pores is polydispersity of bubble sizes and irregularity of the spacing between bubbles giving rise to rapid bubble coalescence. So in the event of forming small bubbles, coalescence can quickly increase the size.

The third reason for generating coarse bubbles from small pores is channelling in a diffuser as illustrated in Figure 2.20. Exit is made easier by the largest bubble that initially forms from that pore, thereby creating a path of least resistance for subsequent bubbles, leading to bubbles growing larger than others in the same nozzle bank.
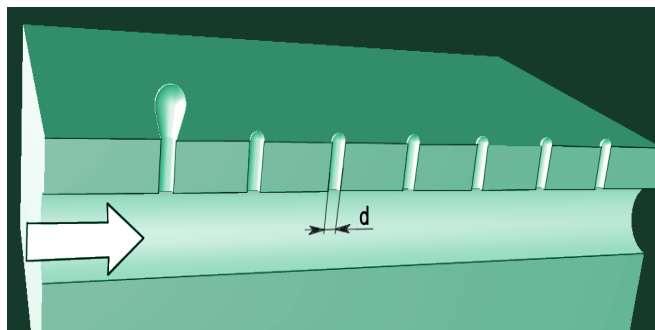
Figure 2.20: Parallel percolation on a nozzle bank system. Source: Zimmerman et al (2008).

2.6.3.3 Bubble Generation by Fluidic Oscillation (FO)

Traditional diffuser systems depend fruitlessly on size of pores, shear and material type for microbubble generation. Unfortunately, due to the cases described in the previous section, it is unlikely that generation of small bubbles can be achieved. However, oscillating the feed air stream by the use of fluidic amplifiers has the potential to pinch off bubbles at an early stage usually known as the hemispherical cap- Zimmerman et *al*., 2009 explain that it is the smallest shape of a forming bubble from a pore.

Engineering breakthroughs that offer robust generation of microbubbles through microfluidics strategies have been very useful. One such development is the fluidic oscillator for microbubble generation (Zimmerman et *al*., 2009; Zimmerman et *al*., 2011a; Tesar and Bandalusena, 2011). Controlling flows with bistable fluidic oscillators has been explored from around about four decades (Raman and Cain, 2002). Initially, oscillators were designed to distribute steady flows, switching from one exit to the other. With the synthetic jets, airflow is distributed intermittently according to the oscillatory frequency but the hybrid-synthetic jets differ from their synthetic counterparts as they utilize the jet pumped into the oscillator to generate suction back into the exit nozzle in an oscillation cycle (Tesar et *al*., 2005).

2.6.3.3.1   Features of the FO

The fluidic oscillator (Figure 2.21) is a bistable device featuring one inlet, two mid-ports and two exit ports and essentially controls a stream of input flow from the inlet, into the mid-ports before transferring it with a regular frequency into one of the two outlets ports per time. Typically, actuators are designed (see: Figure 2.22) in much the same fashion with the inclusion of an inlet, mid-ports and outlet.

2.6.3.3.2   Design and Inlet

The inlet ushers in the continuous air stream, which is then modulated by the pressure difference generated in the mid-port to alternate the flow in the exit nozzles. The region (cavity) around the mid-port is specially designed to allow for the periodic aerodynamic process to occur (Tesar et *al*. 2005). The outlets serve as an exit port for the produced oscillatory flow.

(a) (b)
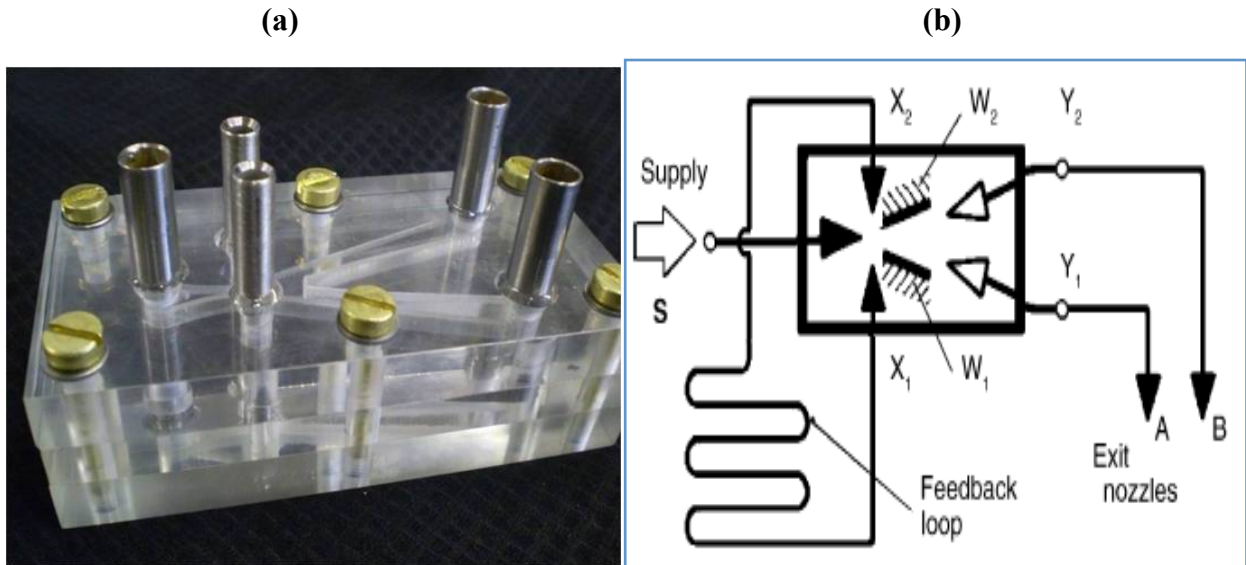
Figure 2.21: The Fluidic Oscillator. (a) Photograph of the assembled equipment as used in the experiment (b) Schematic representation of the fluidic oscillator. A feedback loop connects the two control ports X_1 and X_2 while the outlet ports Y_1 and Y_2 feed the nozzle bank A and B. The use of out-of-plane control loops as used in this experiment is advantageous if tuning the frequency is desirable to maximize the power gain.
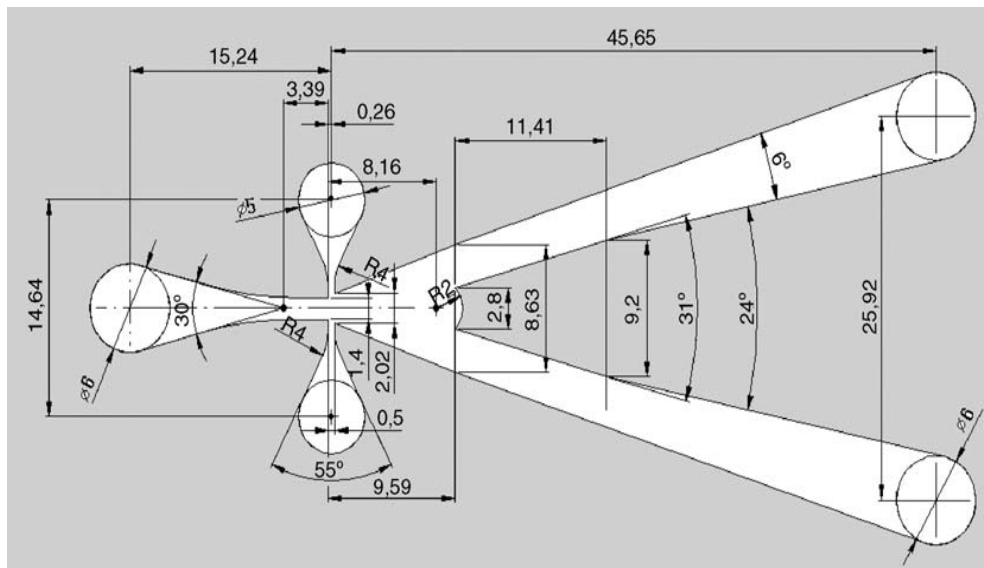
Figure 2.22: Internal geometry of the fluidic oscillator with dimensions. The area after the mid port is the cuspid region from where the two 'legs' –attachment walls extend. Source: Tesar et al., (2005).

2.6.3.3.3   The Feedback loop

The feedback loop is perhaps the most important feature of the fluidic oscillator and can be either external or internal. In either case, its control can be affected by altering the length of the tube (Fig. 2.24). For simplicity and ease of control, the negative (external) feedback loop is more frequently employed. The main driver of the

feedback loop mechanism is the pressure differential between the mid ports due to jet entrainment (Tesar et *al*. 2005). This pressure difference is caused by the Coanda effect, which tends to maintain the jet to one attachment wall (Fig 2.23). On the free attachment wall, however, the pressure is lower and thus prevents additional fluid flow into the entrainment area. Linking the midports with a feedback loop results in a fluid flow in the feedback loop from the high-pressure region to the low region. Gradually, this flow acquires significant momentum to switch most of the control flow into the other nozzle. Eventually, the jet is switched to the opposite attachment wall. Consequently, the pressure difference between the mid ports due to the jet entrainment becomes reduced, reversing the flow direction in the feedback loop. The development of a phase delay occurs when flow reversal (from one end of the mid port to the other) takes time due to fluid inertia. The jet remains for a short duration (often short time), generating an inversed pressure levels in the control ports. Ultimately, the reverse flow increases and attains a limit of 7% of the original supply jet, the jet is transferred back to its original port, setting up an oscillation cycle. Given the crucial influence of the duration of the flow cycle to delay in the loop, it is reasonable to modulate the oscillation frequency by adjusting the length of the feedback loop.
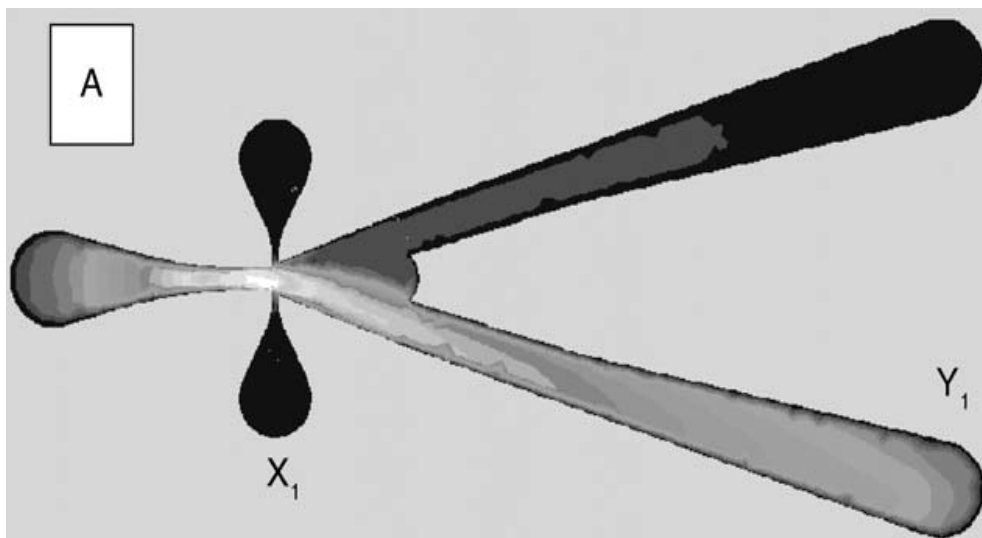
Figure 2.23: Velocity display of flow in a working fluidic oscillator without a control flow (feedback loop length). Lighter shade represents higher velocity region. The bulk flow remains attached to one of the attachment walls in the absence of a control flow. Source: (Tesar et *al*. 2005).
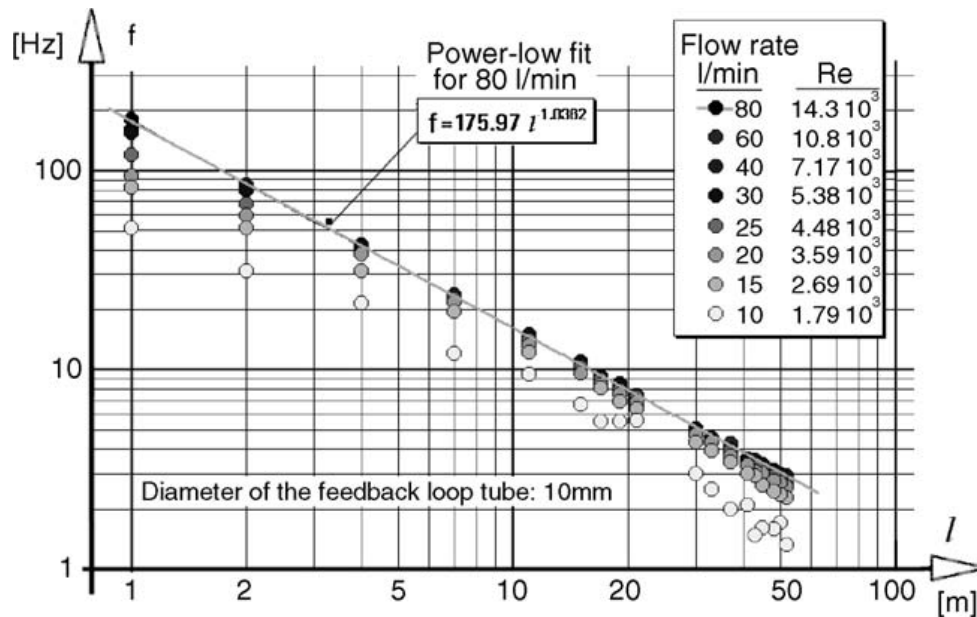
Figure 2.24: Graph of frequency of oscillation as a function of feedback loop length at varying supply flow rate with diameter 10mm. The frequency of oscillation varies inversely proportionate to the loop length. Source: (Tesar et *al*. 2005).

2.6.3.3 Microbubble Generation by Fluidic Oscillation

For microbubble generation with the fluidic oscillator, the basic requirements are: a fluidic oscillator, a microbubble diffuser and an air source. The device as explained in the previous sub-section, functions on the principle of Coanda effect, which tends to attach and maintain a jet to a wall. The control ports on the oscillator (mid-ports) serve to divert this jet from one attachment wall to the other at a regular frequency. By intermittently switching the flow between both attachment walls, the steady airflow is thus converted to oscillatory flow at a regular frequency. The device, when fitted to a diffuser facilitates bubble neck-off through the pulse generated during flow switching. Also, by switching and regulating the supply air flow bubble growth is controlled and limited to the hemispherical stage (stage at which bubble size is smallest), so that uniformly sized, mono-dispersed, cloud of microbubbles; approximately 10 times smaller than those of conventional methods (steady flow bubbling) for the same diffuser are produced with significant savings on energy consumption (Zimmerman et *al*., 2008). Currently, more work has begun to explore the feasibility of the fluidic oscillator driven microbubble generator in many fields concerned with mass, heat and momentum transfer. Examples include the application of ozone as a sterilization agent in the purification of water (Lozano-Parada et al., 2010), as well as rapid and efficient dissolution of CO_2 to promote algal growth for

biofuel production (Zimmerman et *al.*, 2011a, b, c), wastewater treatment and anaerobic digestion (Al-Mashhadani et *al.*, 2011).

Zimmerman et *al.* (2008) claims that the unique ability to switch flow from one of its two exit terminals before the development of boundary layer effect to overcome friction in pipes and conduit is the chief energy saving aspect of the device. Unlike dissolved air flotation, another advantage of the oscillator is its robustness. It has no moving part. It should be noted that the oscillator system can work with only an industrial blower at offset pressures only slightly more than the head of water, so does not require the capital cost of the saturator system and large pumps which cost easily an order of magnitude more. And so, for fine apertures, bubbles almost the size of their exit nozzles can be generated using the fluidic oscillator, consuming 2-3 orders of magnitude less energy density than dissolved air flotation (DAF) and traditional dispersed air flotation, with a similar level of capital cost reduction.

CHAPTER 3

MATERIALS AND METHODS

3.1   Introduction

This project aims to design and develop a fluidic oscillator-powered microbubble generating system that can achieve the production of microbubbles suitable for flotation of colloidal particles (sub-150 micron sized bubbles). The reason for this specific choice is due to the high separation efficiency reported in the literature. In this chapter, details of the materials used are presented and described as are the experimental procedures employed in assessing performance of the Microflotation system. Size is the most influential parameter in separation by flotation. Therefore knowledge of the size of both the colloidal particles to be separated and the size of bubbles for separation is essential. This chapter is divided into two main parts. The first presents the equipment and methods employed in characterising the bubble and particle size distribution as well as the particle zeta potential analyses. In the second part, the materials and methods used in separation and in assessing the performance of the Microflotation system for the different applications (oil, algae and yeast recovery) are described in detail.

3.2   Microbubble Generation

Essentially, generating bubbles by dispersed air techniques requires the use of a microporous diffuser. There are many types of diffusers but traditionally; their main features include: an inlet, plenum chamber and a porous membrane. Diffuser design requires special expertise and an understanding of fluidic dynamics in a confined chamber is essential. Both off-the-shelf (conventional diffusers) and purpose-built diffusers were tested and characterised under steady and oscillatory flow with respect to their effectiveness to generate bubbles suitable for flotation.

3.2.1   Conventional diffusers

The two most common and widely used conventional diffusers are elastic and ceramic diffusers. Elastic diffusers are made of porous elastic polymers and hence are clog-resistant. The disadvantage with elastic diffusers however is their relatively large pore

size (typically ~1 mm), making this diffuser type unsuitable for microbubble generation. Ceramic diffusers by converse are made with silica sand, epoxidic resin and are sintered, forming a matrix pore structure. The diffuser pore size is determined by the grade size of the ceramic media. Apart from the variety of pore sizes available, ceramic diffusers are cheap and efficient. Thus the first approach was to test the performance of the ceramic diffuser (Figure 3.1).

Figure 3.1: Photograph of an Off-the-shelf ceramic diffuser for bubble generation.

3.2.2   *Bespoke Diffusers*

Traditional diffusers are available pre-sealed. Owing to that, it was impractical to retrofit and investigate the performance of various membrane meshes for bubble production. Therefore, in course of this study, purpose built diffusers were made for microbubble generation. The first diffuser (OD 120 mm and ID 80 mm) presented in Figure 3.2 is a simple design essentially consisting of an inlet (ID 6 mm) and plenum chamber (depth 10 mm ID 80 mm) over which a microporous mesh is mounted. Figure 3.3 shows the various membrane materials fitted on the diffuser for use in bubble production. The second design is basically a modification of the first with the inclusion of different inlet channels (Figure 3.4a) through a perforated Perspex plate. Four inlet channels (3 mm ID respectively) were affixed to a circular Perspex-plate and the assembly mounted below the porous membrane (Figure 3.4b). The main

concept of this configuration was to improve the volumetric flow rate through the diffuser without compromising the target bubble size.

(a)

(b)
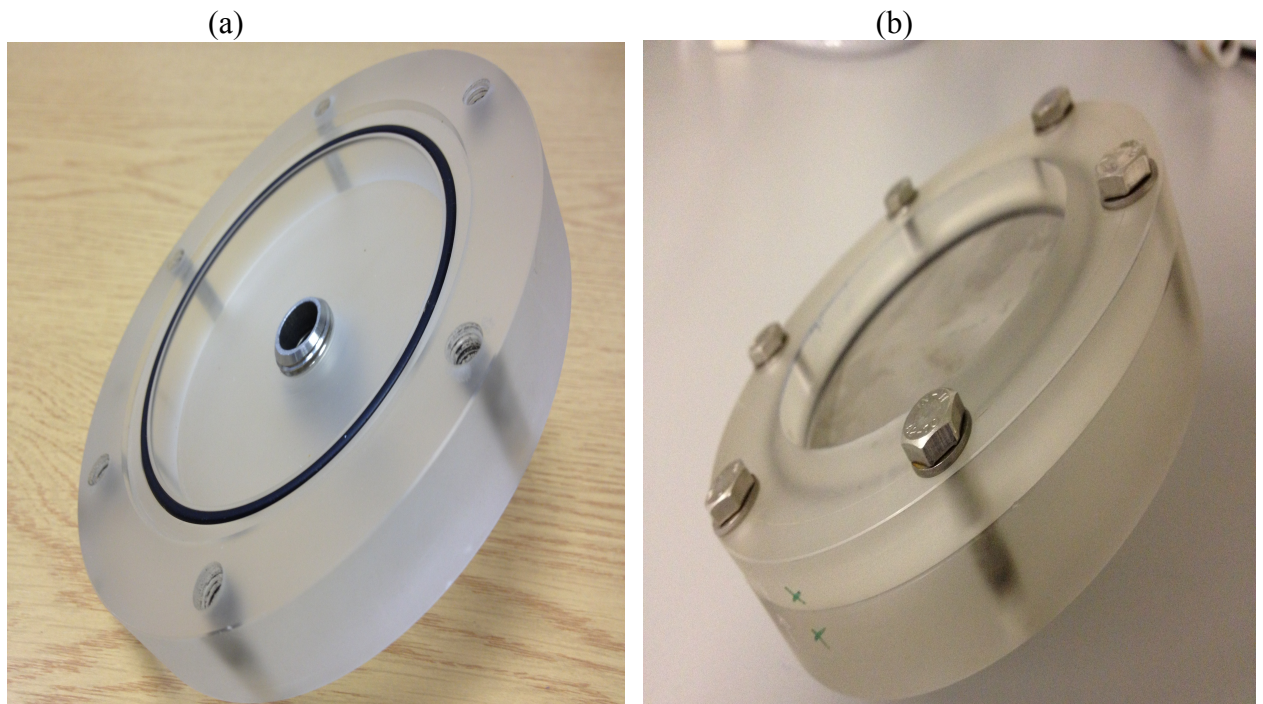
Figure 3.2: Photograph of the first purpose-built diffuser. (a) The plenum chamber. (b) The assembled diffuser showing the microporous membrane mounted over the plenum chamber.

(a)

(b)
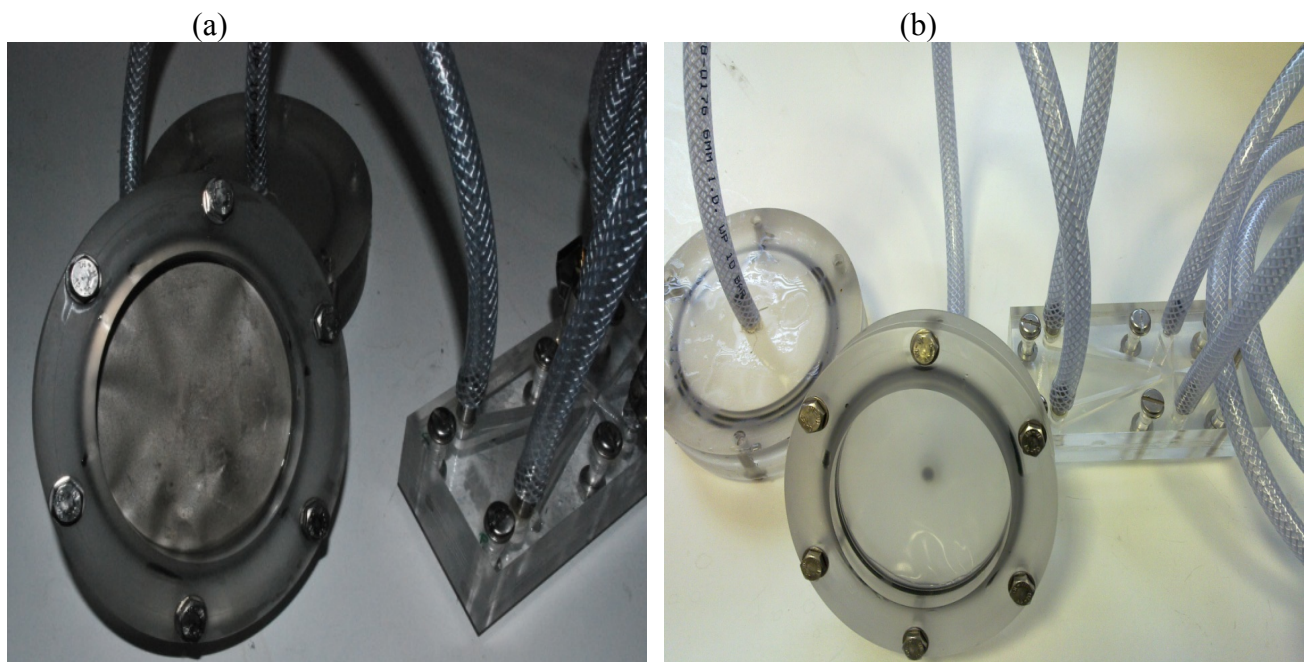
Figure 3.3: Image of the purpose-built diffuser equipped with the Fluidic oscillator for microbubble generation. (a) Diffuser fitted with a Stainless steel (SS) membrane diffuser. (b) Diffuser fitted with a Nylon membrane diffuser.

(a)   (b)
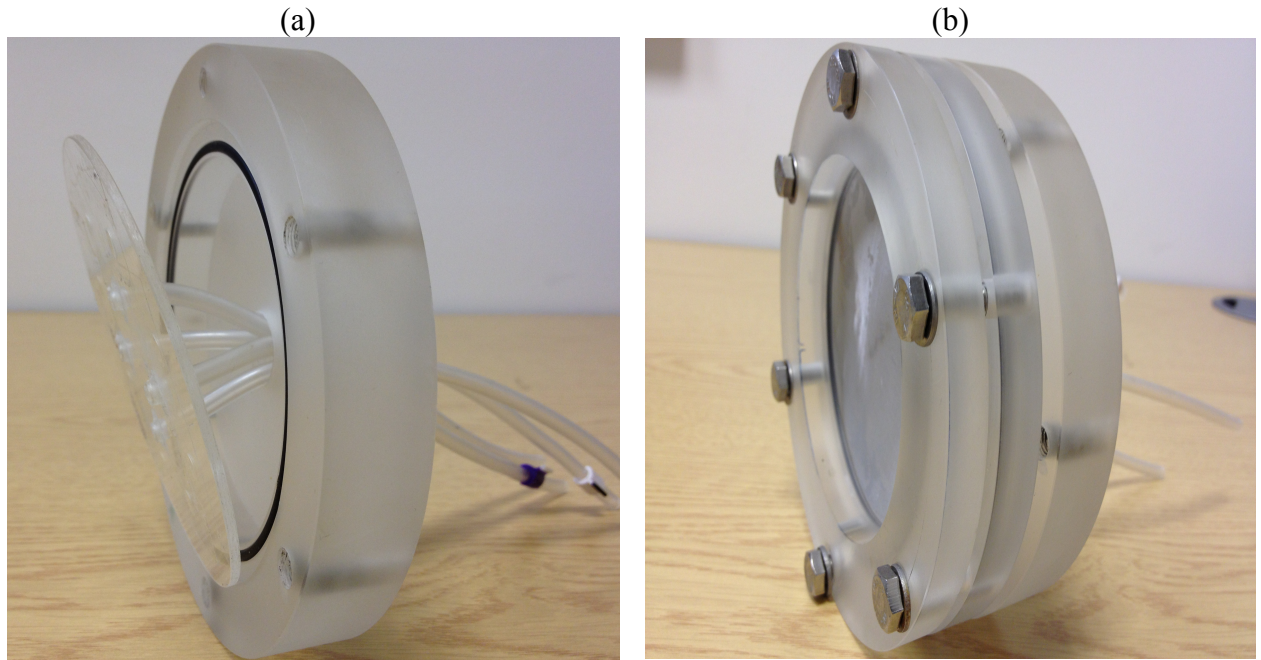
Figure 3.4: The photograph showing the modification made to the first. (a) The plate onto which orifices were drilled connected to an air supply and inserted over the plenum chamber. (b) The complete diffuser with the inclusion of the plate.

The third purpose-built diffuser (Fig 3.5 and Appendix I (a)) was also made with Perspex material to aid imaging and visual studies. The diffuser has an internal and external diameter of 23 mm and 40 mm respectively. It features an inlet a plenum chamber on to which a multiporous membrane is fitted and a clamping ring. The main difference between this diffuser design and conventional plate diffusers is the structure of the plenum chamber, which is configured to have in-built vanes for improved gas distribution. Four vanes measuring ~ 8 mm in length, ~3.5 mm in width and 4 mm in depth respectively are linked at the centre, extending horizontally away from the centre towards the rim of the diffuser. At the top of the vanes, three equidistant outlet ports each measuring 3 mm are drilled vertically from where the supply air exits and eventually passes through to the porous membrane. The distance from the top of the plenum chamber to the membrane is 5 mm. This circuitry design allows the supply air to divert regularly and largely evenly into the vanes. An 'O'-ring is affixed onto the outer rim of the plenum chamber to provide support for the membrane and also prevent air leakage. A clamping ring is mounted over the microporous membrane and the whole unit firmly secured by bolts.
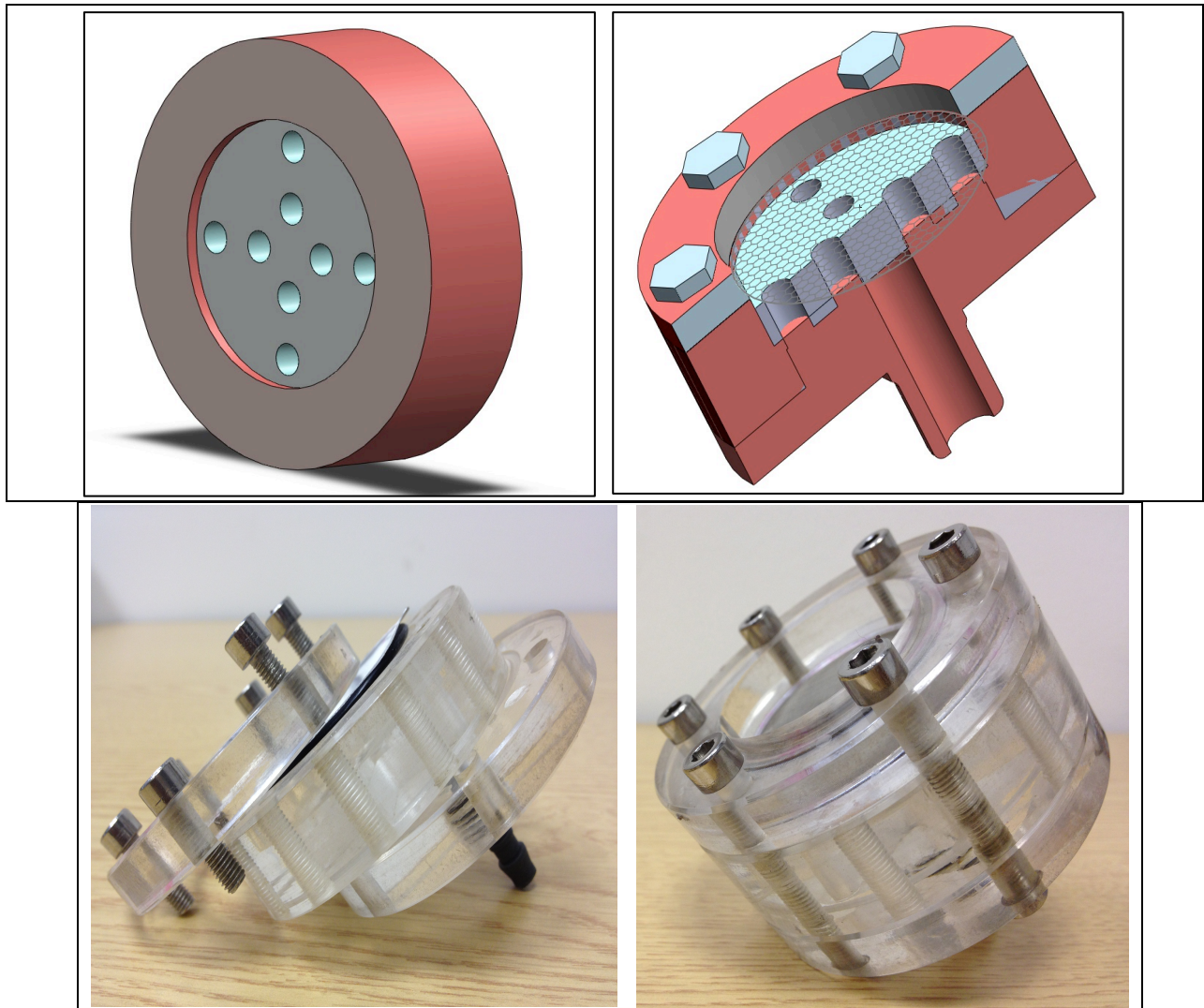
Figure 3.5: Photograph of the bespoke diffuser design with modified plenum chamber. Top Left: Model of the plenum chamber with vane distributors. Top Right: Artistic representation of the diffuser cross sectional view assembly showing the clamping ring, mesh, vane distributor and the inlet. Bottom Left: Picture of the dismantled units of the diffuser. Bottom Right: The diffuser in its fully assembled form.

3.2.3 *Steady and Oscillatory Flow*

To ascertain the efficiency of the fluidic oscillator in generating microbubbles, two experiments (control and main), were conducted for each mesh/diffuser tested (see Table 3.1). Microfiltered compressed air (~0.8 bars) and at room temperature (21 ^{o}C) was fed into the diffuser under steady flow bubble generation. By contrast under oscillatory flow, the diffuser was equipped with an oscillator and the air supply fed into the oscillator. The mode of operation of the fluidic oscillator has been described in the previous chapter (see section 2.6.3.3) as a fluidic amplifier that converts steady fluidic flow into an oscillatory flow. Thus, by passing a stream of continuous air

supply through the device, pulsating air is generated from its outlets, which then is fed to a microbubble diffuser for bubble generation.

Table 3.1: Summary of the operating parameters for microbubble generation.

Operating Parameters						
Membrane Type	Stainless Steel Mesh					
Membrane Pore size	25	38	50	75	100	125	
Air Flowrate (L/min)	61.5	62	62.5	63	63.5	64	64.5
Pressure	0.8 bar						
Feedback Loop Length (FBL)	0.5 m						
Operating Temperature	21°C						

3.2.4 Oscillation Frequency Measurement

Altering the feedback loop length, flow rate and diffuser pore size can modulate the size of the bubble generated under oscillatory flow. For bubble production with the oscillator, the frequency of oscillator was measured with an accelerometer (Figure 3.6). Accelerometers are electromechanical devices that measure vibration or acceleration forces. Frequency of oscillation reading was obtained by fitting the accelerometer 10 cm downstream either of the two outlet terminals of the fluidic oscillator before the bleed line. The accelerometer was connected to a Labview interface to display measurements. Readings were taking at varying operating flow rates and feedback loop length during the experiment to obtain a relationship between flowrate, feedback loop length and bubble size produced.
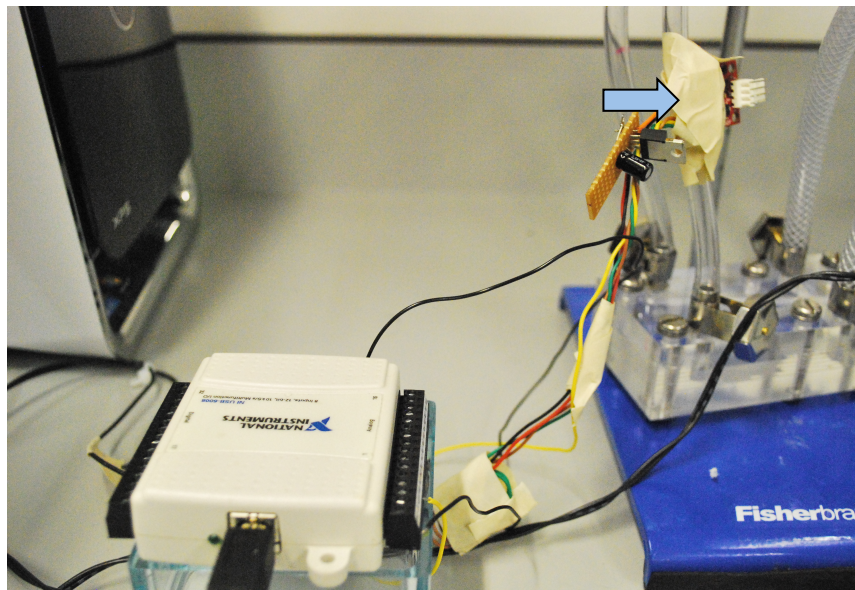
Figure 3.6: Photograph of the accelerometer for frequency of oscillation measurements. The accelerometer is firmly attached to the outlet port of the oscillator (see arrow direction) with its other interface connected to Labview program. By detecting the change in motion of air flow, the value of the oscillatory frequency is obtained.

3.2.5 Bubble size Analyses

In a multi-flow system such as a diffuser system, the mean bubble size is used to describe the system. There are three main methods for measuring the size of bubbles generated in a liquid, namely: optical acoustical and laser diffraction techniques. Bubble size characterisation using optical means is the most widely employed technique. Often times depending on the size and number of bubbles as well as the quality of optical device, the optical method can be both painstaking and time consuming to undertake and its accuracy is a function of factors such as light and medium clarity as well as the software for bubble analyses. These factors if not properly addressed can give rise to errors such as under-predicting or over-predicting the bubble diameter particularly in high bubble flux conditions and turbid media. The three methods employed in this study are described below.

3.2.5.1 Optical Method

The size distribution analysis of gas bubbles was carried out by high-speed photography. The experiment was conducted in clean water contained in a clear glass tank. The main rig components comprise: a water tank, microbubble generator (fluidic oscillator and diffuser) (Figure 3.7). The fluidic oscillator used measures: 10 cm x 5

cm x 5 cm in length, height and width respectively while the water tank (clear glass), where the bubbles were generated measures: 80 cm x 40 cm by 25 cm in length, width and height respectively. For bubble imaging, a high-speed camera system (Photron SA-3) was firmly mounted on a level plain to avoid any vibrations. Illumination was provided using halogen lamps (Model no: HM-682C; 150W Argos, UK). The light sources were positioned on either side of the camera. This technique allowed the bubbles to be well illuminated for proper imaging; otherwise, bubbles were sidelong illuminated with a strong reflection occurring, causing poor bubble contour highlight. A scale rule with clearly marked out dimensions was used to calibrate the area of view to determine the pixel value corresponding to the known calibration. For a representative sampling of bubbles from the diffuser surface, several images were captured at 2000 frames/sec. An image processing software, *Image J* was used in processing and analysing the images. Threshold intensity was set to determine the segmentation so that each pixel in an image is matched with the set threshold. Next the scale of reference was inputted as a known calibration after which the *'Analyse tool'* was employed to measure the area of the bubble. The effective bubble diameter was obtained by calculating the projected area of each bubble from images.
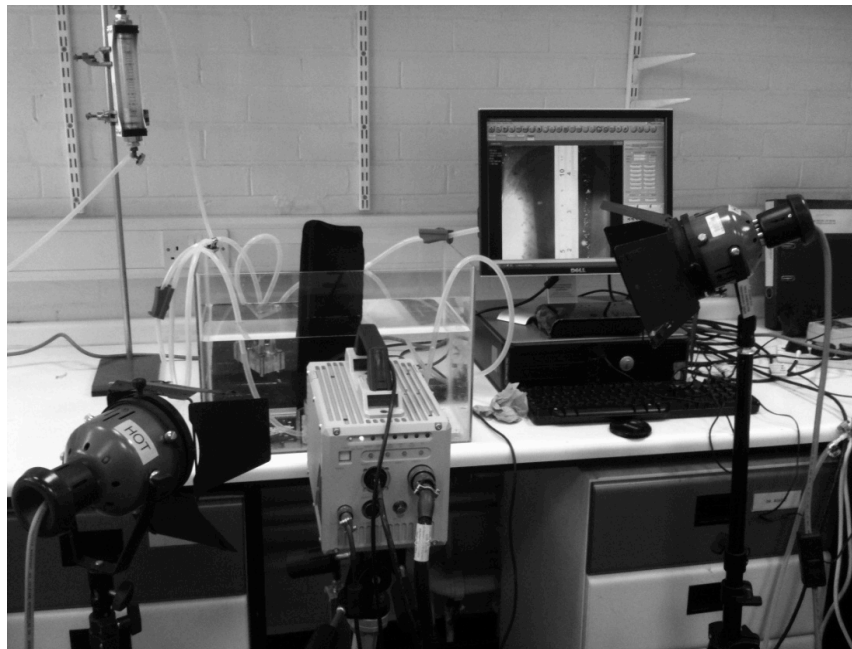
Figure 3.7: Experimental set-up of bubble characterisation during bubble generation. Centre: High speed camera with an optical microscopic zoom lens and two side lite lamps for illumination (Left and Right).

3.2.5.2 Acoustic Method

The acoustic bubble sizer (Dynaflow, Inc.) (Appendix II, Fig 2) was developed to meet the challenges associated with the optical method while being non-intrusive. By exploiting the ability of bubbles to affect acoustic propagated waves, the sound of frequency propagates through a liquid containing bubbles. The bubbles each having a natural frequency and a damping constant depending on their size are made to oscillate and radiate energy back into the liquid. This dispersed complex sound energy is related to the sound energy in the pure liquid medium (without bubbles) through an inverse method solution to obtain bubble size and population at varying frequencies (Wu and Chahine, 2010). The device consists of a pair of transducer hydrophones made of piezoelectric materials inserted in a polyurethane material to prevent contact with water. Both hydrophones are connected to a computer. The transmitting hydrophone generates short bursts of sound signals within a set frequency, which are then received after travelling through the liquid, by the second hydrophone. The signals are analysed by special in-built software for processing the phase velocity and attenuation within the desired frequency range to estimate the size distribution of bubbles. The flat transducer hydrophones (measuring: *7.5x 7.5 x 2.5cm)* were mounted vertically on either side of the flotation column. The signal frequency was set to 40 and three (3) runs were undertaken to determine bubble size distribution under oscillatory condition. The experimental set-up is shown in Figure 3.8.

3.2.5.3 Spraytec Method

Bubble characterisation was done with a Spraytec system (Malvern Instrument, UK), which employs the laser diffraction method to measure bubble sizes. A clear glass tank for bubble generation was placed in between both arms of the open bench Spraytec, so that the laser from the equipment passed through from the transmitter (containing the light source) to the receiver (containing a series of detectors). By introducing bubbles in the tank, the laser beam reaching the receiver is scattered and the receiver lens focuses the scattered beam onto a series of detectors that measure the intensity of the scattered light. The Spraytec software then processes the scattering data to calculate the size distribution of bubbles.
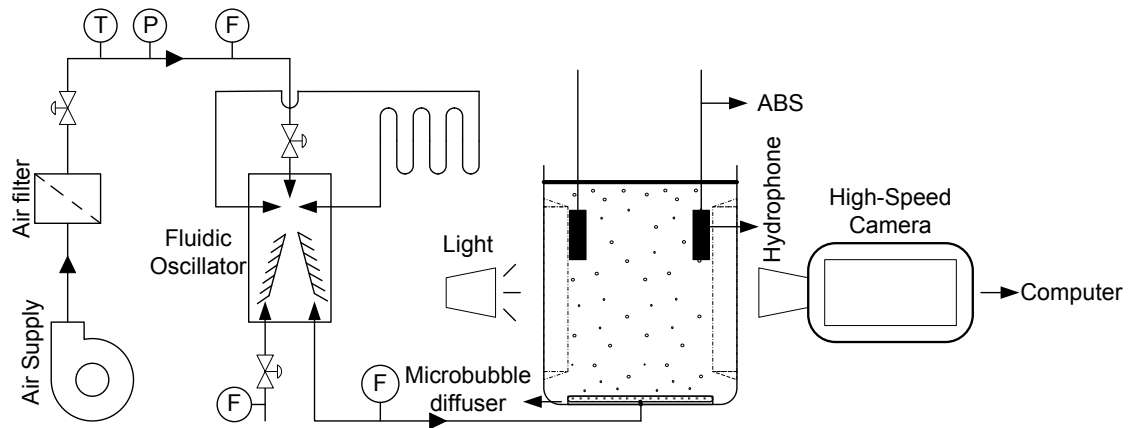
Figure 3.8: Schematic representation of the experimental set-up for bubble size measurement. Microfiltered compressed air (0.8 bars) is fed into the diffuser under steady flow condition otherwise under oscillatory condition into the oscillator, which then feeds the microporous diffuser with a portion of the air bleed-off or channeled otherwise to another set of diffuser. In this study, a portion of the air was bled off downstream of the fluidic oscillator. For measurement with the acoustic method, the hydrophones were inserted into the liquid, just outside the bubble stream. Otherwise, the high-speed camera is mounted with light sources positioned behind for proper illumination.

3.3   Oil/Particle Size Analysis

The particle size distribution was measured with the Mastersizer (Malvern Instrument, UK). The technique uses laser diffraction, which is based on the particles scattering light (laser beam) at an angle corresponding to their sizes. Small particles scatter light at high angles while the reverse is true for large particles. The diffracted light beam is measured using the Fraunhofer approximation as well as the Mie theory, which assumes particle shape to be spherical. Figure 3 (Appendix) presents a photograph of the equipment. Before size distribution measurement was carried out, the instrument was turned on and left for 30 minutes to allow the lasers to warm up. The laser strength was tested and ensured to be at least 70%. High laser strength is essential as it gives an indication of how well the system is aligned. After alignment, a suitable presentation - the standard wet (3OHD)- that accounts for the refractive index of the particles and assumes particle suspension in liquid medium was selected. The residual is an indication of the suitability of the chosen presentation. Typically, a residual of <1% is deemed a good fit. Calibration followed by running a standard sample of known size distribution through the system before the main size measurements. However, slight changes in the sample preparation varied depending on the sample to

be analysed. The methods observed for the three different applications investigated are described below.

3.3.1 Oil Emulsion Droplet

Prior to size distribution measurements of oil droplets the instrument was calibrated by running a standard sample of known size distribution. Measurements of oil droplets were carried out for various surfactant concentrations investigated. After sample preparation and system calibration, the presentation was chosen and then, samples were added to the dispersing unit until an obscurity of 15-20% was achieved. The stirrer was set to 2500 rpm for even dispersion of the droplet and to avoid droplet creaming. The unit was scrupulously cleaned between each run to avoid contamination. Oil emulsion sizes were measured at varying surfactant concentrations.

3.3.2 Algae Cell

Sample of the cultured cells (*D.salina*) were evenly dispersed by rapidly mixing for 30 seconds before measurements were carried out. The system was calibrated before samples were gradually added until an obscurity of 15-20% was reached. The stirrer was running at 2500 rpm. Size measurement was only done for cells before chemical pretreatment.

3.3.3 Yeast Cell

Cells were measured with and without the addition of a flocculating agent. Yeast cells (1g) were reconstituted in growth medium (YPD medium) and immediately dispersed by stirring for 1 minute. Under no coagulant conditions, cells were measured immediately after dispersion in growth medium. Otherwise, the flocculant (Chitosan) was added at varying concentrations and the mixture rapidly mixed (coagulation) for 1 minute. Next the sample was gently added to the Mastersizer until an obscurity of 15-20% was attained with the dispersion unit stirring at 1200 rpm. The stirring rate was chosen in order not to cause floc breakage but also to facilitate good dispersion around the measuring device. It is worthy to mention that samples were taken for measurement soon after rapid mixing to avoid floc settling.

3.4 Zeta potential Measurement

Dry yeast was reconstituted in 10 ml YPD medium and placed in an incubator at 30 ^{o}C and 3000 rpm to keep cells from settling. Following that, 3.7 g agar was made up in 250 ml YPD medium to a concentration of 1.5% w/v before pouring into plates and allowing to set. Then, 20 µl of the reconstituted yeast was cultured in the YPD agar medium for 24 hours. Zeta potential was measured with the zeta potential analyzer (Brookhaven ZetaPALS, UK) using the phase amplitude light-scattering method. Samples were centrifuged at 3000 x g for 5 minutes. After which cells were washed and re-suspended twice in 100 mM potassium chloride (KCl) before centrifugation at 3000 x g for 5 minutes. An electric field of ~2.5 V/cm was used during zeta potential measurements. Triplicate measurements of samples of cells were done for reproducibility.

3.5 Separation

In the next section, the separation methods undertaken for each application is described, starting with the study aim for each application, and then the material and experimental procedure. For all three separation experiments, the recovery efficiency (R) was determined using the formulae:

$$R = (\frac{C_i - C_f}{C_i})100 \qquad \text{Eq. (3.1)}$$

where C_i and C_f are the initial and final particle concentrations respectively.

A schematic representation of the bench scale Microflotation unit is shown in Figure 3.9. The main rig components comprise: a flotation cell, microbubble generator (fluidic oscillator and 40 mm stainless steel baffle distributor diffuser). The fluidic oscillator (Tesar et al. 2006, Tesař and Bandalusena, 2011) measures: 10 cm x 5 cm x 5 cm in length, height and width respectively while the flotation unit measures: 50 cm by 9 cm in height and diameter respectively. The tests were conducted with the diffuser placed at the bottom of the flotation unit.
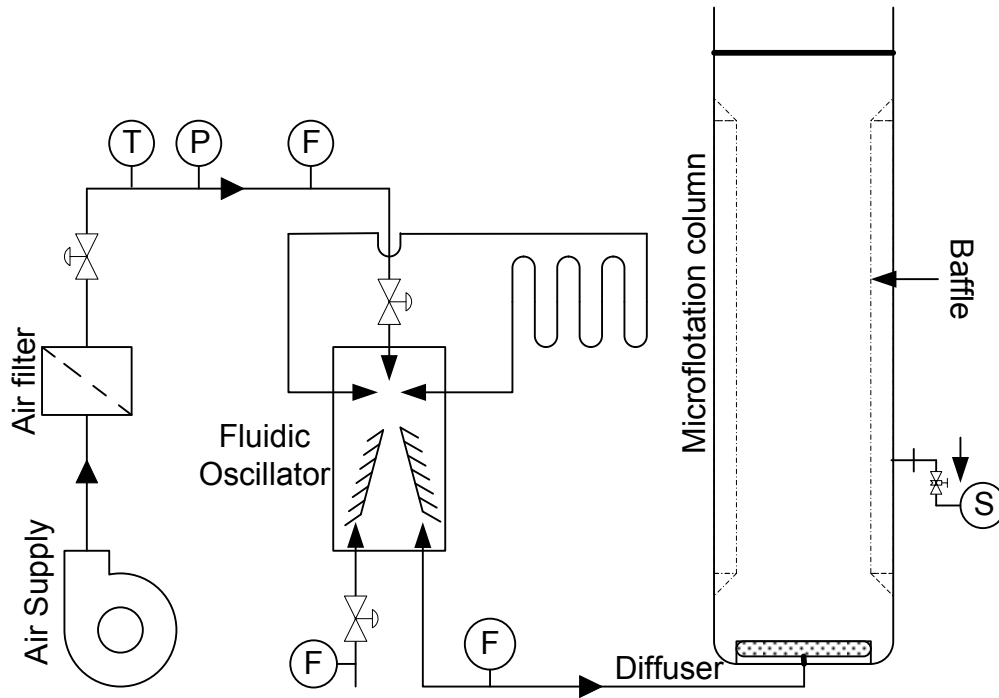
Figure 3.9: Schematic representation of the experimental rig for separation. Microfiltered compressed air (0.8 bars) is fed into the oscillator, which then feeds the microporous diffuser with a portion of the air bleed-off or channeled otherwise to another set of diffuser. Sample ports are fitted vertically along the flotation column at different positions.

3.5.1   Oil Separation

In the oil separation study, the main aim was to test the effectiveness of the fluidic oscillator generated microbubbles in the separation of emulsified oil droplets. The protocol involves the preparation of a typical oily wastewater and then applying microbubbles to separate the oil from water.

3.5.1.1 Material Preparation

Wastewater contains surfactants due to anthropogenic activities and when present, these surfactants stabilize oil in the wastewater, forming an emulsion. However, the degree and stability of the emulsion is a function of surfactant concentration. To replicate this, a test sample of raw water (o/w emulsion) composed of oil, water and an emulsion stabilizer was prepared by adding 10 ml of oil into 1 L of distilled water and surfactant at varying concentrations (0.3, 1, 3, 5 and 10) wt %. The surfactant used was Span 20; a non- ionic surfactant (Sigma Aldrich, UK) with a hydrophile-lipophile balance of 8.6 and density 1050 kg/m^3. The oil used was Vista Oil 100 (Pennine Lubricants, UK) solvent refined base oil with density 880 kg/m^3 at 20°C. All

the components were emulsified at 18000 rpm in a blender (Model no: XB9165; 500W, Argos, UK) for 5 minutes to form a stable emulsion. Table 3.2 presents a summary of the operating parameters.

3.5.1.2 Experimental Procedure

After formation of emulsions, coagulation with aluminium sulphate (Sigma Aldrich, UK) and flocculation were followed for 5 minutes and 7 minutes respectively. The pH value was adjusted to 8 to achieve the highest possible efficiency for aluminium sulphate as reported by Al-Shamrani et al. (2002). Figure 3.9 shows the schematic representation of the experimental set-up. After flocculation the microbubble generating unit was turned on before the prepared raw water was gradually introduced into the flotation column from the top to a level of 15 cm above diffuser. Samples were collected from sampling port located midway the Microflotation column every 10 minutes and oil concentration was measured using a turbidimeter 2100Q and a spectrophotometer DR 2800 (HACH Lange, UK) to assay absorbance at 682 nm wavelength.

Table 3.2: Summary of the operating parameters for oil/emulsion separation.

Parameters	
Surfactant type	Span 20 (Non ionic surfactant)
Surfactant Density	1050 kg/m^3
Surfactant Concentration	(0.3; 1; 3; 5; 10) wt.%
Oil Type	Vista Oil 100
Density	880 kg/m^3
Oil-water Ratio	0.01
pH	8
Coagulant Type	Aluminium Sulphate
Coagulant dosage	(100, 300, 500, 1000) mg/L
Operating Temperature	20°C

3.5.2 Algae Recovery

The Microflotation unit was employed for harvesting and dewatering algae from growth medium. Thus already grown algae was collected and used for this study. The main experimental process basically involved two main unit operations namely: chemical pretreatment of the sample and flotation.

3.5.2.1 Material Preparation

Given that the algae (*Dunaliella salina*) were already dispersed in the medium, a different process was required to calibrate the spectrophotometer for measurement of recovery efficiency. Five samples of the grown algae were taken at varying concentrations to assay chlorophyll content. Determination of the chlorophyll content of *D. salina* cells was done by taking 2 x 5 ml samples from each flask and centrifuging for 10 minutes. Sample supernatant was quickly discarded and sample re-suspended in 1 ml of distilled water before whirl-mixing. Next 4 ml of acetone was added and whirl-mixed again before samples were allowed to stand for 5 minutes away from direct sunlight. After 5 minutes, samples were centrifuged for a further 5 minutes at 3000 rpm until algal pellet was white. Finally, the green supernatant was transferred to a glass cuvette and optical density (OD) measured at 645 nm and 663 nm against an acetone blank. Estimation of chlorophyll content was achieved using equation 3.2 (Gilmour *et al*. 1982) to give μg chlorophyll ml^{-1}.

$$OD_{645} \times 202 = y$$
$$OD_{663} \times 80.2 = z$$
$$(\frac{y+z}{2})/5ml \qquad Eq. (3.2)$$

The result from the assay was then used in calibrating the spectrophotometer (DR 2800 (HACH Lange)) at both wavelengths by establishing a correlation between the algal chlorophyll content and absorbance at 645 nm and 663 nm.

Dunaliella salina 19/30 obtained from the Culture Centre of Algae and Protozoa (CCAP), Oban, Scotland was previously pre-cultured in a 250 L airlift Loop Bioreactor containing 248 L of Dunaliella salina growth medium (Zimmerman et al., 2011b) for 2 weeks. Following that, the microalgae from the laboratory scale 250 L airlift loop bioreactor was transferred to an outdoor 2200 liter ALB for field trials at Scunthorpe. The microalgae was grown with waste CO_2 from steel plant exhaust gas. After ~ 17 days, the cultured microalgae from the ALB was emptied into several drums and delivered back to the laboratory for harvesting.

3.5.2.2 Experimental Procedure

Two litres of microalgae sample at room temperature (21°C) was mixed to break lumps and disperse the cells homogenously in solution following sedimentation and clustering of cells as a result of prolonged storage. Coagulation and flocculation followed for 4 minutes and 10 minutes respectively following pH adjustment. Immediately after flocculating with a mechanical stirrer at 70 rpm, the broth was gradually introduced into the flotation column to a height of 30 cm above diffuser before the microbubble generator was turned on. Three inorganic metallic coagulants used were Aluminium Sulphate; Ferric III Chloride and Ferric Sulphate (Sigma Aldrich, UK), while hydrochloric acid and sodium hydroxide (Sigma Aldrich, UK) were used for pH adjustment. The test was conducted across five (5) pH ranges and five (5) coagulant concentrations (see Table 3.3 for experimental summary). Samples were collected every three (3) minutes and measured with the calibrated spectrophotometer to assay absorbance at 663 and 640 nm wavelength.

Table 3.3: Summary of the key operating parameters for Algae Recovery.

Parameters	
	Aluminium Sulphate
Coagulant Type	Ferric Sulphate
	Ferric Chloride
Coagulant concentration	(25; 50; 75; 100 and 150) mg/L
pH	(5; 6; 7; 8 and 9)
Sample Volume	1L
Operating Temperature	21°C

3.5.3   Yeast Harvest

The aim of the yeast harvest study was to investigate the performance of the Microflotation system on yeast recovery from growth medium. Therefore the main procedure basically entails: preparing a typical growth medium, reconstituting yeast cells in the growth medium and eventually recovering the cells from the growth medium using standard flotation separation procedure.

3.5.3.1 Material Preparation

Sterile Yeast Peptone Dextrose (YPD) medium was made using Yeast broth and Yeast extract (Sigma Aldrich, UK). 8.5 g of the Yeast broth and Yeast extract respectively were added to 1L-distilled water and mixed until dissolved. Meanwhile, Chitosan (Sigma Aldrich, UK) stock was made by dissolving 5 g of dry chitosan (Sigma Aldrich, UK) in 150 ml 0.5 M HCl (Sigma Aldrich, UK) which gives a viscosity of 0.9 Pa s.

3.5.3.2 Experimental Procedure

After pH adjustment of the growth medium, 1 g of dried yeast (Saccharomyces cereviseae, Lallemand, UK) was reconstituted into 1 L of growth medium and mixed for 1 minute to form a homogenous dispersion before chitosan was added. Rapid coagulation with a motorized stirrer at 3500 rpm followed for 1 min before the mixture was stirred for a further 1 minute under low speed at 75 rpm to promote floc growth. After flocculation, the microbubble generator was turned on and the mixture was gradually introduced into the flotation rig where cells were harvested for 20 minutes. Samples were collected every 2 minutes for optical density measurements. Biomass concentration correlates with optical density (OD) and was measured by spectrophotometer DR 2800 (Hach Lange, UK) to determine optical density at 660 nm. For each run, the microbubble diffuser was fitted with different membranes with pore size: 25, 50, 75, 100, 125 μm respectively. Also, the chitosan concentration and the pH of the growth medium was varied. Table 3.4 summarizes the key operating parameters for the experiment. All experiments were conducted under room temperature (21°C).

Table 3.4: Summary of the key operating parameters for Yeast harvest.

Parameters	
Flocculant Type	Chitosan
Flocculant concentration	(0.2; 0.4; 0.6; 0.8 and 1) % v/v
pH	(5; 7 and 9)
Diffuser Mesh (pore diameter in μm)	(25; 50; 75; 100; 125)
Sample Volume	1L
Operating Temperature	21°C

3.6 Moisture Content Estimation

Moisture content was analysed for separation with microbubbles and sedimentation. One gram of freshly harvested particles was weighed into a crucible and heated in an oven (Appendix II, Fig 5) at a temperature of 105 ^{o}C for one hour in order to completely eliminate the moisture content from the harvested samples. After one hour, the samples were removed and cooled to room temperature (21^oC) in a desiccator to avoid moisture reabsorption from the room. The cooled sample was weighed and result recorded. For the calculation of percentage of moisture in the harvested samples, equation (3.3) below was used.

$$\% \text{ Moisture} = \frac{\text{mass of water removed}}{\text{mass of original sample}} = \frac{M_2 - M_3}{M_2 - M_1} * 100 \% \qquad \text{Eq (3.3)}$$

Where: M_1= mass of the empty crucible; M_2= mass of the crucible plus sample before heating; M_3= mass of crucible plus dried sample.

3.7 SEM (Scanning Electron Microscope)

Specimens were fixed in 2-3% Glutaraldehyde in 0.1 M Sodium Phosphate for 3 hours at 4 ^{o}C and then washed in 0.1 M phosphate buffer, twice with 10 minutes intervals at 4 ^{o}C. Secondary fixation in 1-2% aqueous osmium tetroxide for 1 hour at room temperature followed. Next the samples were dehydrated through a graded series of ethanol (75, 95, 100) % for 15 minutes respectively before drying in 100% ethanol over anhydrous Copper Sulphate for 15 mins. Specimen were then placed in 50-50 mixture of 100% ethanol and 100% Hexamethyldisilazane for 30 minutes followed by a further 30 minutes in 100 % Hexamethyldisilazane before drying overnight. After drying, samples were mounted on a 12.5 mm diameter stubs, attached with Carbon sticky tabs, and coated with approximately 25 nm of Gold in an Edwards S150B sputter coater. Finally, samples were examined in a Philips/FEI XL-20 SEM (Appendix II, Fig 6) at an accelerating voltage of 20 KV.

Chapter 4

BUBBLE CHARACTERIZATION

4.1   Introduction

In this chapter, the performance of an off-the-shelf and bespoke diffuser is investigated and presented with the aim of selecting an efficient microbubble unit for application in Microflotation. Both devices were operated with and without the fluidic oscillator and suitability evaluated on the basis of the size distribution of bubbles generated. The methodology of this work is described in Chapter 3 as is the design of the bespoke diffusers. Other investigations carried out relates to the effect of gas flow rate on the size of bubbles as well as the effect of varying diffuser membrane pore size on bubble size distribution. In addition to that, the frequency of oscillation was presented for both diffuser types explored. Except otherwise stated, bubble characterization result presented here was done with the Spraytec and the feedback loop length 0.5m fitted to the fluidic oscillator.

4.2   Bubble Generation

Microbubble generation is an essential part of flotation separation. The size and number of bubbles are essential operating and control variables (Edzwald, 2010) and must be appropriate for effective bubble-particle contact. Thus, characterising the bubbles generated from a flotation unit is a necessary first step and was undertaken prior to separation of colloidal particles.

4.2.1   Conventional Diffuser Performance

The first attempt in developing an efficient microbubble generating technique for application in flotation was to investigate microbubble generation with available (off-the-shelf) diffusers and compare their performances with and without the fluidic oscillator. A 20 μm pore ceramic diffuser was used and the photograph of bubble generation is presented in Fig 4.1 while the size distribution result is shown in Fig 4.2. From the result, the mean bubble size estimated from the ceramic diffuser is 311 μm irrespective of the frequency of oscillation. Contrary to claims of the fluidic oscillator facilitating the generation of bubbles as small as the diffuser nozzle size, the mean bubble size is ~ 15 times larger than the diffuser exit pore. This may be due to the

thickness of the ceramic diffuser plate (10 mm) that attenuates the fluid oscillation. By dampening the fluid oscillation, the accompanying pulsation force is also decreased and as a consequence, bubble neck-off becomes difficult. Another plausible reason for the large mean bubble size is attributable to coalescence. Bubble-bubble agglomeration can occur in a tightly packed pore membrane arrangement such as is found in ceramic plates, making coalescence inevitable. So even in instances when the fluidic oscillation is effective, its benefit is quickly reduced due to coalescence.

Particle-bubble collection efficiency is a function of both particle and bubble size. For effective bubble-particle collection to occur the particle and bubble must be of the right size ratio relative to each other. Several authors (Gaudin et al. (1942); Gaudin (1957); Sutherland (1948); Yoon and Luttrell (1989)) have proved that the particle size must be equal to or preferably larger than the bubble size. Owing to the typical small size of colloidal particles (usually < 10 μm) however, it is often difficult even with chemical pretreatment to increase all particle size to the size of traditionally generated bubbles. Therefore, several investigators have concluded following series of experiments that bubble size range 20-100 μm is the most suitable for effective particle recovery, yielding recovery efficiency >99%. It therefore suggests that bubbles produced with ceramic materials are of size range unsuitable for application in colloidal particle separation.

Figure 4.1: Photograph of microbubble generation from a ceramic diffuser with 20 µm pore size. Average bubble size produced was ~300 µm, 15 times larger than the diffuser pore size.

Bubble Size Statistics (microns)	
Maximum	621.08
Minimum	163.51
Median	655.97
Harmean	133.50
STDEV	199.50
Average	311.87
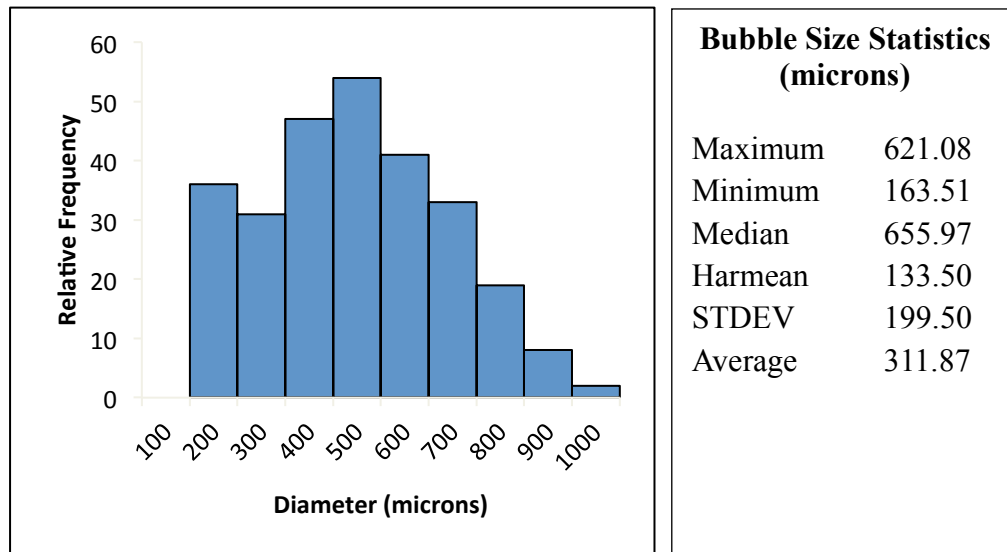
Figure 4.2: Bubble size distribution from a microporous ceramic diffuser with 20 µm pores. Air pressure was ~1 bar. The bubble sizes were analysed with a high-speed camera at 1000 fps and *1024 x 1024* resolution.

4.2.2 Diffuser Design and Fabrication

In light of the bubble size result obtained from the ceramic diffuser, attention was focused on designing and fabricating a more efficient diffuser for microbubble generation to achieve the target mean bubble. Basically, a typical diffuser consists of an inlet and a plenum chamber above which a membrane is mounted. The advantage

of this design type is the possibility for different membrane types to be easily installed and tested but also its simplicity. Figure 4.3 presents the photograph of a diffuser fitted with a 20 μm pore membrane.
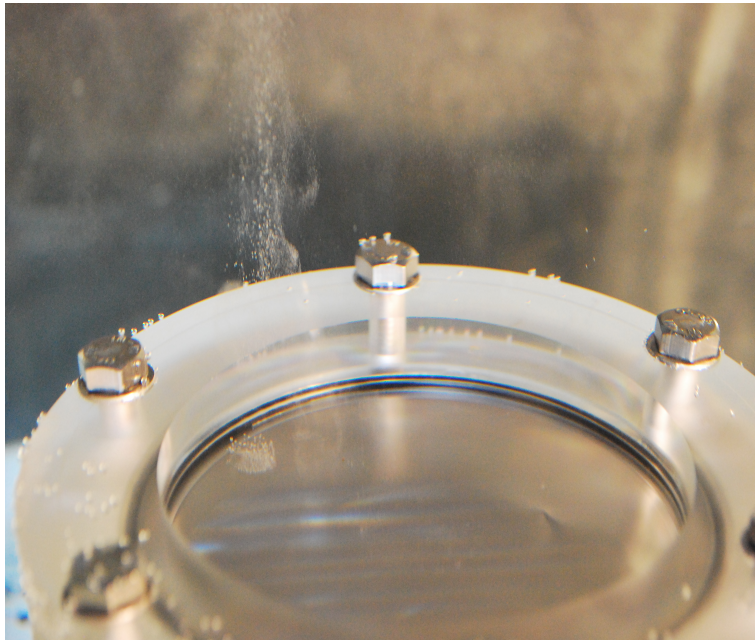
Figure 4.3: Photograph of microbubble generation under oscillatory flow. Microbubble generated emerge from only one side of the diffuser due to maldistribution (see arrow direction).

From Fig 4.3, it is obvious the diffuser was efficient in generating microbubbles (by visual studies), but the bubbles however were observed to exit from only a section of the diffuser during testing. In addition to that, the density and flux of bubbles was abysmally low irrespective of the membrane type used. This outcome is due to channelling in the nozzle bank (Zimmerman et al., 2008). The first set of bubbles that emerge from the pores make the exit pores less resistant for subsequent bubbles. As a result of the pressure differential experienced in the pores, the airflow dynamics can be significantly affected as well as the frequency of oscillation, leading to maldistribution of the supply gas within the diffuser plenum chamber. Further modification attempts with plenum chamber volume scale-down, proved unsuccessful due to liquid weeping.

4.2.3 *Distributor plate Diffuser*

In response to the technical challenges observed with the first diffuser design, an improved design was fabricated and tested. Given that the diffuser plenum chamber is the most important part of a typical chamber-based diffuser, considerable attention

was focused on re-designing the conventional plenum chamber. The bespoke diffuser plenum chamber was therefore modified to have distributor vanes instead of the 'bowl-shape' common with conventional plenum chamber. Primarily, the aim is to overcome maldistribution during bubble generation but also achieve significant gas-liquid contact within the diffuser plenum chamber. Thus, as gas is introduced, it spreads evenly across from the inlet through to the respective vanes on the plenum chamber. The design details however, are presented in the previous section (see section 3.2.2) whereas the result of the microbubble generation and size distribution are presented in the sections below.

4.3   Bubble Size Distribution

4.3.1   Effect of Generation methods

Photographs of bubbles generated under steady and oscillatory flow states from the stainless steel mesh diffuser are shown in Figure 4.4. Here, the bespoke diffuser was fitted with a 38 µm pore size membrane for bubble generation and the size distribution measured with an acoustic bubble sizer (ABS) (see section 3.2.5.2). Under steady airflow (Figure 4.5) bubbles produced are several fold larger than the exit aperture. Conversely, Figure 4.6 shows the mist of microbubbles produced from the same diffuser under oscillatory airflow.

(a)   (b)
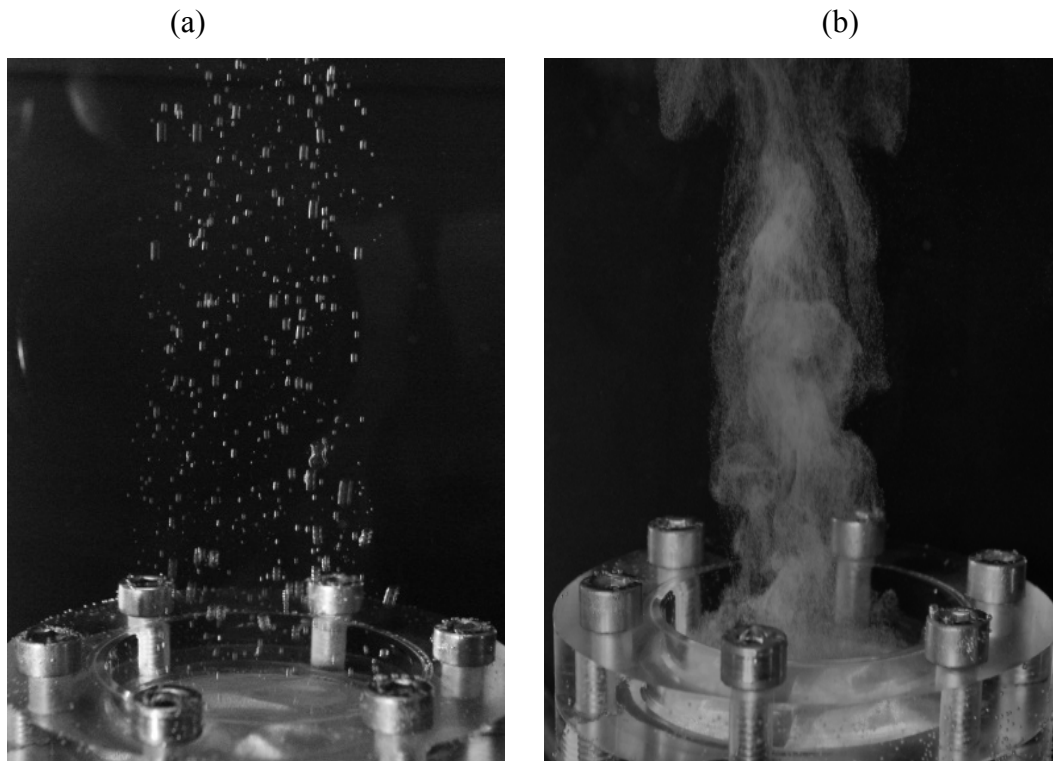
Figure 4.4: Images of bubbles generated from the same microporous diffuser under different conditions. (a) Bubbles generated under steady airflow. Bubbles are coalescent, non-uniform and several fold larger than the diffuser pore size. (b) Bubble generated under oscillatory flow. Formation of uniformly sized non-coalescent mist of microbubbles almost same size as diffuser pores.

Figure 4.5 and 4.6 presents the distribution of bubble size generated under steady and oscillated air supply conditions respectively. Under steady flow state (Fig. 4.5), two peaks are apparent which is evident of a wide range in bubble size distribution. The highest peaks reveal the dominance of bubbles equal to 650 μm and 1350 μm respectively. The smallest bubble produced however was 357 μm while the largest size measured was 1673 μm. Average bubble radius recorded was 1059 μm with 60% of the bubbles less than 1287 μm.
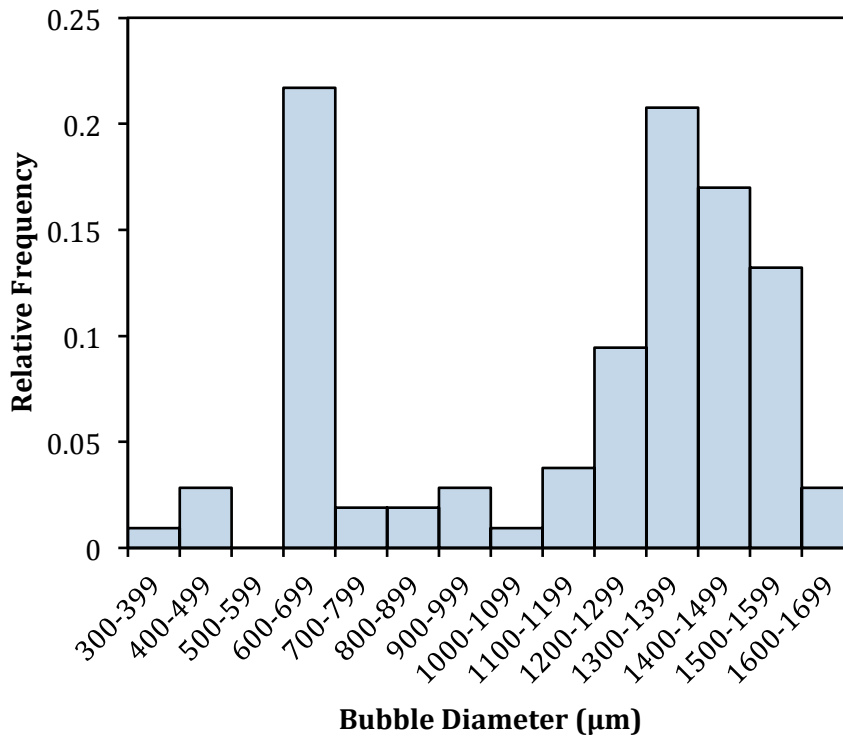
Figure 4.5: Bubble size distribution graph from the stainless steel mesh diffuser. Graph of bubble size distribution under steady air supply. The bubble sizes were analysed with a high-speed camera at 1000 fps and *1024 x 1024* resolution. Minimum and maximum sizes recorded were 181 μm and 1673 μm respectively with an average bubble size of 1059 μm.

From Fig. 4.6, the single peak graph shows a positive skew of bubble size distribution, which reveals the dominance of 24 μm-sized bubbles. The smallest bubble produced was 24 μm while the largest size measured was 260 μm. However, average bubble radius was 86 μm with 60% of the bubbles approximately 74 μm. While the difference between the average bubble size under steady and oscillatory air flow conditions is 967 μm, equally remarkable is that the average bubble size generated with the fluidic oscillator is approximately twice larger than the diffuser pore size (38 μm). By contrast, without the oscillator, the average bubble size achieved is several orders of magnitude (28 times) larger than the diffuser pore size.
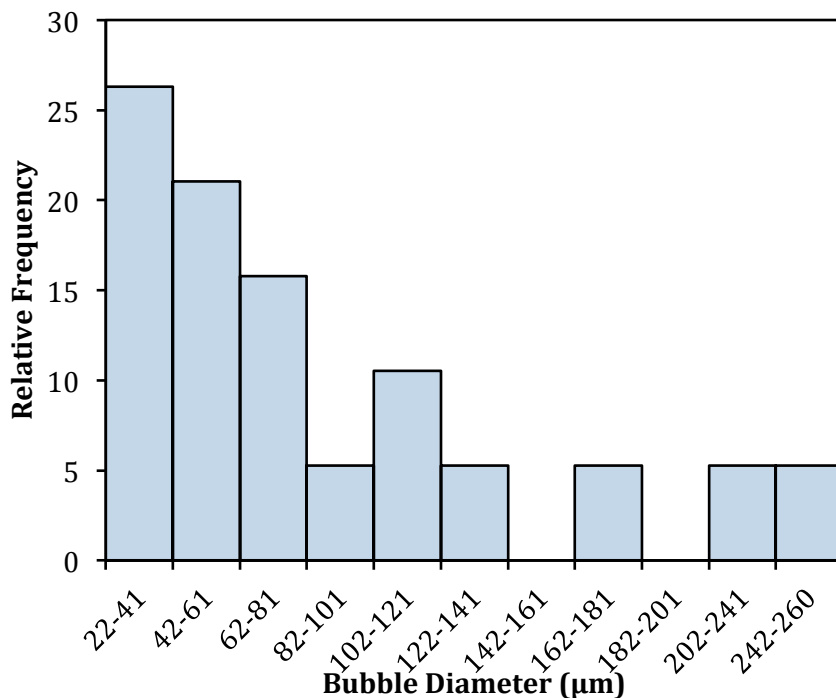
Figure 4.6: The bubble sizes were analysed with the acoustic bubble sizer. The graph shows distribution of bubbles produced under oscillatory flow from the 38 µm pore-sized stainless steel membrane diffuser at operating pressure of ~1bar. A portion of the air supply downstream the oscillator was bled-off to match diffuser capacity. Average bubble size measured with the ABS is 86 µm with maximum and minimum bubble sizes recorded to be ~24 and 260 µm respectively and standard deviation of 60 µm.

4.3.2   Bubble Density Analyses

Another perspective in bubble characterisation considered is the number of bubbles per unit volume for microbubbles generated under oscillatory flow. The bubble density graph presented in Figure 4.7 was determined by measuring the population of bubbles in the column and result showed that 20-40 µm sized bubble made up 95% of the total bubble density, while 5% comprised of bubbles greater than 40 µm in a bubble size distribution of 20-260 µm (see Figure 4.7 for distribution by size). The narrow range of bubbles size distribution not only strongly suggests the production of largely non-coalescent but more particularly, relatively uniformly sized microbubbles.
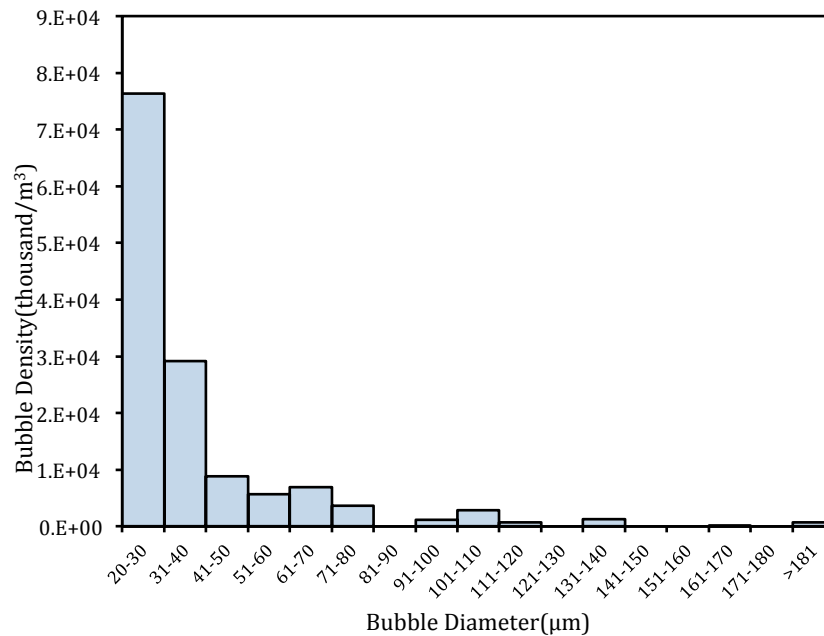
Figure 4.7: Bubble density from the stainless steel mesh diffuser showing the number of bubbles per unit volume. Microbubbles ranging from 24-40 µm in diameter dominate the flux measured by acoustic bubble spectrometer.

The difference in bubble size is simply attributable to the fluidic oscillator. The bistable device facilitates microbubble production by oscillating a stream of continuous air supply. The pulse generated due to the oscillation helps to knock-off bubbles at the developmental stage. In constrast, bubbles continue to grow under continuous flow until such a point when their buoyant force which varies directly proportionate with their size is strong enough to overcome the surface tension forces, before finally breaking off. Under this low pressure state, the force difference is the key to bubble detachment from source and usually, bubbles are several orders of magnitude larger than their exit pore. Likewise, owing to coalescence between neighbouring bubbles, bubbles grow at least an order of magnitude bigger than the exit pore under steady air flow condition. This tendency nevertheless, is reduced under oscillatory air flow regime. The inertia of the pulse arising due to fludic oscillation overcomes the wetting force (see Hanly et al., 2011) directly, and with much less dissipation. Without oscillation, bubbles tend to move irregularly, leading to increased bubble-bubble interaction and consequently production of large bubbles. Regular detachment leads to less coalescence as the bubbles are more uniformly spaced and sized. The level of inertial force in the pulse can be tuned so that bubbles

emerge with little excess kinetic energy over the terminal rise velocity (Parkinson et al. , 2008).

Another interesting behaviour observed with the distributor plate diffusers, which has a significant effect on the diffuser performance, is liquid weeping. The downward flow of liquid through diffuser pores after bubble detachment into the diffuser plenum chamber area is known as liquid weeping and it occurs as a result of the pressure differential in the diffuser plenum chamber and the liquid above the diffuser surface. Akagi et al., 1987 reported that a diffuser plenum chamber pressure fluctuation is characteristic of three basic cycles that make up the entire bubbling period namely, weeping, bridging and bubbling. Plenum chamber pressure level has to be higher than the capillary pressure of the membrane pores in order to initiate bubble formation (Yang et al., 2007). As the bubble grows, the pressure inside the diffuser plenum chamber drops. Immediately after bubble detachment from the pore, pressure drop in the diffuser plenum chamber reaches a minimum value. This pressure value can be substantially less than that at the liquid phase above the diffuser surface region and at this stage, liquid weeping occurs.

Weeping is a major hurdle in bubble production as it causes a change in the plenum chamber volume and as a consequence maldistribution. As in continuous flow weeping also occurs during bubble generation by fluidic oscillation due to flow switching. In principle, as liquid weeps in to the diffuser, it is efficiently and evenly distributed along the vanes within the chamber. By introducing oscillatory air through the diffuser inlet, the pulsating air comes in contact with the liquid and as a consequence, causes it to oscillate. Eventually, both oscillating fluids are pushed through the pores, from where the mixture exits as a fine mist of microbubbles (see Fig 4.4b). A similar concept can be observed in IAF where air is made to contact the liquid for bubble generation (Zheng and Zhao, 1993; Rubio et *al*., 2002; Yan and Jameson, 2004; Li and Tsuge, 2006) but the bubble generation by fluidic oscillation occurs just above the critical pressure drop necessary to produce bubbles.

4.3.3 *Effect of Gas Flowrate*

Figure 4.8 presents the relationship between flowrate and pressure, oscillation frequency and feedback loop length. The plot (Fig 4.5 (a) shows the positive correlation between gas flowrate and pressure. In figure 4.5 (b), the oscillation frequency is observed to decrease with increase in feedback back loop length until a transition regime is reached before a further increase in feedback loop length results in a slight increase in oscillation frequency. A similar behaviour is seen in Fig 4.5 (c), where oscillation frequency is observed to decrease with increase in flowrate before a gradual rise is recorded with further increase in gas flowrate.

(a)   (b)   (c)
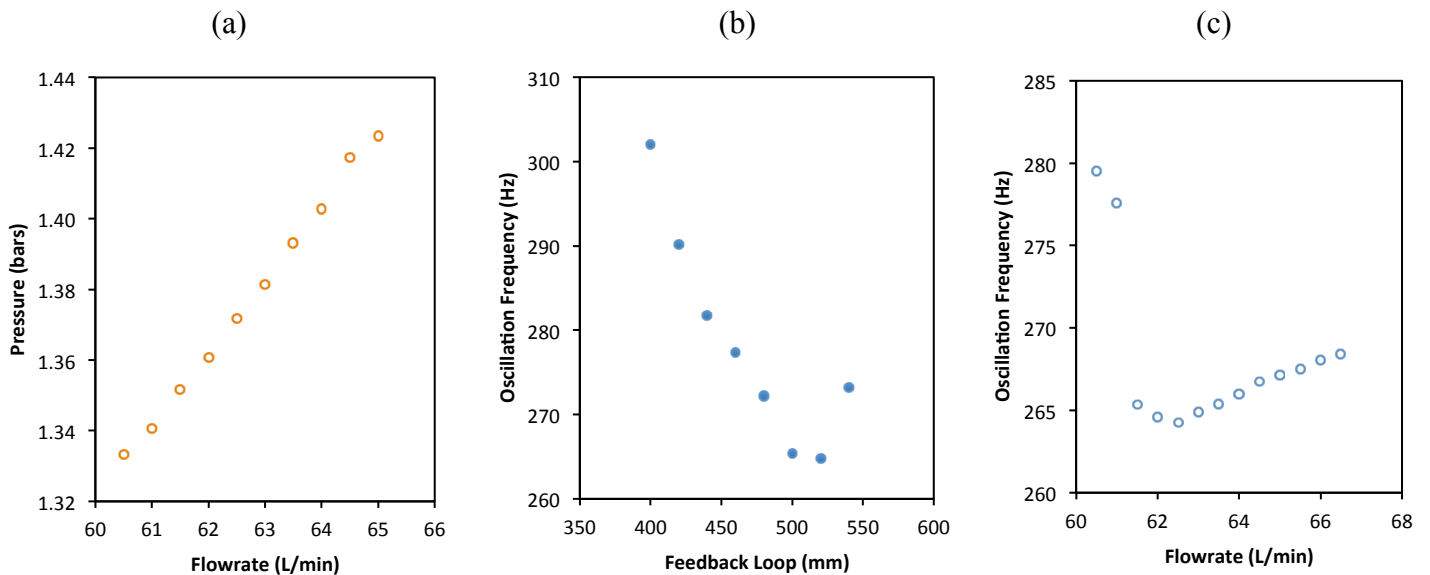
Figure 4.8: Plot of pressure with flowrate. (b) Graph of oscillation frequency as a function of feedback loop length.

In Figure 4.6, a plot of mean bubble size for bubbles generated under oscillatory flow and at varying superficial gas flow rates is presented. Initially, mean bubble size increased directly proportionate with flowrate but more remarkable is the drop in oscillation frequency observed with increase in gas flowrate (as soon as bubble generation begins). At this stage, the gas flowrate is the primary factor influencing the mean bubble size. Eventually, with further increase in flow rate a gradual decrease is observed before the mean bubble size dipped to its lowest size. Conversely, an increase in oscillation frequency is noted, leading to its intersection with the mean bubble size. This intersection between mean bubble size and oscillation frequency is

the optimum operating condition for the production of smallest mean bubble size. At this stage, despite the increase in gas flowrate, the oscillation frequency appears to be the more influential factor affecting bubble size. Finally, with further increase in gas flowrate, mean bubble size begins to increase again. The bubble growth dependence switches back to supply flowrate. Consequently other factors such as coalescence and wetting force become more dominant.
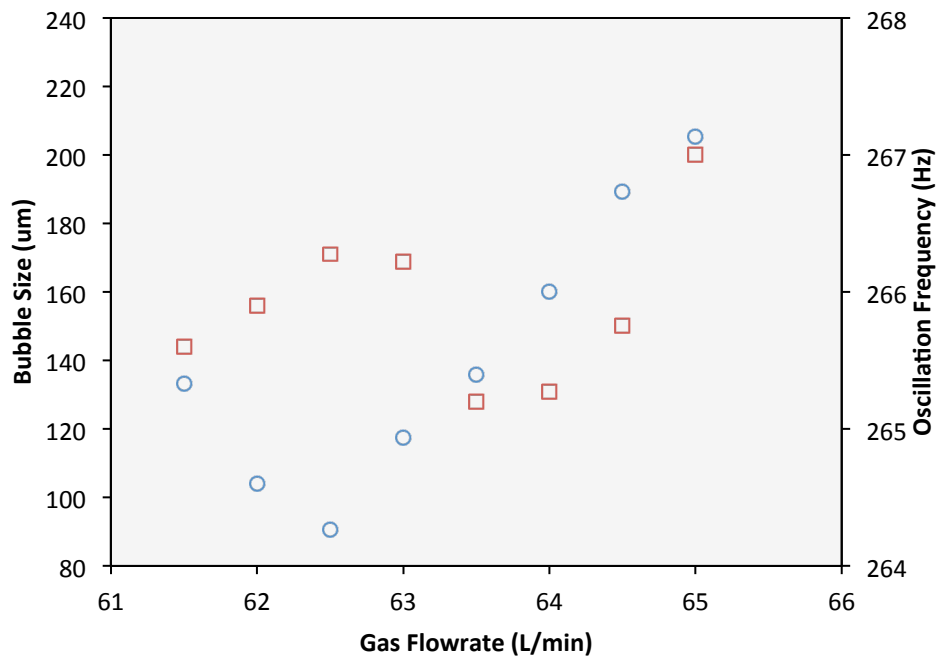
Figure 4.9: Plot of bubble size distribution and Oscillation frequency against flowrate. Average cumulative size distributions calculated for each flowrate bubble generation with a 50- μm pore size stainless steel mesh.

The increase in bubble size as gas flowrate increases can be explained by the growth mechanism of bubbles from their exit orifices (but also, by the frequency of oscillation). Several authors (Akagi et al., 1987; Miyahara and Hayashino, 1995; Yang et al., 2007) have reported bubble production under steady flow state using membrane diffusers. Typically, bubble production generally relies on bubble buoyancy, which implies that in order to attain the buoyant force sufficient to overcome the binding wetting force, bubbles tend to grow substantially larger than their exit pores before detachment (usually 1-5 mm). For single pores, bubbles ascend individually after formation without coalescing. Thus gas flowrate is only the primary cause of growth. However, for multi-porous membranes, a more complex behaviour results. Apart from gas supply, bubble growth occurs as bubbles coalesce with

neighbouring or preceding bubbles during formation leading to increase in their effective sizes. This observation is supported by the findings of Miyahara and Hayashino (1995). Bubbles formed from diffuser plates experience coalescence just after or as formation occurs depending on the pitch size, giving rise to a log-normal probability distribution of the bubble sizes. By oscillating the gas however, relatively uniformly spaced, largely non-coalescent bubbles, ~ 2-3 times greater than their exit pores are produced compared to bubble generation under continuous flow state (Zimmerman et *al*., 2008; Zimmerman et *al*., 2011a). Bubble production is achieved as soon as bubbles grow beyond the hemispherical stage. Zimmerman et *al*., (2008) report that this is the smallest stage for which bubble production from a pore can occur.

Table 4.1: Properties of the stainless steel wire mesh. Source: Plastok, UK.

Pore Size (μm)	Porosity (%)	Pitch (μm)	Pores/inch
25	25	25	500
38	38	25	400
50	34	36	300
75	45.7	36	230
100	44.5	50	165
125	34	90	120

4.3.4 Effect of Membrane Pore Size

The effect of diffuser membrane pore size on bubble size was also investigated and result presented in Figure 4.10 and 4.11. The main factor responsible for the increase in mean bubble size as membrane pore size increases is obviously the membrane pore size. Bubble growth varies directly proportionate to the size of their exit pores. Also influential is the membrane pitch, which is the distance between two adjacent pores. The size of the pitch plays a significant role in bubble-bubble interaction during growth. With an increase in the pore to pitch ratio, the probability of the neighbouring bubbles coalescing increases similarly. From Table 4.1, this ratio decreases with increase in membrane pore size. This further explains the increase in the mean bubble size and the variation in bubble size distribution from 25 to 125 μm pore membrane. Another factor that favours coalescence and as such influences bubble growth is the available free space. Diffuser membrane porosity can induce bubble coalescence.

Under conditions of high porosity, increased bubble flux is achieved and so is the interaction between bubbles.
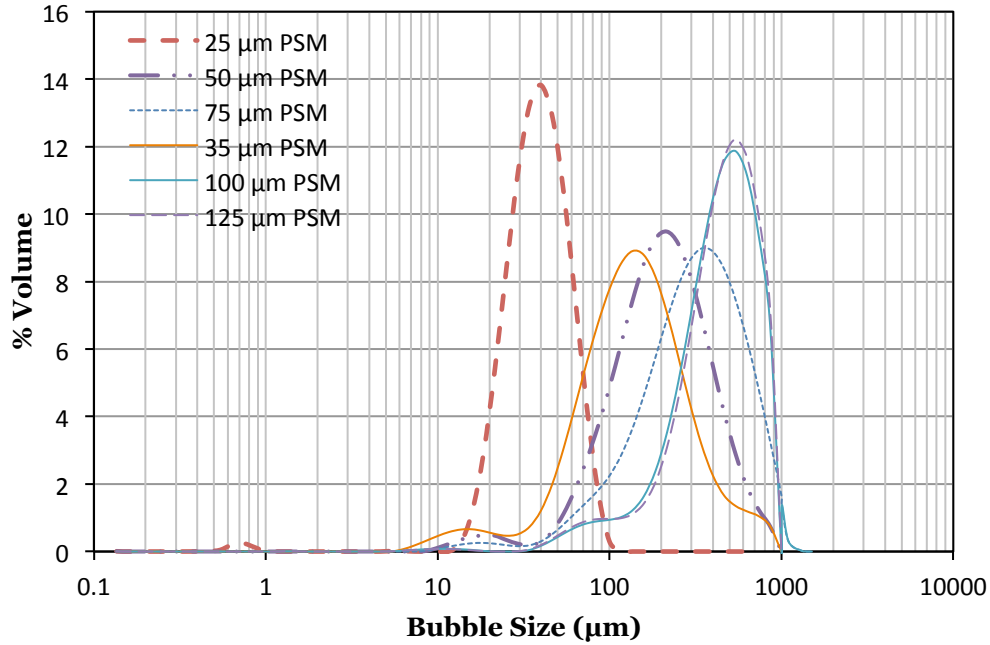
Figure 4.10: Graph of bubble size distribution showing the changes in bubble size for varying membranes pore size.
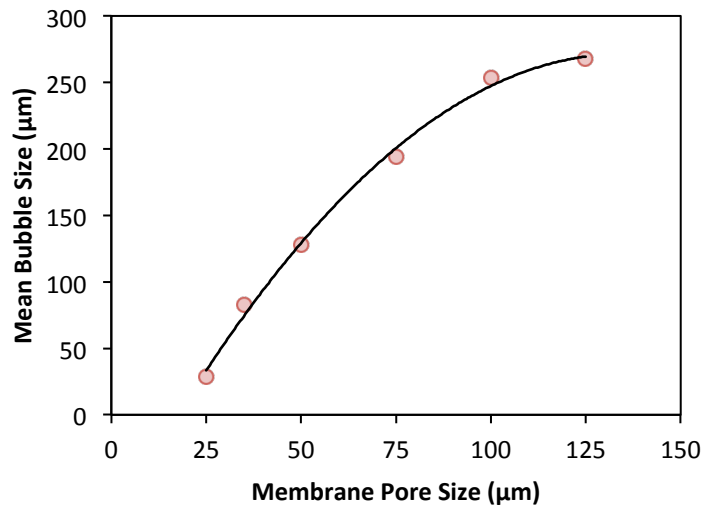
Figure 4.11: Combined plot of mean bubble size distribution at varying diffuser membrane pore size. Bubble mean size is a function of gas flow rate as well as the diffuser membrane pore size.

4.4   Bubble Development

In figure 4.12, a processed image of a cross-section of microbubbles is presented for the varying membrane pore sizes investigated. The photograph provides an insight to the porosity, bubble density as well as the varying nature of the bubble sizes produced from the respective membranes.

| (a) | (b) | (c) | (d) | (e) |
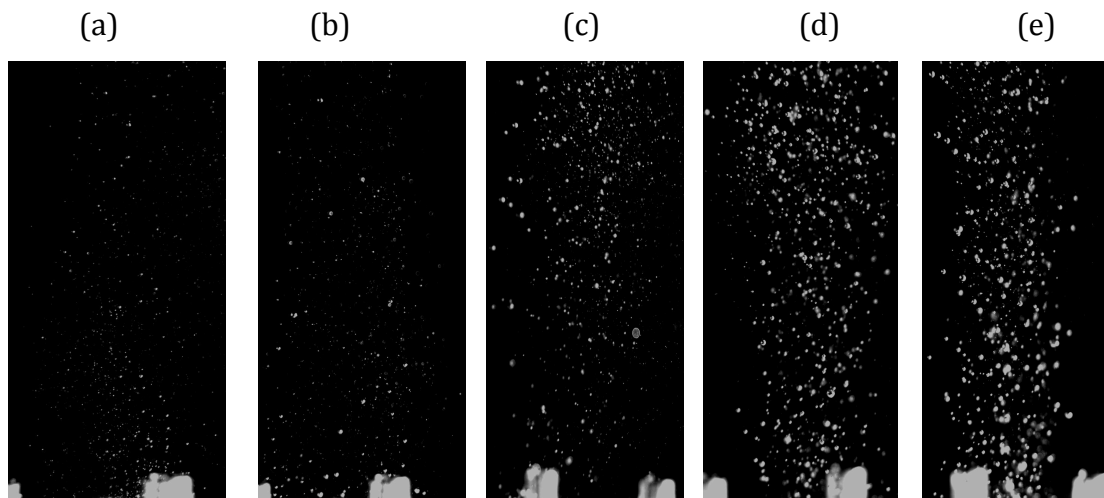
Figure 4.12: Cross sectional image of bubble flux processed using the Gamma tool in Image J. The images are obtained from the different membranes used: (a) 25 µm (b) 50 µm (c) 75 µm (d) 100 µm (e) 125 µm pore membrane. Pressure drop across channels decreases and thus increase in bubble flux is obtained as membrane pore size increases.

The variable nature of the bubble plume observed (under oscillation) at high membrane pore size is confirmed by examining the changes in the measured bubble size as a function of time during bubble generation. This is shown in Figure 4.13 for the generation of microbubble from stainless steel diffuser with two different membrane pore sizes (35 and 50 microns), at an oscillation frequency of ~265 Hz. As can be seen, significant changes in the measured Dv90 are observed over time, representing significant fluctuations in the coarse bubble fraction. This suggests that bubble coalescence is relatively less controlled under this condition and at increased membrane pore size. With a smaller membrane pore (Fig 4.10 a), the variation in the Dv90 is considerably less, representing a relatively uniform bubble plume.

(a)   (b)
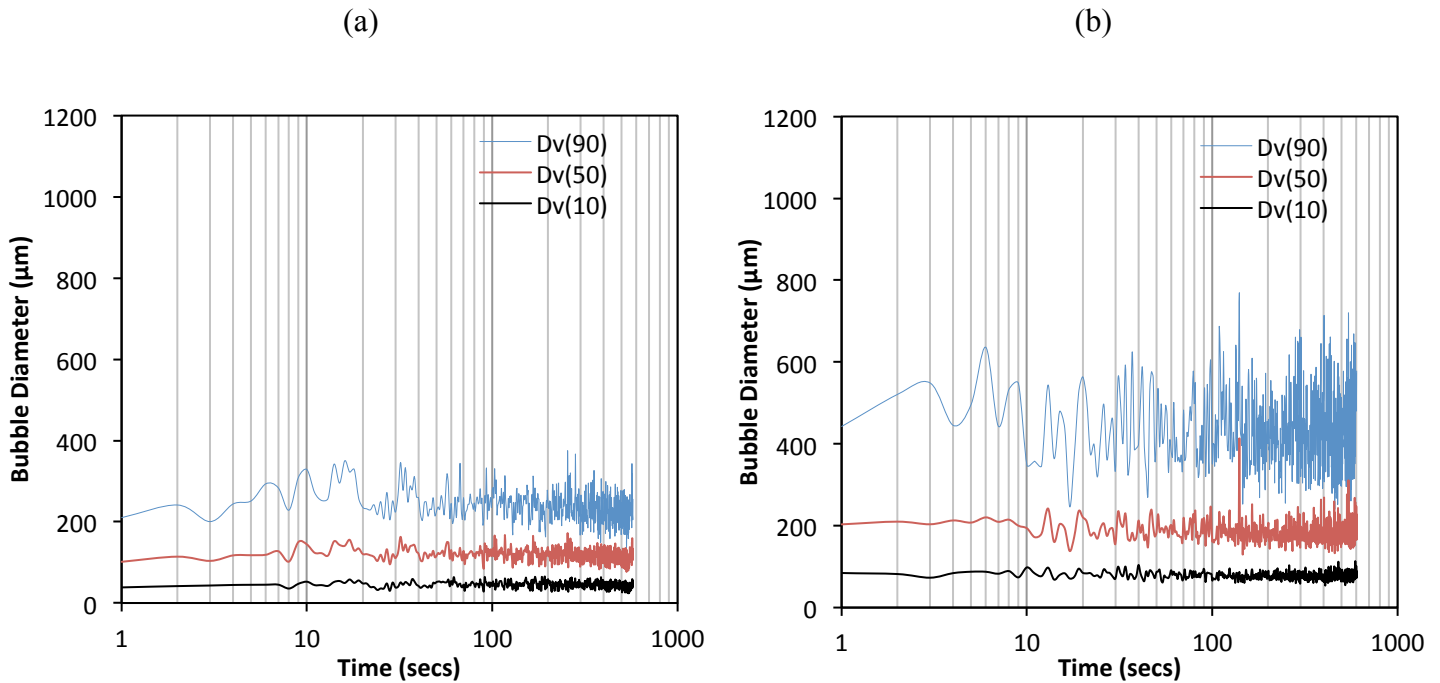
Figure 4.13: Size history showing the changes in bubble size during generation by oscillation over time. (a) 35-μm pore size membrane. (b) 50-μm pore size membrane.

Although the diffuser pore size did not seem to have any significant effect on the oscillation frequency (for the pore size range investigated), the frequency of oscillation however influenced the rate of weeping, and consequently the bubble size distribution. From visual observation, the fluidic oscillation seemed to falter beyond a particular flow range. Given the unstable condition, it was not possible therefore to characterise the bubbles at varying feedback loop length. Preliminary measurements using the ceramic diffusers also revealed a similar outcome. The result shows frequency of oscillation dependence on flowrate and feed back loop length. The frequency of oscillation is clearly seen to vary directly proportionate to the supply flow rate and inversely proportionate to the feedback loop length. These results are in good agreement with the findings of Tesar et *al*. (2005).

Table 4.2 presents a summary of the materials tested, the average bubble size range and cost of material per square meter.

Table 4.2: Summary of the diffuser materials tested (mean pore size ~ 20 microns) and their associated cost per square meter of material.

S/n	Material	Cost / m2	Performance	Remark
1	Ceramic	~2-3k	~ 300µ bubble	Not suitable
2	Microchip	Unconfirmed	~300µ bubble	Not suitable
3	Polypropylene	< £200	No bubble	Not Suitable
4	Nickel	~£2k	~25 – 45µ	Suitable
5	Stainless Steel	£90	~ 20-150µ	Suitable
6	Nylon	<£200	~60µ	Suitable
7	Osopyrene	<£200	Not yet tested	-

4.5   Summary

A low-pressure offset technique utilizing just gas for the production of microbubbles have been designed and characterised. First attempt was made to solve the problem with bubble generation using existing diffusers but the target mean bubble size was not achieved. Subsequent attempt to design a diffuser was met with maldistribution and hence deemed unsuitable for use in Microflotation. An improvement on the bespoke diffuser was made by modifying and incorporating a vane distributor into the plenum chamber to facilitate high bubble flux whilst also achieving the desired mean bubble size, which proved successful. Furthermore, the diffuser performance was tested by studying the effect of gas flowrate on bubble size distribution as well as by varying the diffuser membrane pore size. Result showed an increase in mean bubble size and wide size distribution of bubbles as supply gas flowrate was increased. A similar outcome was observed with varying membrane pore size. The use of the fluidic oscillator in generating microbubble proved effective in comparison with conventional steady flow technique for the same diffuser.

Chapter 5

MICROFLOTATION FOR OIL EMULSION SEPARATION

5.1   Introduction

This chapter presents the application of fluidic oscillator generated microbubbles for the separation of oil-water emulsion. The materials and method employed in this study are described in Section 3.2.2 for bubble size measurements; Section 3.2.3 for particle size distribution and Section 3.3.2 for separation. The diffuser used for this investigation is fitted with a 50 μm pore size membrane (see Fig 4.9f for bubble size distribution). The chapter is organized as follows: in the next section, the effects of separation techniques are discussed and comparison drawn by exploring the separation efficiency of bubbles generated under steady and oscillatory flow conditions. The other section provides insight into the effect of surface-active molecules on the stability and separation of emulsified oil droplets.

5.2   Effect of Separation Methods

To compare the performance of microflotation with traditional techniques, experiments were carried out with fine bubbles (~3 mm) and 'no bubble' (gravitational separation). Experimental conditions such as surfactant concentration, pH, and coagulant dose were kept the same with conditions for these experiments (see section 3.3.1). Three experimental runs for each technique were done and the mean separation efficiency presented in Figure 5.1. With fine bubbles, oil separation efficiency of 14% was recorded while gravity separation showed relatively higher recovery efficiency 77% compared to 91% from microflotation (mean bubble size ~ 131 μm Fig 4.9f).

The oil droplet size measured using the Mastersizer is shown in Fig 5.2. Oil droplets are small with diameters < 5 and < 80 μm before and after coagulation with aluminium sulphate respectively. As a consequence of their small diameters, oil droplets have high residence time (practically non-buoyant) in the medium, making separation by gravity time consuming and relatively less efficient. The attachment of microbubbles to oil droplets increase the density difference, between the agglomerates and the medium. Due to the density difference, the agglomerates rise faster,

facilitating rapid separation from the medium. However, emulsion separation is largely dependent on collision frequency and attachment efficiency between bubbles and oil droplets (Grattoni et al., 2003; Moosai and Dawe, 2003), bubble surface mobility and ultimately on bubble size due to increased surface area with smaller bubbles (Tao, 2005).

Compared to microbubbles, fine bubbles have lower surface to volume ratios and lower residence time. These properties of fine bubbles render them ineffective in the separation of colloidal substances from aqueous solutions. Even in instances when oil-bubble collision occurs, the instability of the aggregates eventually leads to early detachment. The instability associated with fine bubbles is due to their large buoyant force and high terminal rise velocity. Also, because flocs are fragile, their weak structures are readily susceptible to shear resulting from system disturbance. The passage of a single large bubble imparts significant shear stress upon particles on its travelling path and within its vicinity. When these flocs break, the recirculation of their disintegrated parts makes it even more difficult for oil-bubble collision to occur. Grammatika and Zimmerman (2001) suggested that a critical particle-bubble size ratio exist within which collection efficiency approaches unity (i.e, the product of the collision, attachment and stability efficiencies approaches 1).

Compared with fine bubbles, microbubbles have increased surface area to volume ratio and high residence time. The gentle sweep of a cloud of microbubble affords many separation advantages. As microbubbles rise, they do so with minimal shear stress on flocs. As a consequence, floc size and structure is preserved. Thus upon collision and attachment to flocs, aggregate stability is maintained. Under this circumstance, neighbouring bubbles can be entrapped in the aggregates and in some cases; microbubbles can be entrapped by aggregates resulting in increased separation efficiency. This observation is corroborated by the DAF separation mechanism reported by Rubio et al. (2002).
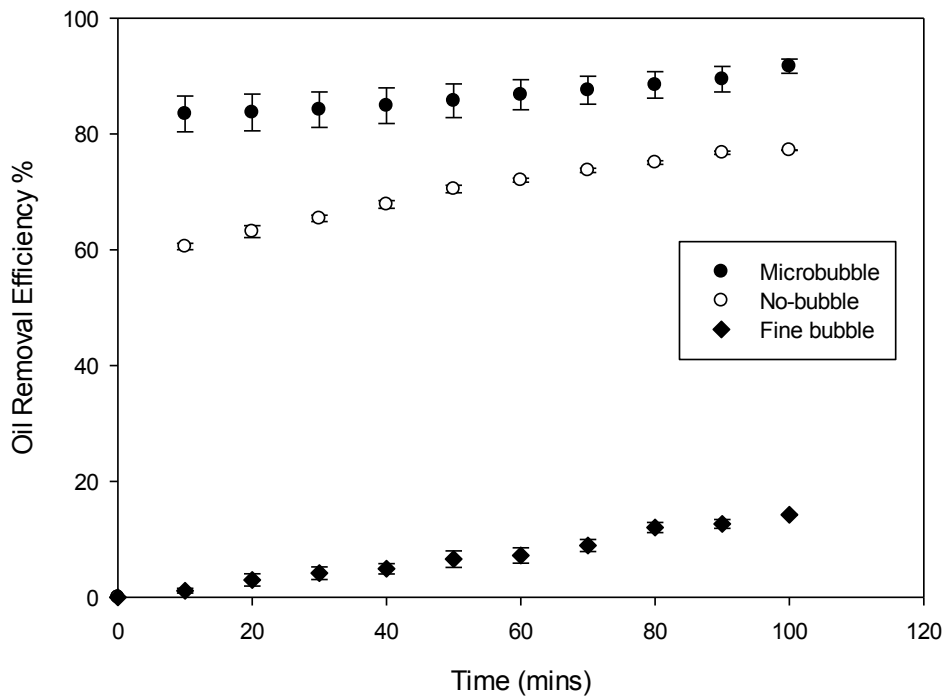
Figure 5.1: A plot of oil removal efficiency against time at 0.3 wt% Span 20 concentrations and Aluminium concentration of 500 mg/L. The graph shows results from main and control experiments under optimum operating conditions. (a) Coarse bubbles (>1 mm) were generated without the use of the oscillator. Oil removal efficiency was 14%. (b) Gravity separation (No bubble) with oil removal efficiency of 77%. (c) Microflotation (sub-150 μm bubbles) with efficiency of 91.3%. The error bars represent the standard error.

5.3 Effect of Surfactant Concentration

To investigate the effect of surfactant on separation of oil, surfactant was introduced at varying concentration in the raw effluent. The oil removal efficiency depends on surfactant concentration due to alteration of surface tension. The results are presented in Fig. 5.3 and 5.4. The overall maximum oil removal efficiency was obtained at the lowest (0.3wt%) surfactant concentration with separation efficiencies reaching 91.3%. With 1wt% surfactant dose removal efficiency reaching 82.4% was obtained. The efficiency dropped to 75% at 3 wt% concentration before decreasing to its lowest at 36.3% and 36.5% for 5 wt% and 10 wt% surfactant concentrations respectively.

(a)

(b)
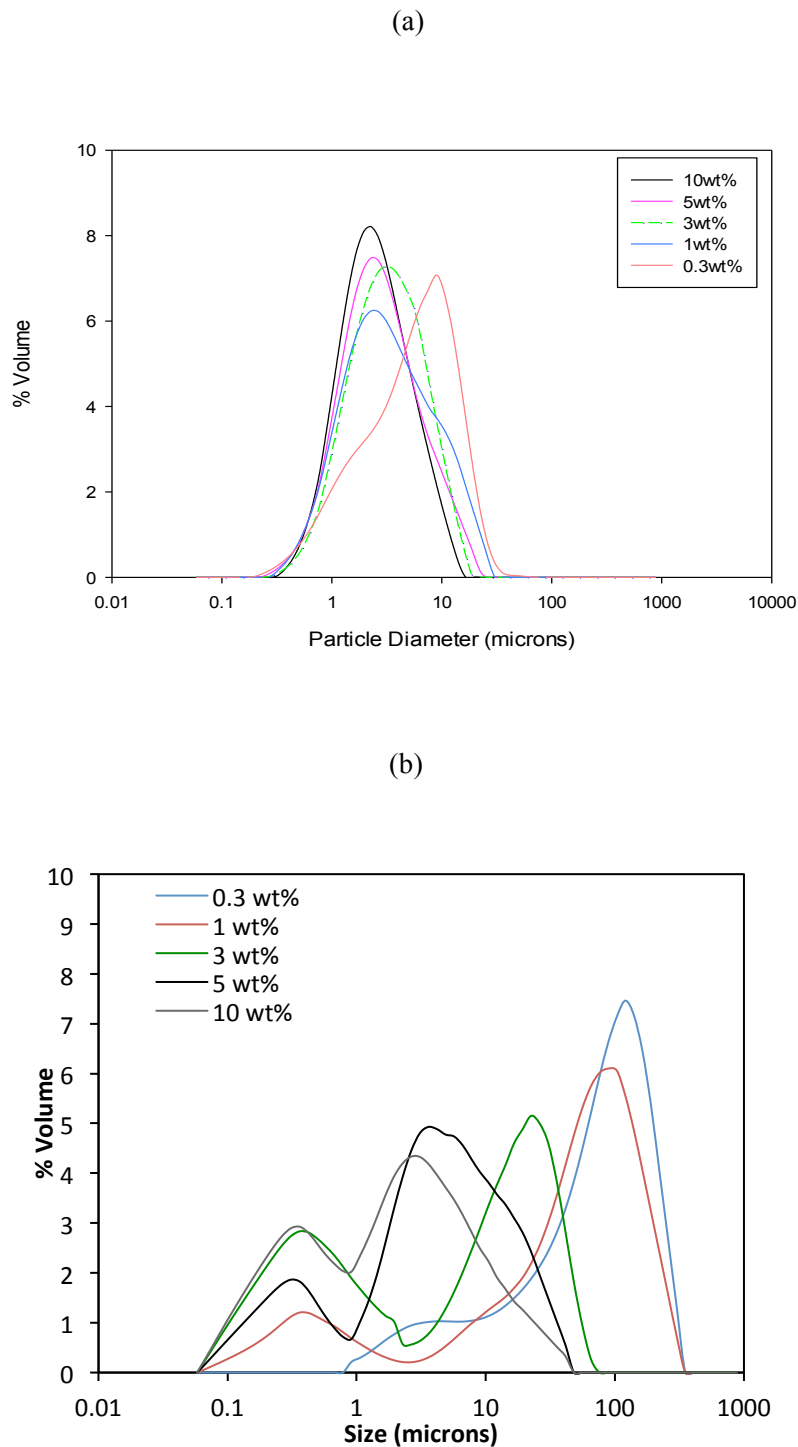
Figure 5.2: Size distribution of oil droplets under varying surfactant concentrations (a) Before chemical coagulation: Average size of droplets in general was less than 3 µm for all surfactant doses apart from 0.3 wt% with mean droplet size of 5. (b) Size distribution after chemical coagulation: Maximum floc size measured was 80 µm at 0.3 wt%. Generally, mean size of droplets and flocs varied inversely proportional to increase in surfactant concentration.

The results presented in Fig 5.3 and 5.4, show that increase in surfactant concentration from 0.3 wt% to 10 wt% leads to a reduction in oil removal efficiency. Contrary to the understanding that surfactant reduces interfacial tension and surface tension of liquids (Moosai and Dawe, 2003) which are commonly conjectured to lead to further reduction in bubble size, oil removal efficiency dropped as surfactant concentration level increased. The reason for this outcome is that, surfactant molecules attach firmly to the oil-liquid interfaces and at increased surfactant concentrations emulsions are highly stable. Under these conditions, auto-flocculation or droplet coalescence is significantly reduced and consequently, separation efficiency is low. In addition, at high surfactant concentration, substantial coagulant quantity will be required to de-emulsify oil droplets and promote flocculation. Conversely, at reduced surfactant concentration, the emulsion is less concentrated and less stable which allows for increased efficiency for the same volume of air throughput. Another explanation for the high efficiency recorded under this condition relates to the large flocs formed at low surfactant concentration. In addition to the increased collision probability they offer, large flocs are good transport media and can serve as collision and entrapment vehicles for neighbouring flocs in the liquid.

Another reason for this outcome is that oil droplet size is negatively correlated to surfactant concentration (see Fig. 5.2). The relatively small size of oil droplets at high surfactant concentrations decreases the oil-bubble collision probability. Apart from their low buoyancy that keeps them deflected when approached by a rising bubble (Grattoni et al., 2003), smaller oil droplets have low-rise velocity and increased residence times, which are influential factors in their separation from a liquid medium. The rate of flotation increases with increasing size (Hanotu et al., 2012; Miettinen et al., 2010; Pyke et al., 2003). This explains why larger flocs are preferentially separated before small flocs.

Furthermore, oil droplets attach to bubbles either by point contact or spreading over the bubble surface. Attachment by point contact is less effective and often gives rise to oil-bubble detachment during the aggregate ascension. Spreading by contrast is a more robust and effective attachment mechanism but its effectiveness is a function of the oil droplet size. Larger oil droplets relative to gas bubbles upon collision with

bubbles spread relatively evenly over a wider region on the bubble surfaces, producing a relatively robust attachment to the bubbles and the aggregates are maintained during ascension to the sludge layer. Small oil droplets by comparison, spread less over the bubble surface because of their size and low spread velocity. The degree of spreading can be defined by the spread coefficient. It is the imbalance of forces between the interfacial forces acting on the planes of the respective fluids in contact (Grattoni et *al*., 2003; Moosai and Dawe, 2003). Its importance relates to the stability of the oil-bubble agglomerate. At positive spread coefficient, total spreading is achieved whilst relatively low spreading is the result at negative spread coefficient values. Grattoni et al., (2003) report that the velocity of spread is proportional to the spreading coefficient, which must be positive for spreading to occur. Also, because the spreading coefficient is influenced by factors such as: interfacial, gravitational and viscous forces, small droplets have low spreading efficiency. The resulting low attachment efficiency gives rise to aggregate instability and consequently detachment. Moosai and Dawe (2003) report that a 50 µm oil droplet will have a spread layer 13 µm in size over a 50 µm bubble; while a 20 and 10 µm droplet will form a spread layer of 1 µm and 0.15 µm respectively on the same sized bubble. Generally, interaction by spreading between two fluids is characteristic of the spreading coefficients. However, in order for optimum separation efficiency, attachment by spreading must be sought and optimized through flocculation and droplet coalescence. Here we have varied coagulant concentration in order to promote flocculation and improve the effective size of droplets.

(a) (b)

(c) (d)
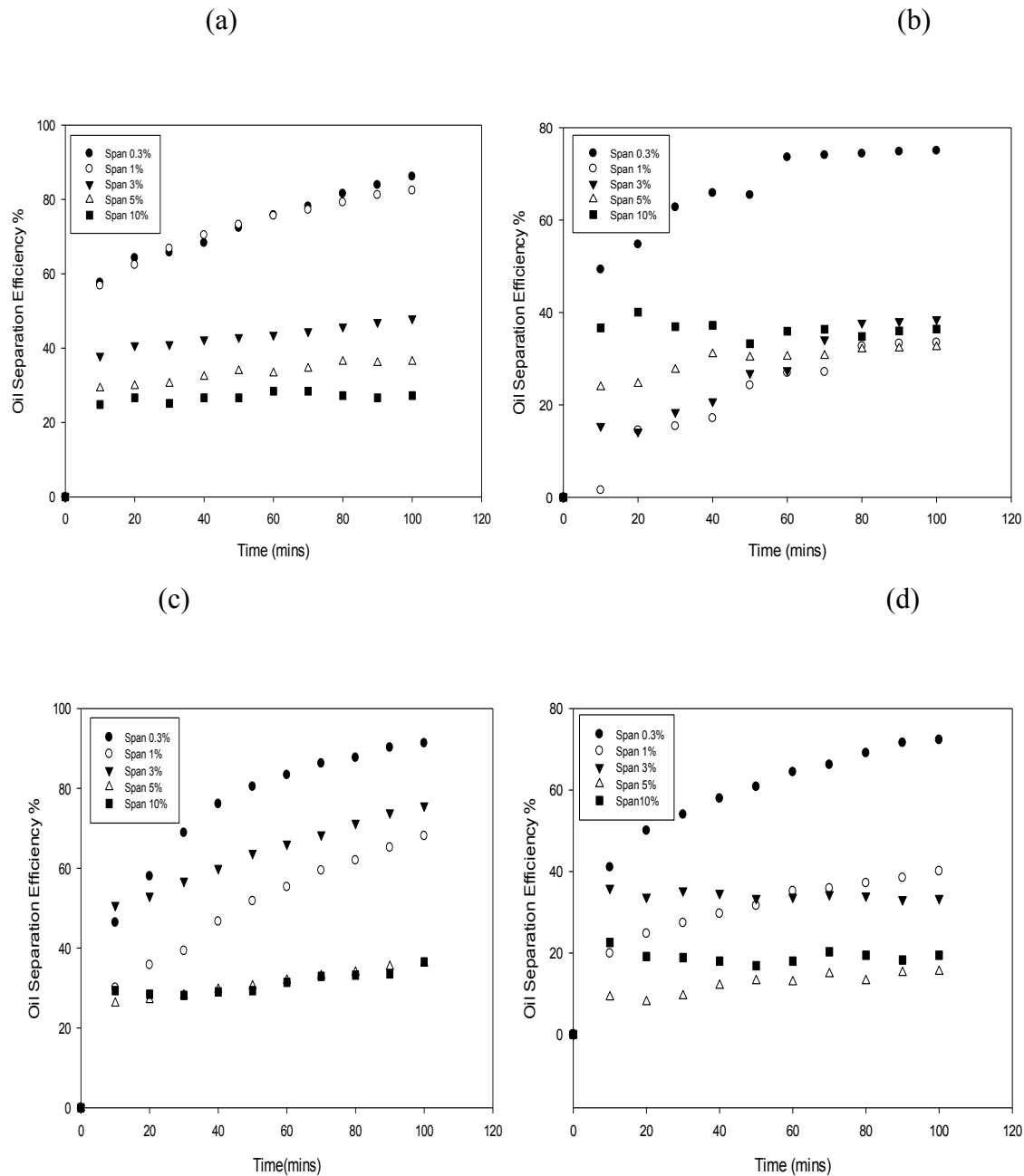
Figure 5.3: Graph of oil removal efficiency against time at varying surfactant and coagulant concentrations. (a) Coagulant concentration of 100 mg/L showed highest separation efficiency to be 86.70% at 0.3 wt% surfactant concentration and the lowest recorded as 27.3% at 10 wt% surfactant concentrations. (b) Coagulant concentration of 300 mg/L. Highest efficiency obtained was 74.4% at 0.3 wt% surfactant concentration and the lowest 34.8% at 10 wt% surfactant concentration. (c) Result at coagulant concentration of 500 mg/L showed highest separation efficiency to be 91.3% at 0.3 wt% surfactant concentration and the lowest recorded as 36.5% at 10 wt% surfactant concentrations. (d) Result at 1000 mg/L coagulant concentration. Highest efficiency obtained was 72.30% at 0.3 wt% surfactant concentration and the lowest 19.4% at 10 wt% surfactant concentration

The decrease in separation efficiency with increase in surfactant concentration can also be explained by a retardation in bubble upward surge as total adsorbed surfactant molecules increased at higher levels of surfactant concentrations. At high doses, surfactants in liquids naturally trail to the lower hemisphere from the upper hemisphere of the bubble leaving the lower hemisphere immobile (Clift et al., 1978; Nguyen, 1998; Nguyen and Evans, 2004; Schulze, 1992). The resulting overall bubble deceleration compels the liquid streamlines away from the bubble-liquid interface preventing liquid thinning and consequently, resulting in a reduced bubble-particle collision and attachment efficiency respectively (Schulze, 1992; Dai et al., 2000). Conversely, mobility of the microbubble surface increases with decrease in surfactant concentration (Parkinson et al., 2008). Essentially, spherical, non-deforming surfaces of microbubbles have a higher capture efficiency of particles/oil droplets as described by Grammatika and Zimmerman (2001). Furthermore, unlike larger droplets, small oil droplets are harder due to high internal pressure. Each oil droplet is susceptible to an upward rise in a process known as creaming. Creaming is indicative of the instability of emulsions.

Above the critical micelle concentration (CMC), the droplets gain increased positive charge and repel each other, which reduce oil-oil agglomeration and consequently separation efficiency. The higher the surfactant concentration, the closer towards the critical micelle concentration the emulsion approaches. Conversely, at extremely low surfactant concentration the conditions are less optimal and flotation will also be less efficient (Moosai and Dawe, 2003).
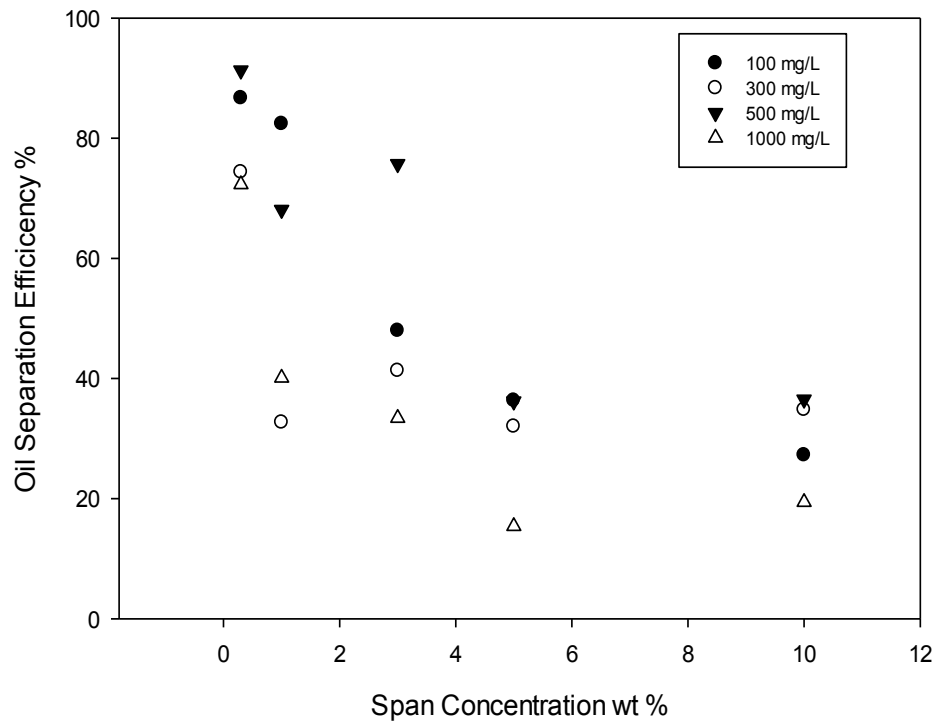
Figure 5.4: Plot of oil removal efficiency against surfactant concentration at varying coagulant (aluminium sulphate) doses.

Although the maximum oil removal efficiency observed in this study is less than the efficiency reported by Al Sharamni et al (2002) (98%) and Zouboulis (2000) (95%), it is significantly higher than the efficiency result reported by Liu et al (2010) (40%) for dissolved air flotation. The main difference in experimental conditions is the higher surfactant concentrations, oil type and concentration used in the current study. Nonetheless, the potentially high-energy savings with microflotation far outweighs those of dissolved air flotation. Hanotu et al. (2011) reported higher separation efficiencies (up to 99.2%) for microflotation of microalgae, using the same bubble column. The significant difference is that microalgae are solid particles approximately 10 μm in diameter, significantly larger than the droplets in this emulsion. Grammatika and Zimmerman (2001) demonstrate that matching the size of the bubble and the generalized particle in flotation separations is crucial in achieving high collision efficiencies. Tuning of the bubble size distribution with microflotation is possible with selection of membrane and surface properties of the membrane and influenced by the contents in the media.

The major limitation of our system is the gas hold-up, which can be improved by continuous flow systems (such as DAF) by ducting the flow over a wider area packed with diffusers. This is possible in a 'no-liquid' flow clarifying tank as here (fig 1). Although low bubble holdup is a drawback in our approach, it has redeeming features. The common interpretation of DAF is that bubble-particle flocs are formed due to the collision efficiency. DAF systems causes turbulent flow by highly energetic release of supersaturated liquid into the clarifying tank, high shear instability breaks down flocs after they have formed. The birth-death competition in DAF for flocs is not mirrored by Microflotation. The flow field is laminar, which does not break up flocs once formed. This suggests that turbulent break up of flocs dominates the floc formation mechanism, so turbulence is net counter-productive and partly a waste of energy in the separation process.

5.4   Summary

In this chapter, the treatment of oil-contaminated water by microbubbles produced via fluidic oscillation has been investigated. It was found that the presence of surface-active agents can influence the size of the oil droplets present in an emulsion and consequently affect the separation efficiency. It was observed that an increase in the surfactant concentration resulted in a decrease in the oil droplet size and enhanced stability of the emulsion, thereby leading to a decrease in separation efficiency. The combination of fluidic diverter valve and a pair of micro-porous diffusers used in this experiment has produced gas bubbles with a narrow size distribution with a mean diameter of 131 μm. These bubbles were successful in separating oil droplets in the order of 5 μm with an efficiency of 91% at a surfactant concentration of 0.3%. The pilot experiments carried out with fine bubbles (~3 mm) and no bubbles showed relatively low efficiencies. Although the separation time for fluidic oscillator driven microbubbles is longer than that of the conventional DAF, low-energy consumption associated with the former technology could potentially offsets the operational cost incurred with the latter. Even thought the results of this study suggest suitability of microbubbles in oil-water separation, a pilot scale study is recommended to fully assess the feasibility in effluent water treatment.

Chapter 6

MICROFLOTATION PERFORMANCE FOR ALGAL SEPARATION

6.1   Introduction

This chapter presents the results of algae separation by Microflotation. The work mainly focuses on algal recovery from growth medium but the process and technique can be applicable to separation or treatment of effluents containing algae particles.

The determination of recovery efficiency is based on the difference in the concentration of the algal biomass in the liquid medium. Unless otherwise stated, the recovery efficiency plots are for samples from port 1 (SP_1) two (2) cm from the microbubble diffuser. Given the number of experimental runs, limited time and the associated cost, it was practically difficult to triplicate all experiments to obtain the standard error. Therefore, only for the optimum results under each coagulant type and concentration were re-run conducted to obtain the standard error, which reported in Table 6.1. The materials and method employed in this study are described in Section 3.2.2 for bubble size measurements; Section 3.2.3 for particle size distribution and Section 3.3.2 for separation. The diffuser used for this investigation is fitted with a 38 μm pore size membrane (see Fig 4.7 for bubble size distribution).

This chapter is outlined as follows: In the next section, the size distribution of the algal cells is presented. Also, the recovery efficiency results are plotted against time, highlighting the effect of pH, sampling port position and coagulant concentration. Next, the effect of coagulant type was investigated using the three most common metal coagulants as well as the recovery efficiency across the column sampling ports. Finally, a cost analysis is presented in section 6.3 for the coagulant types used before a general summary is drawn in section 6.4.

6.2   Algal Recovery

Understanding the step-wise processes prevalent in a multi-floc system between particle-bubble interaction in a flotation column is both interesting and informative. Figure 6.1 presents the size distribution of algal cells before chemical pretreatment. The graph is a single peak distribution indicating the presence of relatively uniformly sized algal cells.
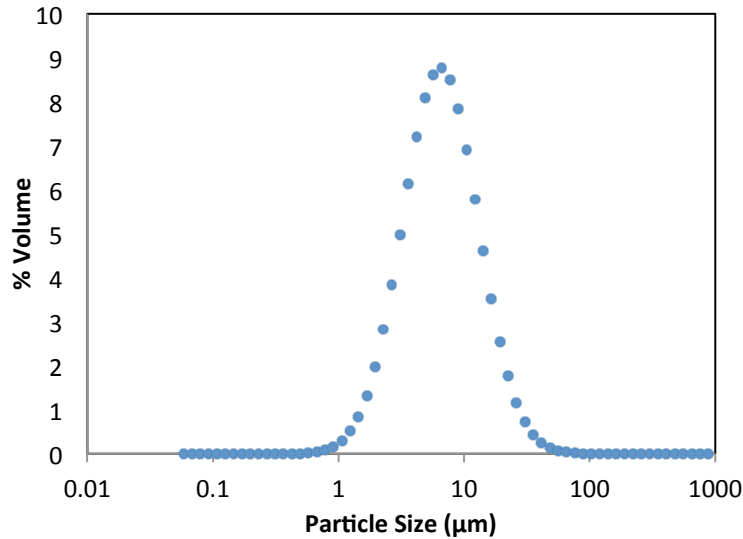
Figure 6.1: Size distribution of algal cells before chemical pretreatment. The algal cells were measured after growth as described in Chapter 3. Average cell size measured was 10 μm.

The photograph of the flotation unit illustrating key stages in the recovery process is shown in Figure 6.2. At first (Fig. 6.2a), the sludge blanket begins to form and sludge build up intensifies. Here, larger flocs are preferentially collected first before smaller flocs and the removal efficiency decreases sharply as gradient of biomass versus time (Fig 6.3). This outcome is simply attributable to their large surfaces, which readily render them susceptible to bubble collision and adhesion, bubble formation at particle surface, microbubble entrapment in aggregates and bubble entrainment by aggregates. Edzwald (2010) reported these bubble-particle interaction mechanisms in the review of flotation as a wastewater treatment. These large flocs also engage in sweep flocculation as they travel upwards under the lift of microbubbles hence the exponential biomass recovery efficiency recorded at the early stage.

After half the separation time (Stage 1), the amount of large flocs decreases markedly in the continuous phase; smaller flocs become prevalent in the flotation unit, indicating the second key stage. Biomass concentration (Fig. 6.3) only reduces slightly and as such recovery efficiency therefore increases fractionally with time because at fixed bubble size, bubble-particle contact is more effective with large flocs. In the second stage (Fig 6.2b), sludge build up continuous but also observed is the thickening of the sludge blanket. As more bubbles rise to the top, these bubbles compress the sludge layer from underneath, reducing the water content of the sludge.

Schulze (1992) provides some supportive theoretical and experimental insight as to why this is. Bubble-particle interaction upon approach has been found to occur either by attachment or driftage. While the former often results in collision and bubble surface deformation following the extension of the thin liquid film between bubble surface and particle to create a three-point contact, the latter process occurs across bubble surface and only causes minimal surface deformation without extension of the liquid film.

(a)	(b)	(c)
t = 0	t =12mins	t =30mins
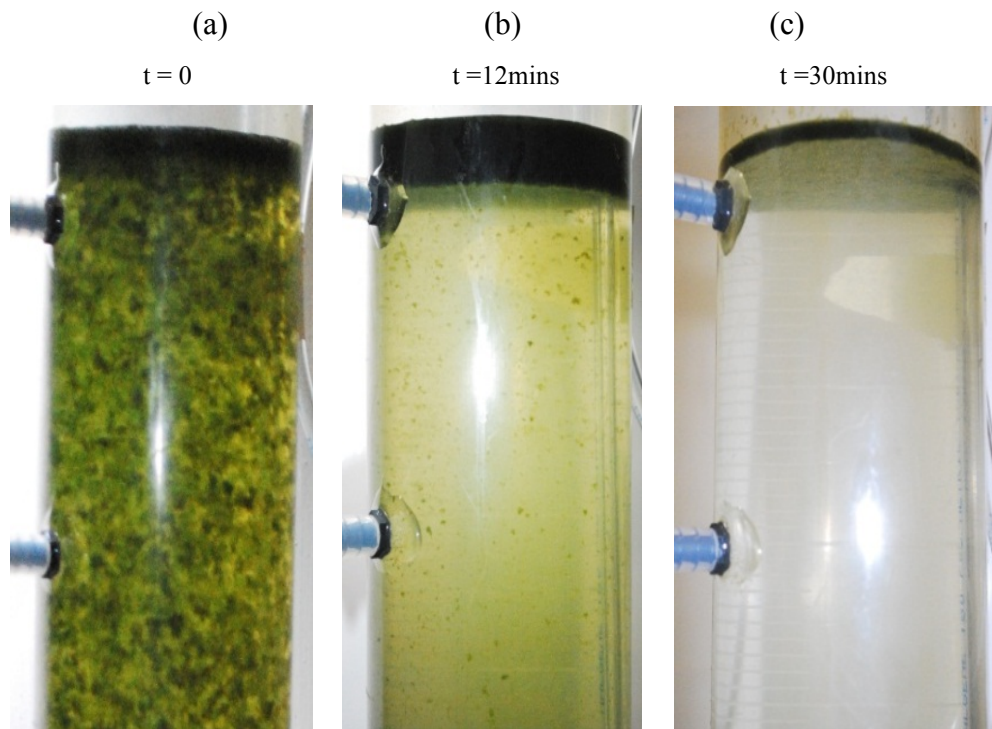
Figure 6.2: Photograph of the flotation unit showing the separation at three different key stages. (a) Few minutes after flocculated algal cells were introduced into the unit. Development of the sludge blanket outline begins to occur immediately as microbubbles transport large flocs. (b) Image of separated continuous phase clearly showing the algae sludge blanket minutes afterwards. Small flocs are predominant at this stage but the sludge layer is clearly outlined and fully formed (c) Third stage is marked by much slower separation as relatively smaller flocs but intense sludge thickening is observed. Clear continuous medium indicating full separation is obtained.

The possibility of particle-bubble collision in a flotation unit is higher with heavier and large particles at high radial particle velocity. By contrast, at relatively low velocities and with smaller particles, sliding (driftage) dominants the bubble particle contact mechanism (Schulze, 1992). And as such collision and attachment between particle and bubble is relatively low. Furthermore, the particle-bubble encounter probability and the collection probability are only equal when the collision as well as

attachment probability approaches 1 and the detachment probability, zero. This condition is rapidly obtainable given the two circumstances: particles are hydrophobic and sufficiently large for collision (Nguyen, 1998). The third key stage (Fig 6.2c) is primarily characterised by intensive sludge thickening and thinning. At this stage, the majority of the particles have been separated (Fig. 6.3) therefore microbubble rise velocity is increased as relatively very few particles are present to cause rise retardation and the rate of water removal from the sludge is high. The sludge layer is reduced to almost a quarter of the initial size.
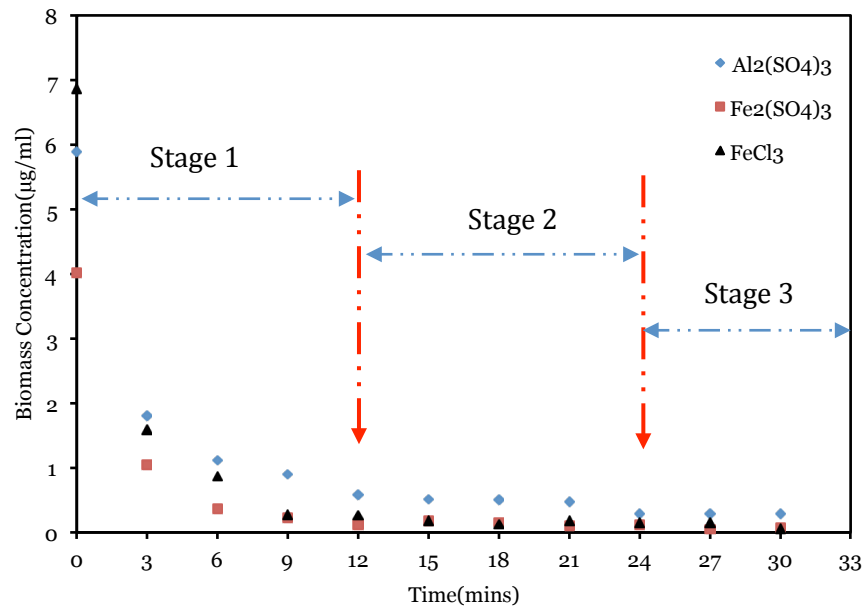
Figure 6.3: Graph of Algal biomass concentration as a function of time illustrating the different key stages in the flotation experiment. The first stage is characterised by sludge formation and intense sludge build-up, at this stage, separation efficiency is exponential and concentration of residual biomass drops sharply. Second stage still supports sludge build up but a transition into sludge thickening is observed. Here, separation efficiency is rather linear and biomass concentration reduces only gradually. Stage 3 is primarily dominated by sludge thickening and thinning; almost no significant separation efficiency result is recorded.

6.2.1 Effect Sampling Position

Table 1 provides useful information on the difference in results at various sampling points for all coagulant type. A total of four (4) ports were installed 80 mm apart across the flotation column (see Fig 3.14). Depending on the position of the port relative to the diffuser, efficiency is positively correlated. Away from the diffuser, recovery efficiency decreased continuously at all sampling ports. This is probably due to the difference in bubble density/flux away from the bubble diffuser, which

decreases away from bottom to top of column. Two factors are primarily influential on the bubble density in a liquid viz: coalescence and gas dissolution. The former reduces with decrease in bubble diameter (Esp. sub-100 micron bubble), and is therefore the unlikely cause of the difference in recovery efficiency. Until, saturation is achieved, bubbles introduced in a liquid continue to transfer their content (gas) into the surrounding liquid due to the pressure differential between the internal of the bubble and the surrounding liquid as well as into relatively larger bubbles (Ostwald ripening). The result is a decrease in bubble diameter and eventually, a collapse of the bubble, so that the number of bubbles available for separation (surface area ratio) in the column decreases away from the diffuser.

Table 6.1: Recovery efficiencies for the various sampling ports under best operating parameter (pH5 and 150mg/L coagulant dose). Efficiencies of 94-99.2% are reported across all ports and coagulant types. However, Teixeira and Rosa (2006) reported removal efficiencies of 92-98% and 70-94% for DAF and sedimentation respectively of blue-green algae while Wyatt et al., (2011) obtained 90% removal efficiency of fresh water algae by flocculation.

Sampling Ports (SP)	Height from Diffuser (cm)	Coagulants		
		$Al_2(SO_4)_3$	$Fe_2(SO_4)_3$	$FeCl_3$
		% Recovery (+/- 0.5)		
Sp1	2	95.2	98.1	99.2
Sp2	10	94.2	98.3	98.9
Sp3	18	94.6	98.6	98.9
Sp4	26	93.9	96.9	98.2

Another possible explanation for the difference in recovery efficiency regards the particle concentration. As bubbles emerge from their pores, they quickly attach to particles and the bubble-particle agglomerate rise, increasing the concentration of particles at each sample port as they travel towards the column top where the sludge blanket is formed. In other words, the concentration of particles is non-uniform at each port.

6.2.2   Effect of pH

Chemical pre-treatment is very essential in decreasing the effect of repulsive charge between bubbles and flocs. The success of chemical pre-treatment depends on pH because pH determines the solubility of chemical constituents of nutrient and metals in solution and influences the form and quantity of ions produced. Optimum pH and coagulant dosing reduces the charge on particles to about zero causing particles to be more hydrophobic (Edzwald, 2010). To investigate the effect of pH on separation, trials were conducted across different pH levels and results reported in Figure 6.3.

Figure 6.4 and 6.5 presents the flotation results for three metallic coagulants. The effect of pH on algal removal efficiency from Figure 6.4(a) showed that with aluminium sulphate coagulant, efficiency increases with decrease in pH to the lowest at pH 7 before rising again as pH increases to 9. Optimum recovery result of 95.2% was obtained at pH 5 with efficiency gradually decreasing to 71.9% at pH 6 and 50.6% at pH 7. At pH 8 however, a sudden increase to 74.6% was obtained and 81.5% at pH 9 indicating the other peak of result with aluminium sulphate. Data from Figure 6.4(b) can be compared with the data in Fig.6.4 (a) which showed a similar trend in the effect of pH on algal recovery efficiency. Again two peaks were observed on either side of the pH range experimented in this study. Best results were obtained at pH 5 with 98.1% followed by 91.6% at pH 6. The drop in performance continued to 83.2% at pH 7 before hitting the lowest with 80% at pH 8. At pH 9 however, the performance was observed to rise sharply to 85.5%. From the result in Figure 6.4(c), it is apparent that the result with this coagulant was different. Algal recovery efficiency dropped monotonically and nearly linearly with pH decrease. Optimum result of 99.2% was achieved at pH 5 and then 93.1% at pH 6. The recovery result further decreased to 90% for both pH 7 and pH 8 respectively and finally to 86.4% at pH 9. Graph 6.4(c) is quite revealing in several ways. First, unlike the first two graphs, overall efficiency was higher. The least efficiency at pH 9 was higher than the 80% mark. Thus with this coagulant, efficiency ranged from 86.4%-99.2%.

(a)

(b)

(c)
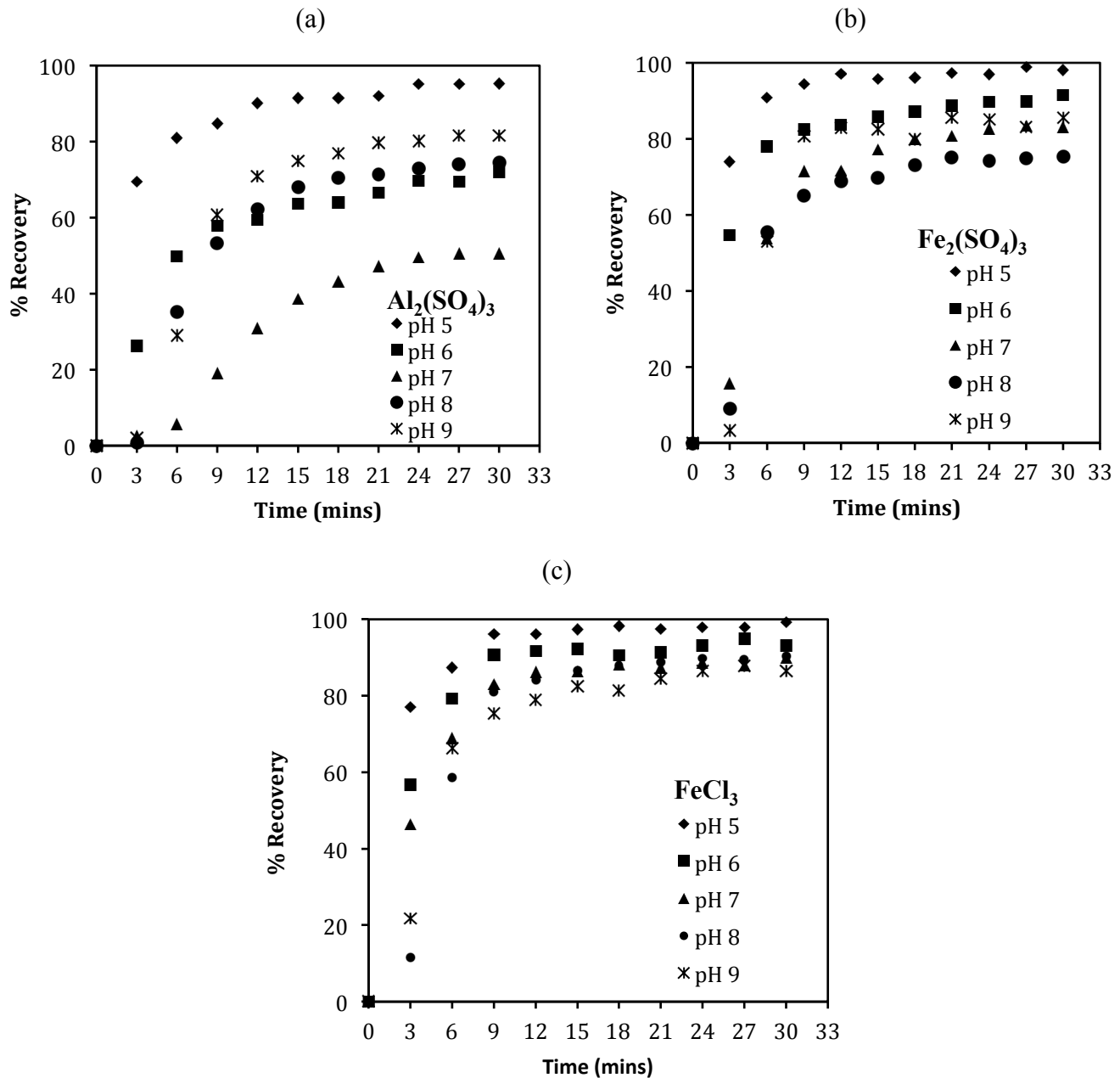
Figure 6.4: Graph of recovery efficiency at 150mg/L coagulant dose against time at varying pH levels for all three metallic coagulants. Recovery efficiency for all three coagulant used is highest at pH 5. Under this condition however, Ferric Chloride gave overall best result followed by Ferric Sulphate then Aluminium Sulphate.

In general, the optimum cell recovery result in these experiments was found at the lowest pH studied. Figure 6.5 reveals a peculiar trend in recovery efficiencies for the different coagulants studied with aluminium sulphate exhibiting a non-monotonic tendency across all concentrations studied followed similarly with ferric sulphate. Recovery efficiency with ferric sulphate nonetheless shows a fairly monotonic response as pH drops. One explanation for the non-monotonic behaviour observed

116

for ferric sulphate is contactless flotation (Jiang et al. 2010). One would infer that isoelectric points for all three coagulants are achieved with acidic conditions, so the alkaline high separation with ferric chloride would not naturally be achieved by zeta potential neutrality. By adding metallic inorganic coagulants such as iron and aluminium salts in solution, coagulation is achieved with the coagulants dissociating into Fe^{3+} and Al^{3+} respectively as well as other soluble complexes having varying high positive charges. Essentially, the rate and extent to which these trivalent ions and other complexing species adsorb onto colloidal surfaces is pH dependent. At room temperature, under acidic pH, trivalent species-Fe^{3+} (Wyatt et al., 2011) and Al^{3+} (Pernitsky and Edzwald, 2006).are the dominant species in the continuous phase These predominant trivalent species are the most effective in colloidal charge neutralization and attach to the negatively charged algal cell. The excess H^+ present under low pH react with hydroxides of these metals to further release the trivalent metal species. As a consequence, more Al^{3+} and Fe^{3+} species become available again for charge neutralization but the amount of hydroxides species is reduced. As pH shifts away from acidity however, H^+ concentration becomes less than OH^- and the amount of trivalent ions present in solution reduces. These prevalent OH^- react freely with the available trivalent metallic species to form the corresponding metallic hydroxide species. As such, hydroxide species become predominant under alkaline conditions attaching to algal cells and precipitating as large gelatinous flocs. Pernitsky and Edzwald, (2006) and Wyatt et al. (2011) reported increased concentrations of hydroxide species for aluminium and ferric salts respectively as pH moves beyond pH 7 at room temperature. This explains the large flocs generated under alkaline condition. It is for these reasons the recovery efficiency is observed to increase again under alkaline pH.

(i)

(ii)

(iii)
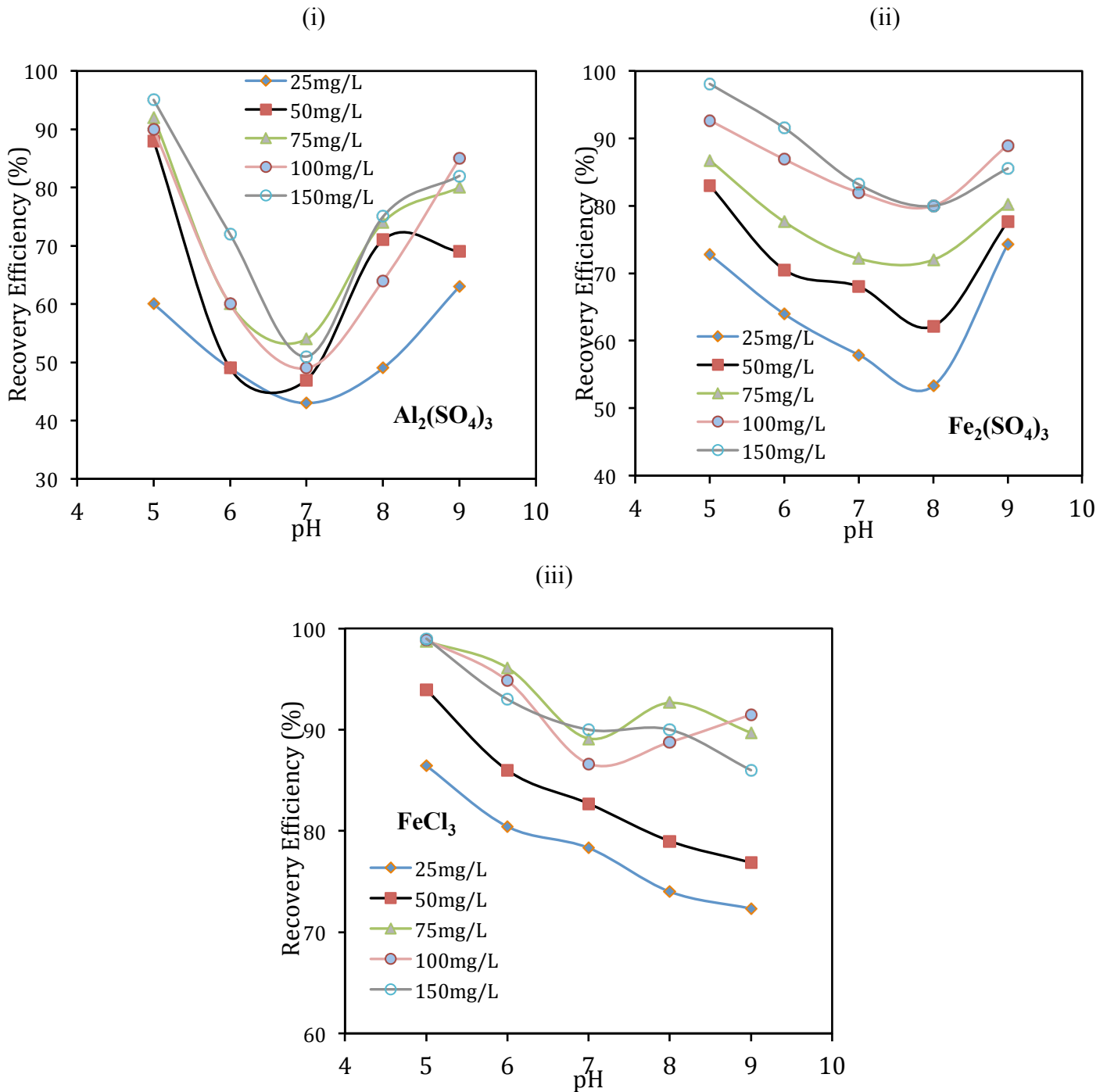
Figure 6.5: Plots of algae recovery efficiency as a function of pH at different coagulant concentrations. In general, efficiency increased as coagulant concentration increased. However, the graph shows unique trends in recovery efficiency results with change in pH for the respective coagulants. (i) Aluminium sulphate influences a non-monotonic trend across the investigated pH range. (ii) A similar outcome is observed with ferric sulphate but in this case, the recovery efficiency decreases with drop in pH until pH 8 before a sharp rise in recovery efficiency in pH 9. (iii) A fairly monotonic response was found with ferric chloride coagulant for recovery efficiency, anticorrelated with pH.

Considering that large flocs are good vehicles for sweep flocculation - large aggregates of $Al(OH)_3/Fe(OH)_3$ that are formed when Al/Fe salt is added to water, which colloid and drag colloids with them as they are transported by microbubbles, - one might wonder why despite the relatively large flocs formed at pH greater than 7, the overall efficiency under alkaline condition recorded for aluminium and ferric sulphate coagulant was still lower than results under acidic state. Under the same operating conditions of flowrate, bubble size and flux, this observation can be explained by the difference in charge density of species. The higher the size and charge of the species, the more effective the coagulation process will be. Because these charges increase with increasing acidity, recovery efficiency is highest under acidic pH. In addition, relatively larger flocs are developed under alkaline state and given that as particle size increases the residence time of the rising microbubble-floc agglomerate also increases leading to prolonged flotation time. Moreover, the lifting force of microbubbles diminishes with increased particle size (Miettinen et al., 2010).

By contrast, the condition is quite different for $FeCl_3$ though. Whilst a similar tendency occurs under acidic condition, $FeCl_3$ exhibits a rather different behaviour under basic pH. It is note-worthy to reiterate that ferric chloride produced the overall best recovery result. The justification for this is that ferric salts are relatively less soluble than aluminium salts. This observation corresponds with the findings of Chow et al. (1998) on the concentration of iron speciation in solution. Their results showed that the soluble ion concentrations were less than 1% of the total iron chloride amount initially added. In addition, hydroxides of aluminium are amphoteric- containing both basic and acidic functional groups. Furthermore, the addition of ferric salts decreases the solution pH and the closer the pH tends towards acidity, concentration of trivalent species in the solution increases. Wyatt et al. (2011) observed the same occurrence in their study of critical conditions for ferric chloride-induced flocculation of freshwater algae. The optimum pH for algal separation ranges from 5-7 for ferric chloride but for aluminium and ferric sulphate, two ranges are effective- 5-6 and 8-9. Overall, the process governing these reactions is very complex and by no means easy to fully detail especially also as the growth medium contains vital and very reactive chemical constituents.

In Figure 6.6 the SEM images of the algal flocs are shown for the different metallic salts used. The photographs provide a useful insight as to the cell destabilization mechanisms of the coagulants. Cells coagulated with Aluminium sulphate salt appear strongly bound in a cemented fashion. The same is true for Ferric sulphate salt. It therefore suggests that the binding mechanism is perhaps predominantly influenced by the sulphate species on both salts. For ferric chloride salt however, a rather different occurrence was observed with the formation of polymers that serve to link cells together. Cell destabilisation with Ferric Chloride appears to occur via enmeshment. This strongly suggests that the different salts may have varying charge neutralisation and binding mechanisms, which ultimately influence the recovery efficiency.
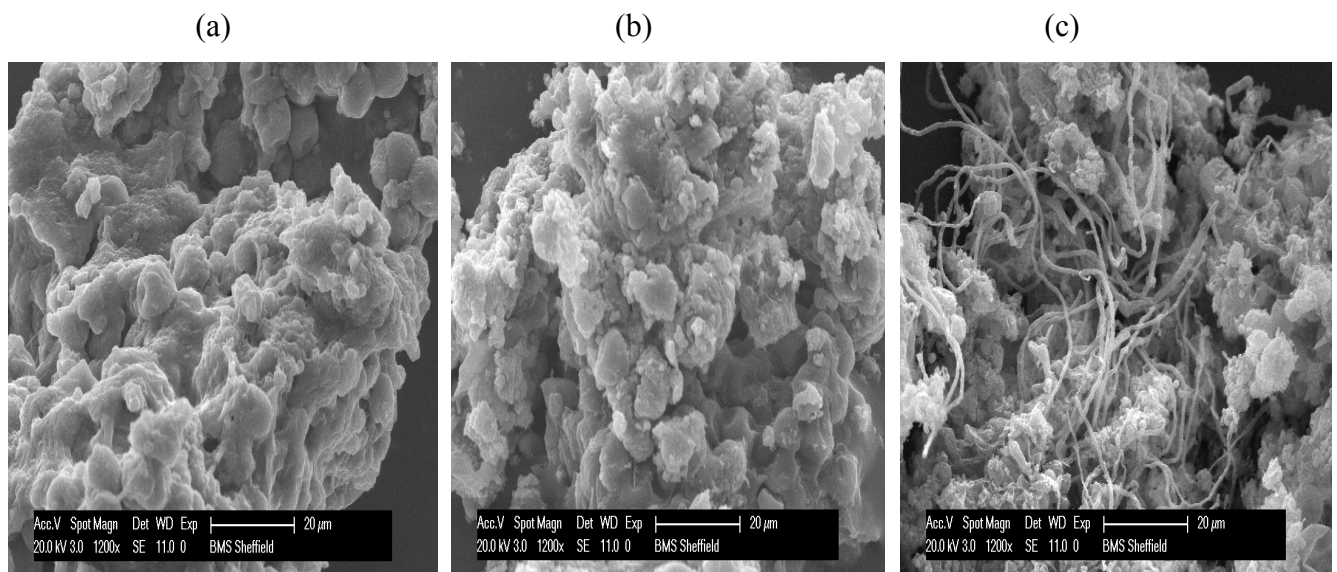
Figure 6.6: SEM photomicrograph of flocculated algal cells with the different metallic coagulants at 50 mg/L. (a) Aluminium Sulphate. (b) Ferric Sulphate. (c) Ferric Chloride.

6.2.3   Effect of Coagulant Dose

To ensure charge neutralization and proper particle agglomeration, good coagulation not only involves the type of coagulant but also the right amount of coagulant. By neutralising particle charge, collision between particles and bubbles is proliferated. The effect of coagulant concentration on separation efficiency was studied. Figure 6.7 shows the results of the effects of coagulant dose with time for the three metallic coagulants used.

A steady drop in efficiency was recorded with Aluminium Sulphate as the concentration of coagulant reduced from 150mg/L to 25mg/L. Highest result obtained was 95% at 150mg/L. At 100mg/L, 89.7% efficiency was obtained followed by 87.9% at 50mg/L and then 80.5% for 75mg/L before recording the lowest – 60.1% - at 25mg/L. With Ferric Sulphate, lowest yield in recovery efficiency was recorded at 25mg/L, which gave a maximum of 72.8% algal recovery followed by 83%, 86.8% and 92.7% for 50mg/L, 75mg/L and 100mg/L respectively. However, best algal recovery result recorded for this coagulant was achieved at 150mg/L with a recovery efficiency of 98.1%. The same exponential trend is observed with ferric chloride. Under this condition however, the lowest results registered were 86.4% and 93.9% at 25mg/L and 50mg/L respectively then, at 75mg/L of coagulant dose, the results rose to 98.7% and then to 98.9% at 100mg/L. For 150mg/L however, overall recovery efficiency of algal biomass obtained was 99.2%.

(a)

(b)

(c)
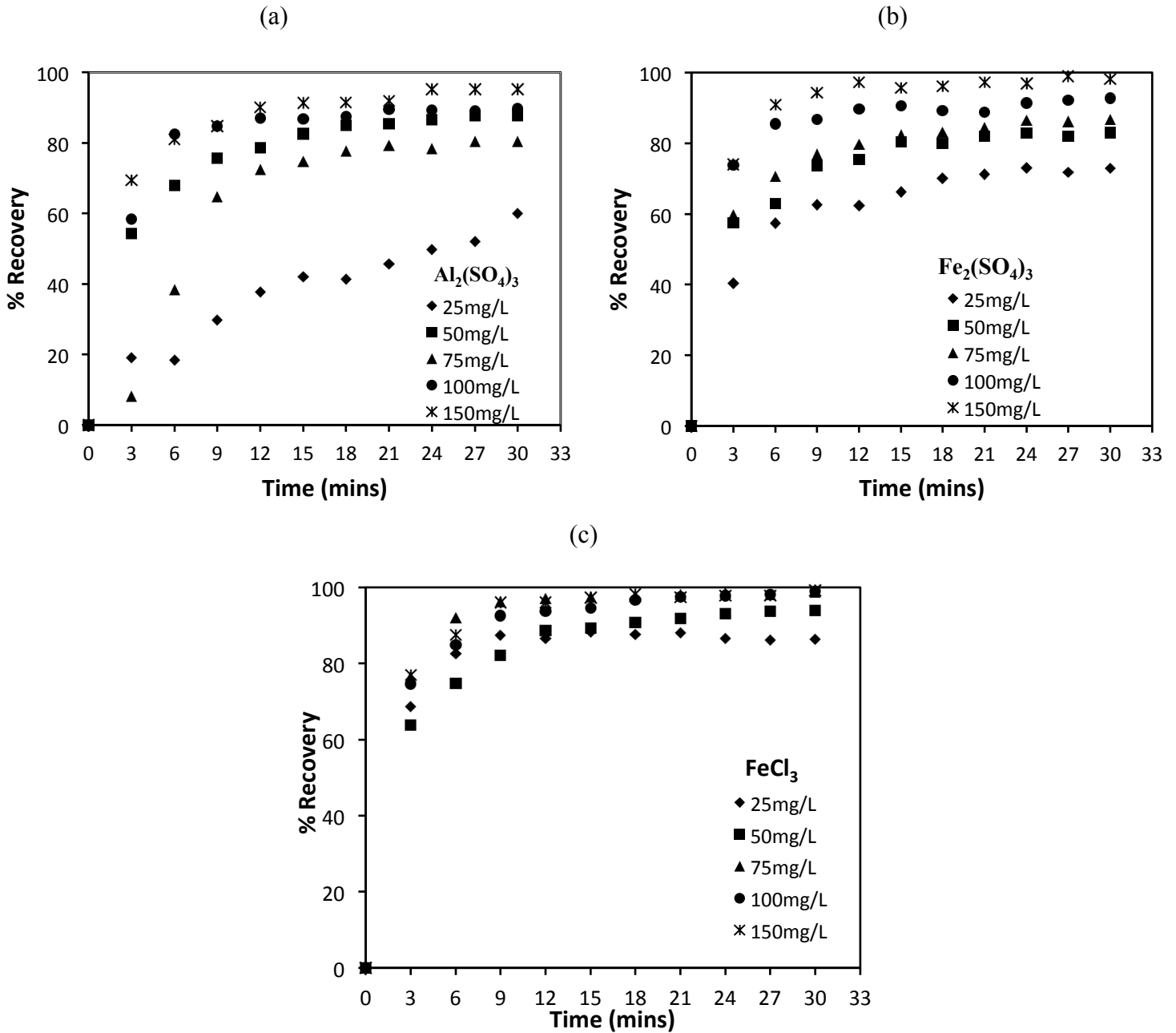
Figure 6.7: A plot of Algae recovery efficiency at pH 5 as a function of time at varying coagulant concentrations for the three metallic coagulant types. A steady increase in algal cell recovery was recorded with increasing concentration of coagulant. For all three coagulants, highest result was obtained at 150mg/L coagulant dose whilst the lowest results were recorded for 50mg/L and 25mg/L respectively.

The graphs in Figure 6.7 and 6.8 reveal in all cases an increase in the recovery of algal cells as concentration of coagulant increases. This is so because compression of the double layer effect is essential for particles to agglomerate and within the isoelectric point, increasing the dosage of coagulant, provides more trivalent ions necessary for double layer compression. Bubble particle attachment and detachment

in flotation studies by (Ralston et al., 1999) rightly supports this observation. The authors reported that increasing the amount of electrolytes decreases the interaction potential energy existing between bubble and particle. This phenomenon is more effective with hydrophobic particles. Also, when electrolyte concentration increases and at high particle hydrophobic strength, attachment efficiency becomes less dependent on size of particle.

The ability of a chemical coagulant to produce good coagulation is reliant on both the electric charge of the species and the size of the species used as coagulant. The higher the size and charge of the species, the more effective the coagulation process will be. Because these charges increase with increasing acidity, recovery efficiency increases at low pH. Coagulation of effluent is the most vital operating control variable influencing the performance of flotation. At low or no coagulation, particles remain negatively charged and hydrophilic which is why bubble-particle attachment is low or zero.
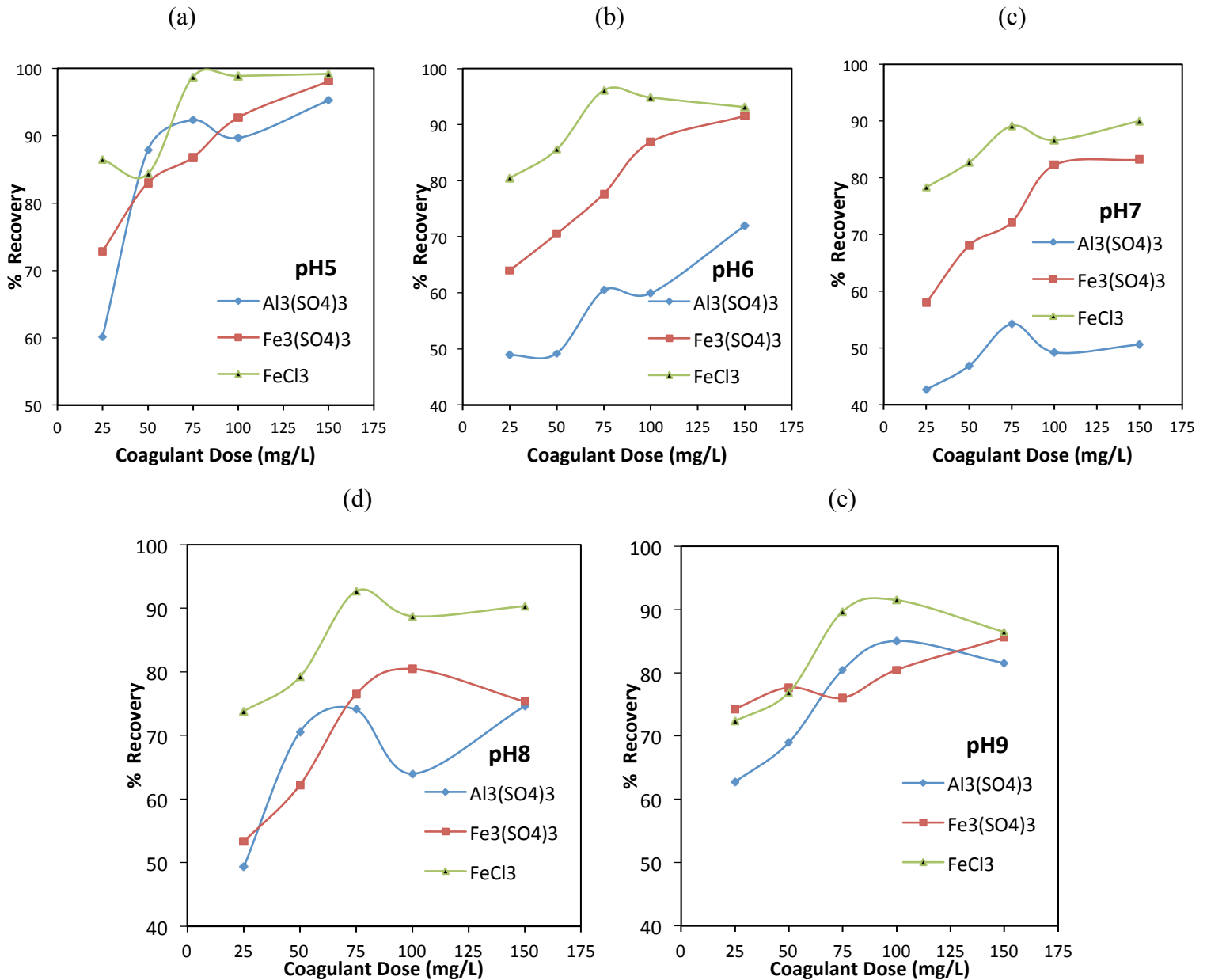
Figure 6.8: Graph of recovery efficiency versus coagulant concentration for the three coagulant types. (a) pH 5. (b) pH 6. (c) pH 7. (d) pH 8. (e) pH 9. Across the different pH levels, ferric salts showed higher efficiency than their alum counterpart. Most notable is the performance of ferric chloride, which was highest across all coagulant dosage levels.

6.3   Chemical Cost Comparison

With many studies laying emphases on the importance of the use coagulant in flotation processes and most especially for its use in this research work in the removal of algal particle from water, an evaluation of its economics is important. From the experimental studies done on dispersed air flotation in treating an algae-water

solution, the best performance was recorded at pH 5 and coagulant dose of 150 mg/L. The coagulants used in the experiment are aluminium sulphate, ferric sulphate and ferric chloride; these chemicals were purchased from Sigma-Aldrich Co. LLC. The tables below present the cost of 150mg/L of coagulant and the cost of coagulant required for a 1000L capacity tank contain wastewater.

Table 6.2: Cost analyses of coagulant types.

Aluminium Sulphate;

Quantity	Price (£)
5kg	77.00
For 150 mg of optimum dose per litre	2.31×10^{-3}
For 1000L capacity tank of algal solution which will require 150 g of Coagulant	2.31

Ferric Sulphate;

Quantity	Price (£)
500g	18.30
For 150 mg of optimum dose per litre	5.49×10^{-3}
For 1000L capacity tank of algal solution which will require 150 g of Coagulant	5.49

Ferric Chloride;

Quantity	Price (£)
2.5kg	86.70
For 150 mg of optimum dose per litre	5.202×10^{-3}
For 1000L capacity tank of algal solution which will require 150 g of Coagulant	5.202

6.4   Summary

This study considered the performance of microflotation on algal biomass recovery. There are 4 (four) conclusions that can be drawn from the results. First, the fluidic oscillator generated bubbles about twice the size of their outlet pores. Second, fluidic oscillator generated microbubbles were effective in the recovery of algal biomass from growth medium. Third, algal biomass recovery was enhanced with increasing coagulant dose. Fourth, the effect of pH was a key factor in flocculation and recovery efficiency was optimum under acidic condition.

Good coagulation chemistry relies on coagulation pH and coagulant concentration. Best coagulation conditions for bubble-particle capture efficiency are a balance between appropriate pH and coagulant dose to generate flocs with reduced surface charge and high hydrophobicity. Optimum results was obtained at lowest pH for all

three metal coagulant used. However, recovery efficiency showed exponential result with increasing coagulant dose.

As interest in sustainable energy continues to intensify, developing an energy efficient harvesting technique has never been more important. With the high energy cost associated with dissolved air flotation and the inefficiency of conventional dispersed air flotation to generate the right size of microbubbles, microflotation facilitated by the fluidic oscillator is a viable technology that promises to meet both the generation of microbubbles and its application in water treatment or algal biomass recovery for biofuel production.

Chapter 7

HARVESTING AND DEWATERING YEAST BY MICROFLOTATION

7.1   Introduction

The chapter presents the application of Microflotation in yeast harvest. Here a bioflocculant was used instead of the traditional coagulant and flocculant. In addition to studying its effect on yeast recovery, the study also explored the effect of varying bubble sizes in the recovery of yeast cells.

The determination of recovery efficiency is based on the difference in the concentration of yeast biomass in the liquid medium. The recovery efficiency plots are for samples collected 2 cm above the microbubble diffuser. The materials and method employed in this study are described in Section 3.2.2 for bubble size measurements; Section 3.2.3 for particle size distribution and Section 3.3.2 for yeast harvest. In addition to the materials and experimental method employed for zeta potential measurement, which are described in Section 3.2.4, that of moisture content analyses are given in Section 3.4. The diffuser used for this investigation was fitted with varying membrane pore sizes (see Figure 4.7 for bubble size distribution). Scanning electron micrograph analyses is described in Section 3.5.

The chapter is organized as follows: the next section presents the size distribution of bubbles analyzed in the yeast growth medium as well as the particle size distribution under varying pH conditions. Following that, yeast recovery results are presented highlighting the effect of pH, Chitosan concentration and bubble size on recovery efficiency. Finally, comparison of the recovery efficiency between two separation methods is presented as is the moisture content analyses of cells harvested using both methods.

7.2   Bubble Size Measurements

Bubble size was measured in water as well as in the yeast culture medium. The result of average bubble size measured is shown in Figure 7.1. Mean bubble size for measurement in water was 82; 131; 183; 341 and 436 μm for 25, 50, 75, 100 and 125 μm pore size respectively. In the yeast medium, however, bubble size (61 μm) as

recorded from the 25 μm pore size membrane followed closely by the 50 and 75 μm membrane with 68 μm and 87 μm respectively. As membrane pore size was further increased, higher average sizes (104 μm and 140 μm) were observed for the 100 and 125 μm pore size.
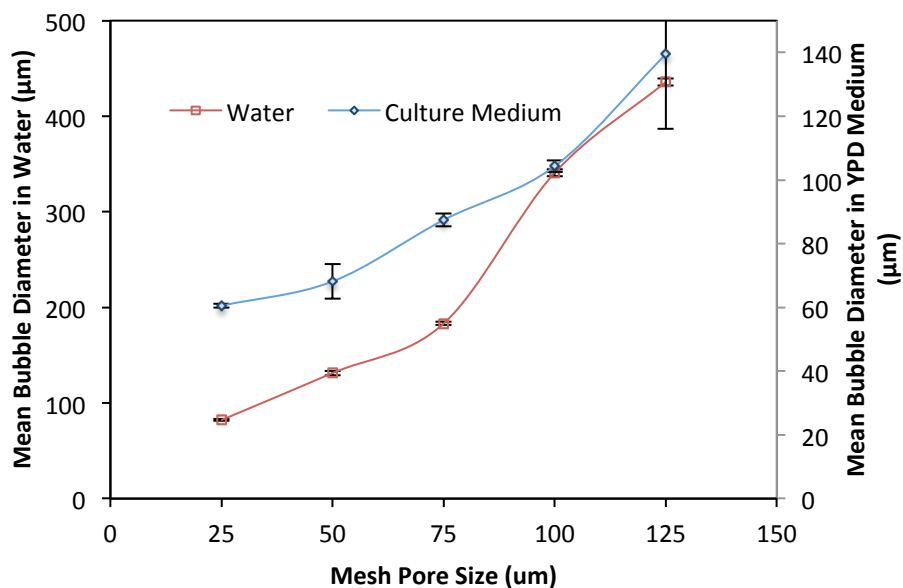
Figure 7.1: Graph of mean bubble size versus diffuser membrane pore size. (Blue-Right axis) mean size result for bubbles generated and measured in growth medium. (Red-Left axis) mean size for bubbles generated in water. The error bars represent standard error.

Mean bubble size is a function of the diffuser membrane pore. Bubbles produced in water are approximately 2-3 times larger than their exit pores. For bubbles generated in the growth medium however, the bubbles are almost same size as their exit pores. The difference in size is attributed to the surface tension (wettability) of both liquids.

7.3   Particle size distribution

The average particle size (yeast cell) for each flocculant dose is plotted in Figure 7.2 for both pH 5 and pH 7. Size of particles was improved as particles aggregated owing to the addition of chitosan. The size of the yeast cells (without flocculant) was found to range from 17-20 μm but otherwise, particle size reached 251 μm.

(a)

(b)

(c)
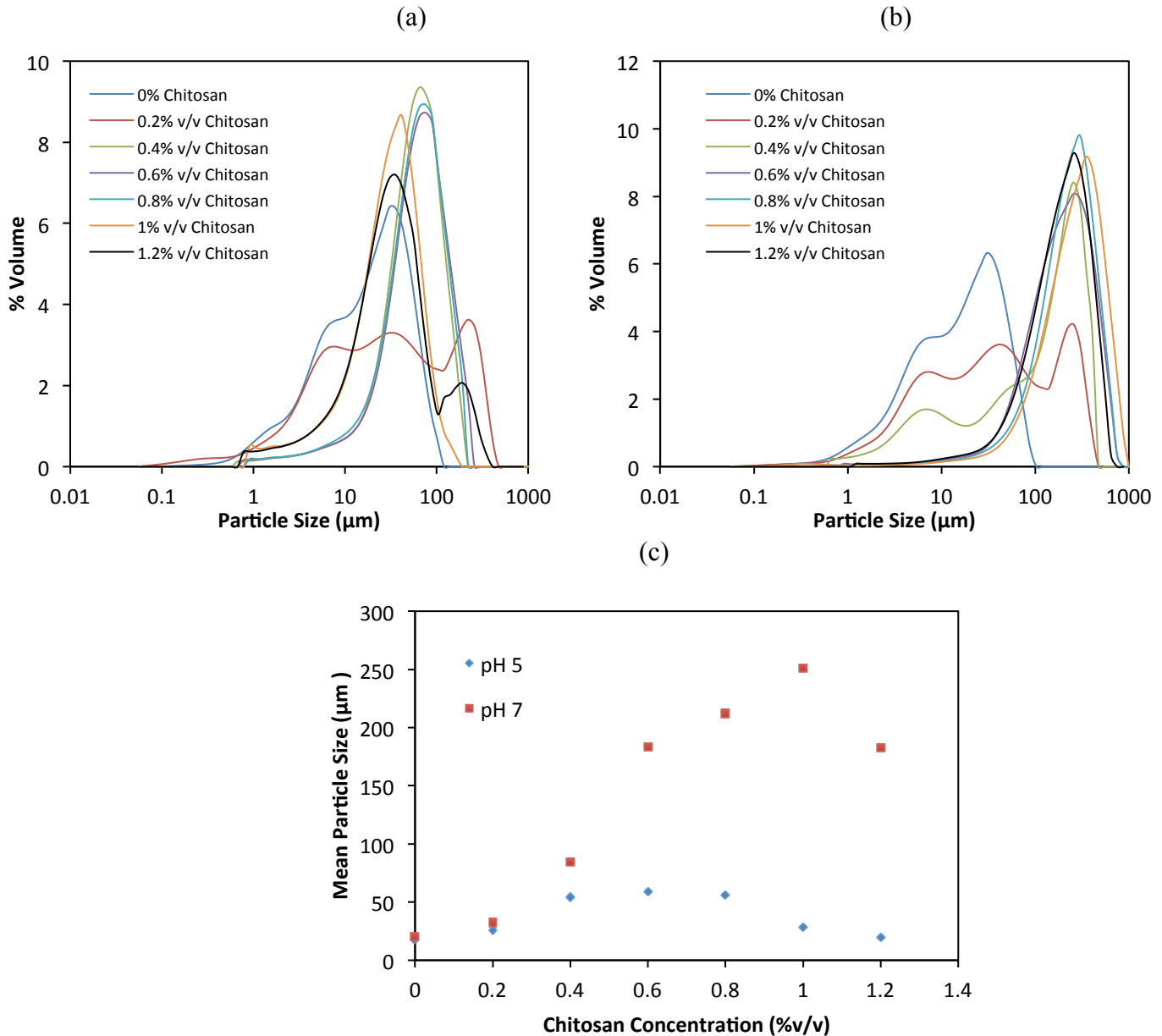
Figure 7.2: Size distribution of yeast cells at varying flocculant concentratons and pH for yeast floc sizes. (a) Size distribution at pH 5 (b) Size distribution at pH 7. (c) Combined plot of mean particle size.

Average particle size increased with flocculant concentration until the critical flocculant concentration was exceeded. Across the flocculant concentrations investigated, flocs generated at pH 5 showed a relatively narrow size distribution. Contrastingly, flocs generated under pH 7 exhibited a wider size range and are larger than flocs produced under pH 5. The size distribution results agree well with recovery efficiency results under the same conditions.
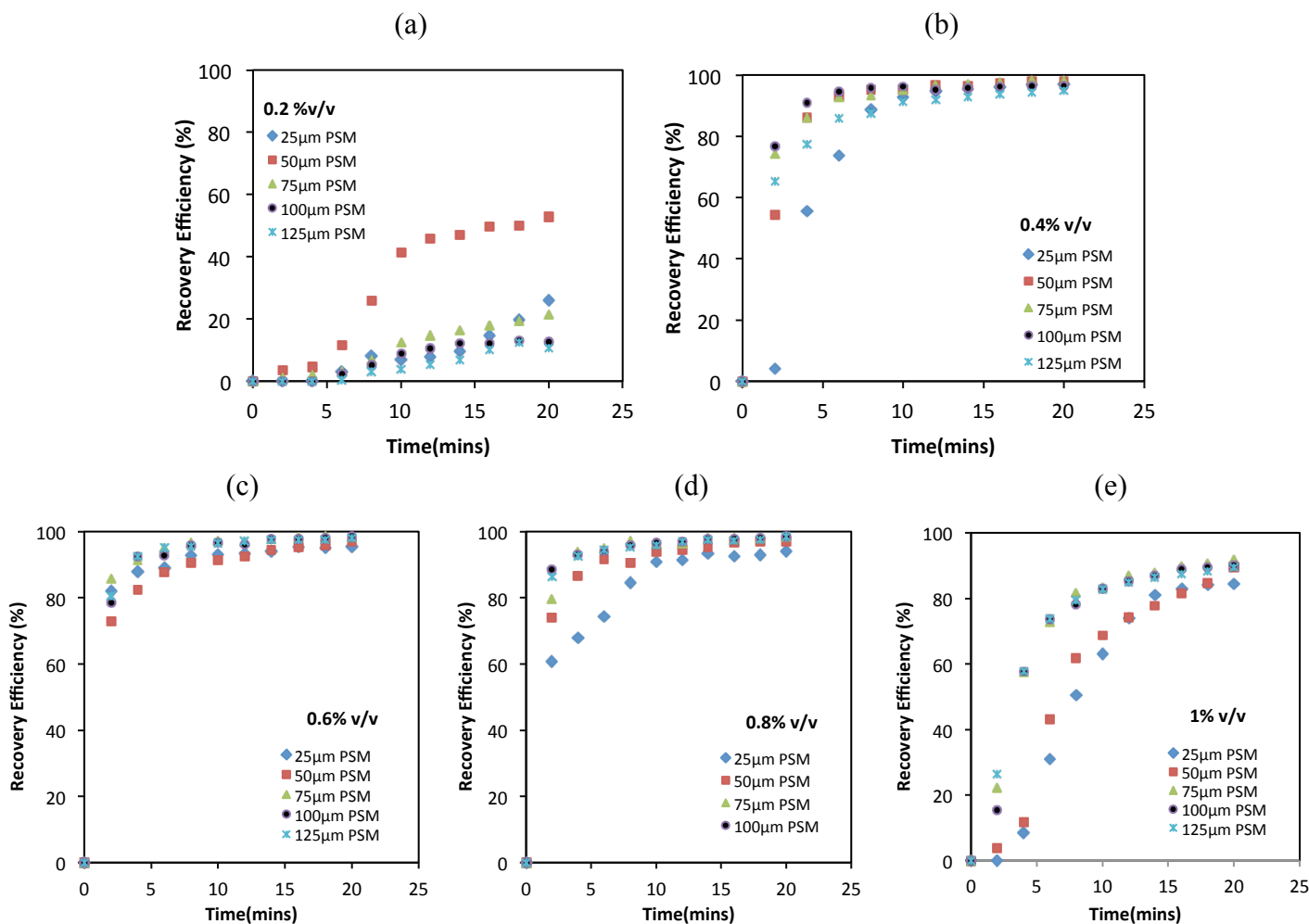
Figure 7.3: Plots of recovery efficiency with time at pH 5 under varying membrane pore sizes and chitosan concentrations of: (a) 0.2 %v/v (b) 0.4 %v/v (c) 0.6 %v/v (d) 0.6 %v/v (e) 1 %v/v. N/b: PSM- Pore size of membrane. Increase in efficiency is observed as coagulant concentration increases up to a maximum before a decrease in efficiency occurs with further chitosan increase. The effect of pore size on cell recovery was influenced by the medium wetting properties. Across all chitosan concentrations, bubbles generated from the 25 μm pore mesh produced the lowest efficiency. As the mesh pore size increased to 50, 75 and 100 microns respectively, efficiencies were comparable but dropped slightly with further pore size increase to 125 μm. The difference can be clearly observed outside the optimum chitosan concentration.
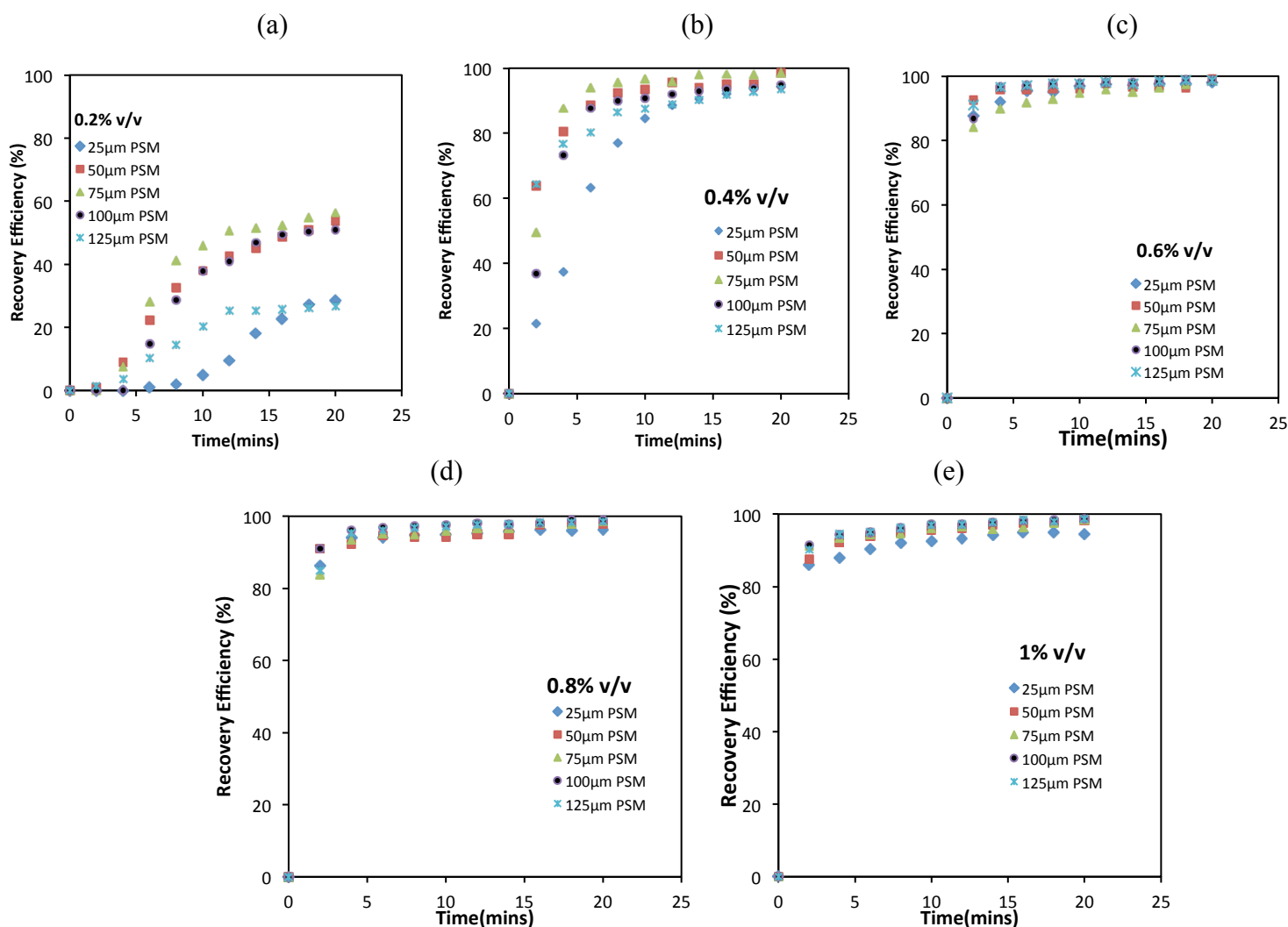
Figure 7.4: Plots of recovery efficiency with time at pH 7 under varying membrane pore sizes and chitosan concentrations of: (a) 0.2 %v/v (b) 0.4 %v/v (c) 0.6 %v/v (d) 0.6 %v/v (e) 1 %v/v. Increase in efficiency is observed as coagulant concentration increases up to a maximum before a decrease in efficiency occurs with further chitosan increase. The effect of pore size on cell recovery was influenced by the medium wetting properties. Across all chitosan concentrations, bubbles generated from the 25 μm pore mesh produced the lowest efficiency. As the mesh pore size increased to 50, 75 and 100 μm respectively, efficiencies were comparable but dropped slightly with further pore size increase to 125 μm. The difference can be clearly observed outside the optimum chitosan concentration.

7.4   Effect of Chitosan dose

The influence of chitosan on the performance of yeast separation was investigated by varying the concentration of chitosan in the medium. The results are presented in figure 7.5. At pH 5, recovery efficiency improved with increase in chitosan concentration from 9% at 0.2% v/v to ~99% at 0.4% and 0.6% v/v similarly before slightly dropping at 0.8% v/v to 98%. Further decrease in efficiency to ~88% was recorded at increased

131

chitosan concentration of 1% v/v. Overall, separation efficiency increased with increasing chitosan dosage up to a maximum before dropping with further dosage.

The success of flotation separation is largely dependent on the mechanisms governing particle-bubble interaction. Separation or collection efficiency as proposed by Derajguin and Dukhin (1987) is a product of three sub-steps viz; particle-bubble collision, attachment and the aggregate stability efficiencies. Ideally, the product of these three processes must be or approaches unity for optimum collection efficiency (i.e. successful cell harvest). In practice, collision and attachment efficiencies are connected through the drainage and rupture of the thin liquid film separating the particle and bubble but are however independent steps that are usually considered separately. While collision efficiency (E_c) is a function of the ratio of particle size to bubble size (Yoon 2000) and thus relatively low for small particles and coarse bubbles, attachment efficiency (E_a) is mainly influenced by particle zeta potential and floc size (Hewitt et al., 1994; Yoon 2000; Dai et al., 2000). Nonetheless, stability efficiency (E_s) is largely dependent on inertial force and system hydrodynamics in the flotation cell (Yoon 2000). Given conditions when collision efficiency is unity, attachment and stability efficiencies become the rate limiting factors. Therefore, increase in chitosan concentration, increases particle hydrophobicity as well as particle size and consequently, attachment and stability efficiencies increase (Hewitt et al., 1994). But at low concentrations however, attachment and stability efficiencies become less than unity and resultantly, recovery efficiency drops.

Furthermore, when the repulsive forces that exist due to the presence of the double layer are high, colloidal particles will repel each other and hence prohibit agglomeration. In such an instance, the particle must be destabilized by pre-treatment through one of the four known destabilization mechanisms for colloids. The energy forces between colloidal particles must be balanced for optimum agglomeration of particles. In the presence of enough counter ions, colloidal particles become electrically neutral (Iso-electric point). Under this state, optimum flocculation can be expected. Contrarily, insufficient flocculant dose often leads to partial particle destabilization and ultimately poor floc formation. On occasion, some particles still remain completely stabilized in the liquid medium. This explains the low recovery efficiency obtained at chitosan concentration dose of 0.2% v/v (see Fig 7.3a and 7.4a). By converse, over-dosing with

chitosan is similarly counter productive as it gives rise to charge reversal or polymer fold-back. To investigate this hypothesis, tests were conducted under pH 5 and 7 with incremental chitosan addition until efficiency began to drop (see Fig. 7.5). Excessive chitosan dosage re-stabilizes particles. Cheng et al., (2005) reported a similar observation and suggested particle re-suspension was due to the reversal of surface charge at higher doses. Similarly, results at neutral pH showed increase in harvesting efficiency as chitosan dosage increased. However, pH 7 revealed a rather higher tolerance for flocculant concentration (Fig. 7.5). This outcome corroborates the findings of Cheng et al., (2005) with recovery of organic matters from brewery wastewater. Divakaran and Pillai (2001 and 2002) also reported that particles exhibited a higher tolerance for chitosan flocculation at pH 7 as well as optimum algal removal efficiency under the same pH state.
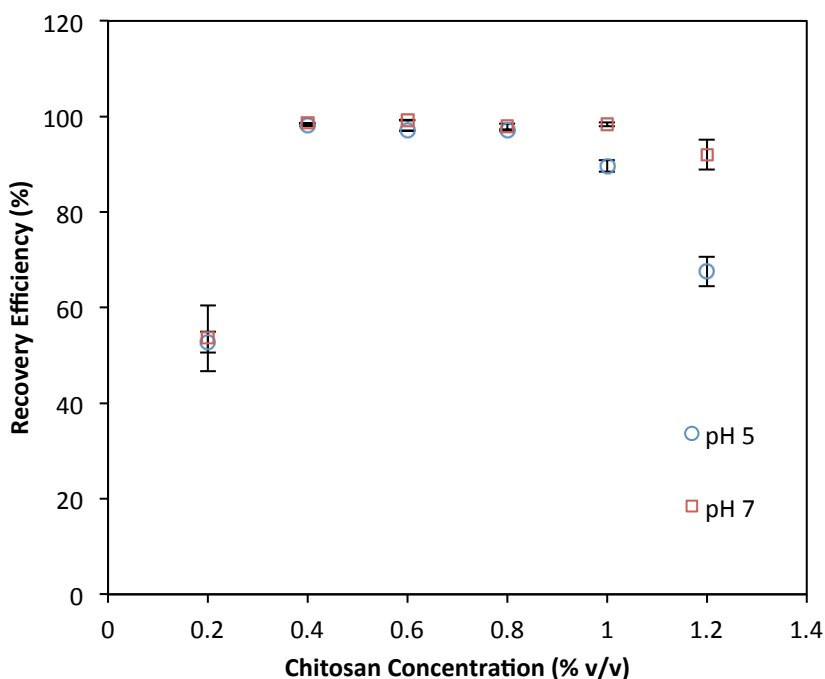
Figure 7.5: Effect of chitosan dose on yeast cell recovery efficiency across pH 5 and 7. Recovery efficiency increased with chitosan dose up to an optimum concentration. The optimum chitosan concentration ranged from 0.4 to 0.8 % v/v for pH 5 and efficiency remained rather constant within this range. Drop in efficiency occurred however beyond the optimum chitosan concentration. This trend is comparable with pH 7 but pH 7 showed a wider optimum chitosan concentration range (0.4 - 1.2% v/v). Beyond the optimum chitosan concentration however, efficiency was also observed to drop with further chitosan addition. The error bar represents standard error.

7.5   Effect of pH

Unarguably, pH can be a rate-limiting factor in particle separation from an aqueous solution. As with other coagulant and flocculants, the performance of chitosan as a bioflocculant is highly influenced by medium pH (Fig. 7.3 and 7.4). Acidic and neutral pH conditions favored cell harvest more than alkaline states. Recovery efficiency results reaching 99% was obtained under both acidic and neutral pH states. By converse however, no significant separation was recorded as pH became alkaline.

The pH effect can be attributed to the protonation difference of the amine groups and changes in the macromolecular chain conformation of chitosan. Solubility of chitosan varies with pH, giving rise to a difference in the distribution of the acetyl groups, which is crucial in defining the interactions with negatively charged cells. Chitosan is a positively charged polymer at pH lower than its pKa (6.4) (Aranaz et *al.*, 2009), in these conditions negatively charged cells bind easily to chitosan. pH affect not only the size but the structure of flocs (see Fig. 7.6). In neutral pH, chitosan due to its coiled structure, generates larger and denser flocs (Fig. 7.2). Conversely under acidic state, the biopolymer has increased charge density and extended chain and as such generates relatively smaller, largely less dense flocs (Huang et al. 2012). Given their hydrophobic nature and unstable intervening thin liquid film, the flocs generated are readily susceptible to aggregation with microbubbles. Yoon and Luttrell (1989) provide experimental evidence to show that the formation of a three-phase contact line is short for hydrophobic particles since the liquid film rupture time is approximately 10^{-9} s. Additionally, Hewitt et al., (1994) experimentally showed that attachment efficiency (E_a) increases with increasing particle hydrophobicity.

(a)　　　　　　　　　　　　　　　　　　　(b)
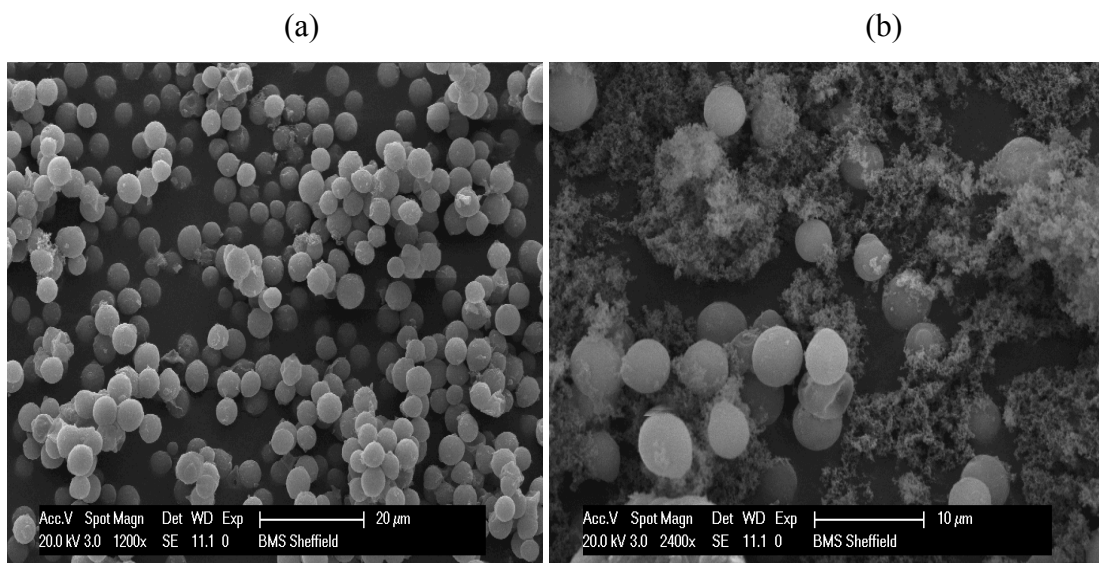
Figure 7.6: SEM photomicrograph of yeast cells. (a) Reconstituted yeast cells. (b) Yeast cells with the bioflocculant-Chitosan at pH 7.

A completely different outcome however, was observed under pH 9 where no significant yeast cell recovery was recorded across the different chitosan doses. One reason for this outcome is the gelatinous flocs formed. Gelatinous flocs have been widely reported at higher pH levels (Gochin and Solari 1983; Hanotu et al., 2012). Generally, gelatinous flocs often have slight negative charge and high affinity for the containing medium (aqueous phase). Apart from being hydrophilic, gelatinous flocs have slippery surfaces and the intervening liquid sheet existing between a particle and bubble is usually stable with hydrophilic surfaces (Miettinen et al., 2010), leading to no liquid film drainage and reduced attachment efficiency and consequently decreased collection efficiency. Even in rare instances when collision occurs, hydrophilic particles do not adhere to the surface of air bubbles (Yoon 2000). Gochin and Solari (1983) using dissolved air flotation (DAF) also reported that hydrophilic quartz particles or flocs would not be recovered. Their dispersion is stabilized by hydration and as such are thermodynamically stable. Agglomeration of hydrophilic colloids requires the significant dosage of ions, which compete for water molecules with the colloids, thereby causing dehydration of the colloidal particles.

7.6　Effect of bubble size

The mean bubble size result presented in Fig. 7.1 showed that average bubble size was influenced by the liquid type and varied directly proportionate to diffuser pore size. The

effect of bubble size on recovery efficiency was investigated and the result presented in Figure 7.7.
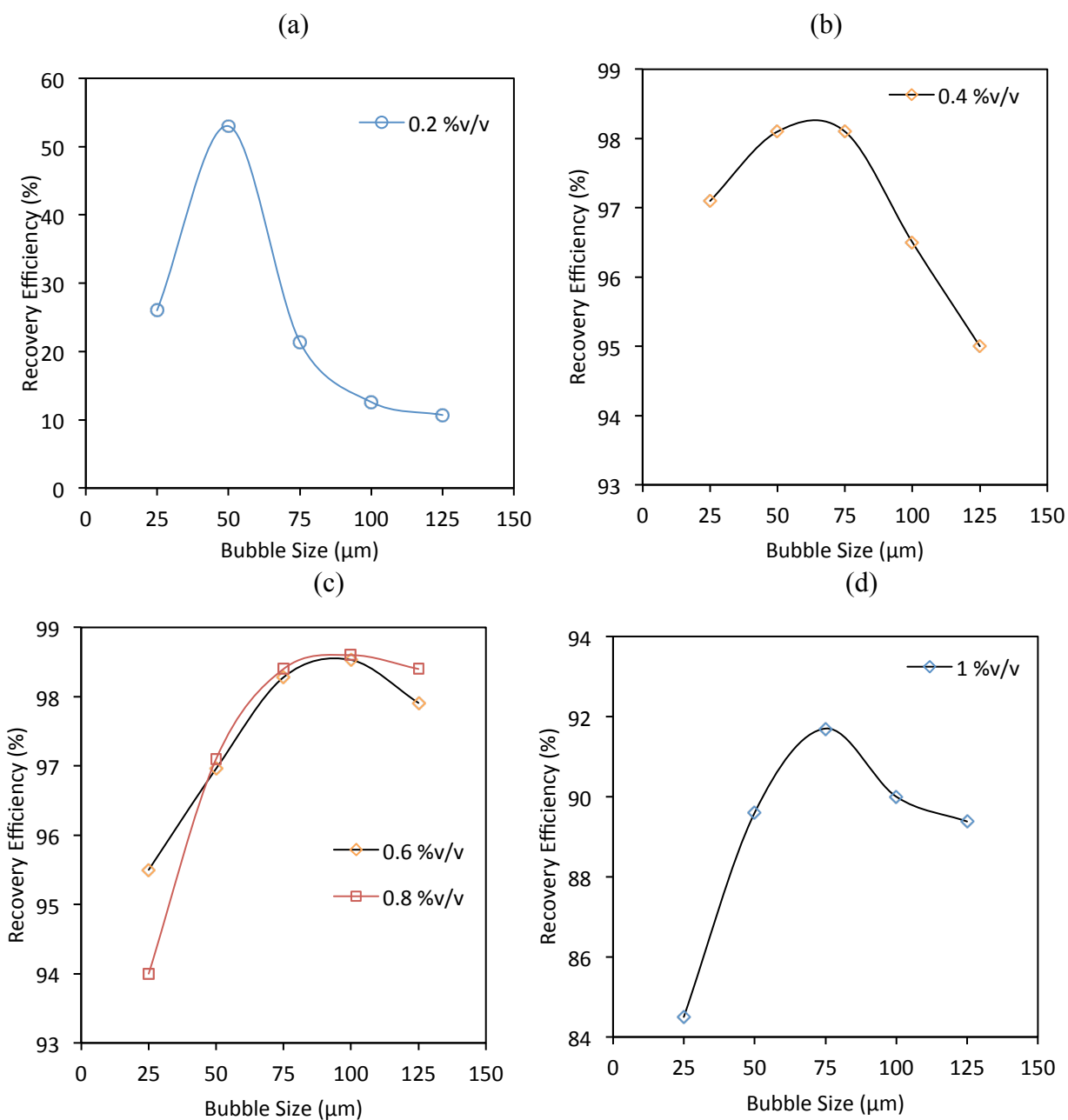
Figure 7.7: Plots of recovery efficiency against bubble size and varying flocculant concentrations. (a) 0.2% v/v- (b) 0.4% v/v (c) 0.6% v/v; 0.8% v/v; 1% v/v. (a) Low concentration of flocculant yields increase in recovery efficiency as bubble size increases and eventually decreases with increasing bubble size. The poor flocculation of cells and the resultant small flocs is the reason for this outcome. Generally, when small flocs are formed separation with larger bubbles is ineffective. Conversely, the low rise velocity of smaller bubbles results in increase residence time and consequently decrease in recovery efficiency. (b) Although the floc size marginally increases, a slight increase in recovery efficiency as flocculant dose increases is observed. (c) As floc size increases with further flocculant dosage, recovery efficiency favors relatively larger bubbles.

From the results, recovery efficiency was influenced by bubble size but also important was effect of the particle size. It might seem that under the influence of the high bubble density formation the underlying principles of effects of bubble-particle induction time can be neglected due to increased probability of collision. The experimental results above suggest otherwise. Particle/floc size is essential in determining the average bubble size required for a flotation (Yoon 2000). But it is dependent on flocculant concentration as is the recovery efficiency. Note how for a given floc size (Fig 7.7), efficiency generally increases with bubble size to a maximum before gradually dropping with further increase in bubble size. One main justification for this outcome is the low terminal rise velocity of microbubbles, which is intrinsically linked to their low buoyancy as well as size but also influential, is the changing floc size at varying flocculant concentration.

At reduced chitosan concentration (Fig 7.7a), small flocs (see Fig 7.2) are produced due to insufficient counter ions necessary for particle destabilization. Particle aggregation is largely low given this condition, yielding relatively small, loose and less dense flocs. Thus, recovery efficiency favours smaller microbubbles (<70 μm) because smaller microbubbles are gentler with small, loose and less dense flocs for their collision kinetic energy is too small to distort or break the flocs. Also, the probability of particle-bubble collision is a function of the ratio of particle to bubble size and varies indirectly with bubble size for small particles (Yoon 2000). Under this condition where particle density approaches density of surrounding fluid, long range hydrodynamic interaction (LRHI) - dominant force governing bubble-particle collision mechanism for relatively small particles - influence dominates particle-bubble collision mechanism and therefore dictates the trajectory of the particles with respect to the fluid streamlines (Miettinen et al., 2010).

However, as the (particles) flocs increase in size and become denser with higher flocculant dose (see Fig 7.7b graph: 0.4 %v/v), the optimum recovery efficiency shifts towards relatively larger microbubbles (~70-90 μm). Inertial forces become the influential collision mechanism given the inability of coarse and dense flocs to follow fluid streamlines and also given that their densities are greater than the containing medium, they posses a settling velocity which deviates their trajectory from the fluid streamlines (Miettinen et al., 2010). Microbubbles experience a tangential stress due to

this settling velocity (Ralston et al., 1999). Furthermore, this stress decelerates bubbles, ultimately causing their terminal rise velocity to approach that of a solid sphere and as consequence resulting in an increase in particle-bubble residence time. This is a key reason for the low efficiency below the bubble size range 70-90 μm for the same time. Above this range, however, the recovery efficiency drops as the size ratio of particle to bubbles becomes low due to the increased bubble size.

Boussinesq (1885) first described the tangential stress effect on microbubble as 'surface viscosity'. Velocity results less than those predicted by Stokes' law were reported by Takahashi (2005) when the author studied the rise velocity of bubble swarm (10-55-μm) produced by a vortex in distilled water. Subsequent investigation by Kelsall et al. (1996) for bubble swarms in water agree with Levich's (1962) condensation of Hadamard-Rybczynski equation and those of electrolytically generated bubbles of oxygen in 10^{-4} M NaClO$_4$ solution.

Auspiciously, as microbubble size increases, their buoyant force increases consequently and balances out this tangential stress. In other words, larger bubbles experience less tangential stress for a given particle size. Therefore, further increase in flocculant concentration (Fig. 7.7c: 0.6 and 0.8 %v/v) results in much coarser and denser flocs and again, efficiency is observed to shift favourably towards relatively large bubbles (90-100 μm). A limit is reached nonetheless, where further flocculant addition yields no more increase in floc size. Beyond this limit actually (Fig. 7.7d: 1% v/v), overdosing occurs due to excess flocculant concentration and resultantly, floc size significantly reduces. Therefore, optimum efficiency tips back towards smaller microbubbles (70-90 μm) again. Excessive flocculant dosage contributes to particle re-suspension and reduction in process efficiency (Huang et al. 2012). Note however, that whilst the critical coagulant concentration (CCC) is reached at 8% v/v for pH 5, pH 7 shows a higher tolerance for flocculant dose (see Fig. 7.5).

7.7   Effect of harvest method

In order to explore the effectiveness of Microflotation against a control, tests were set up with and without bubbles to simulate flotation and sedimentation separation

techniques respectively. Figure 7.8 displays the optimal results for either technique under the three (3) pH states.
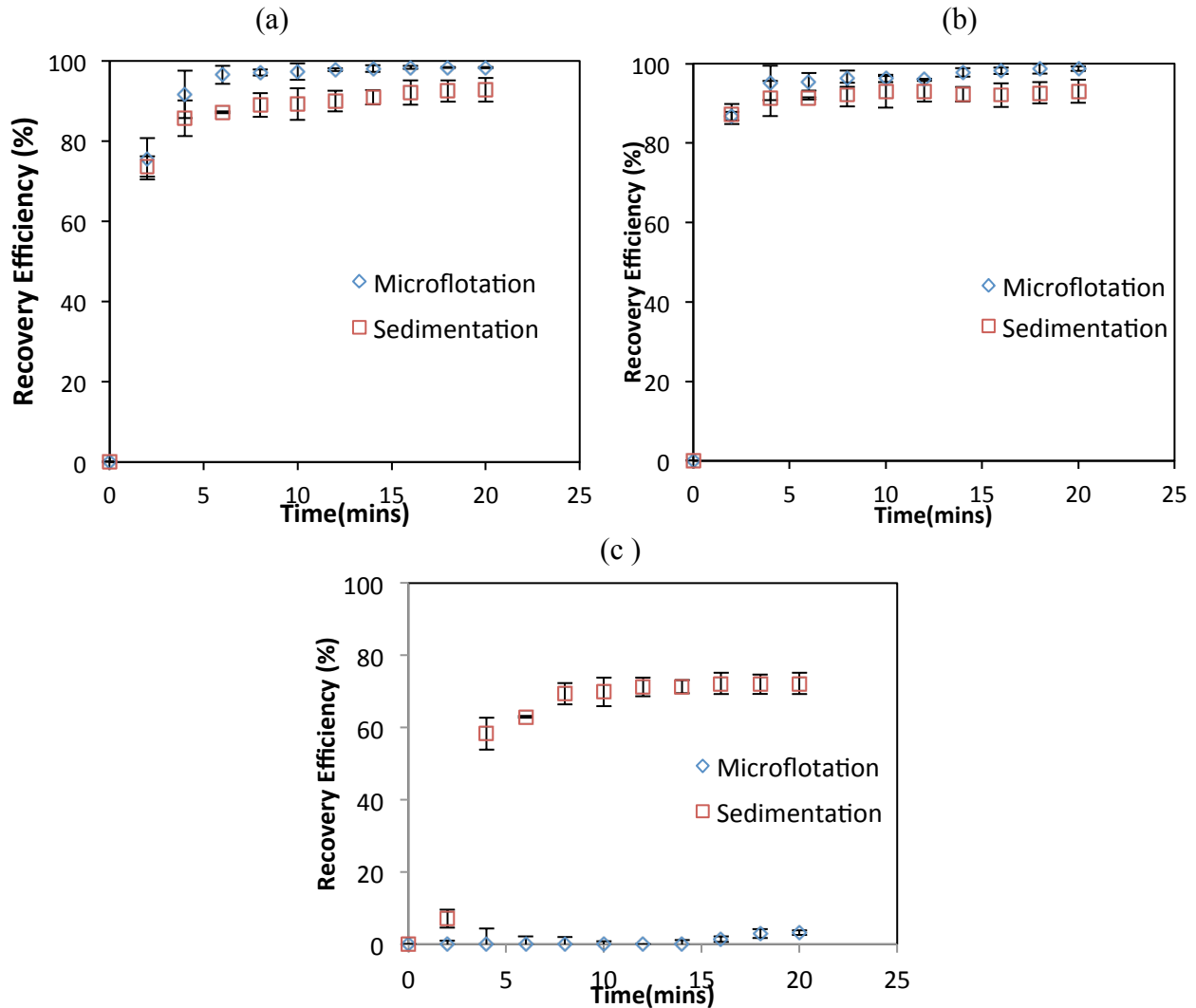
Figure 7.8: Comparison of recovery efficiencies with time of yeast cells between two separation techniques: Microflotation and Sedimentation at varying pH conditions. (a) pH 5 (b) pH 7 (c) pH 9. The results from pHs 5 and 7 are comparative. Higher recovery efficiency was obtained with microflotation than sedimentation to the tune of 6% under either pH state. Under pH 9, no significant separation was recorded (with the introduction of microbubbles) due to the gelatinous hydrophilic flocs formed. Collision and attachment probability is low with hydrated colloids. Therefore, recovery by sedimentation yielded higher efficiency. It is worth noting however, the overall drop in recovery efficiency under alkaline pH.

Yeast recovery by Microflotation and sedimentation was 98% and 93% at pH 5 and 99% and 93% at pH 7 respectively but at pH 9, Microflotation yielded no significant separation whilst sedimentation resulted in 72% recovery efficiency.

Bubble based separation systems are preferred over their non-bubble based counterparts primarily because, particle sedimentation velocity is substantially lower than their rise velocity when attached to bubbles. Thus, flotation improves separation by enhancing buoyancy force over sedimentation. Also, unlike sedimentation where some particles cling and remain attached to the flotation cell wall, microbubbles ensure a clean sweep of particles along their path. Another advantage over sedimentation is the sludge moisture content level after harvest. Moisture content measurement (see Fig 7.9) of recovered yeast cells showed a reduced water amount with the microflotation-harvested cells than with cells allowed to sediment. As they rise, microbubbles transport the attached flocs and dispatch the floc particles at the liquid-air interface to initiate formation of the cell (sludge) blanket layer. Once formed, microbubbles continue to transport attached flocs to thicken the blanket but also begin to compress and compact this cell blanket layer, thereby thinning it (forming a closed packed bed). When fully thinned, further injection of microbubbles accumulate at the rear of the blanket layer, so that the layer becomes suspended in the foam structure rather than immersed in the liquid continuous phase as is the case with sedimented cells. Hanotu et al. (2012) reported a similar occurrence for algae. Moisture content results for cells harvested with microbubbles is ~ 7% less than cells harvested by sedimentation. The significance of this result is obvious when further processing is required. Dewatering is one such example particularly in cases where yeast cells are needed just as 'cream yeast'. Alternatively, heating can be employed for cell drying. The difference in moisture content between sedimentation and microflotation-harvested cells can represent significant energy savings especially for large-scale productions. Microflotation facilitates dewatering through thickening and thinning of the sludge blanket.
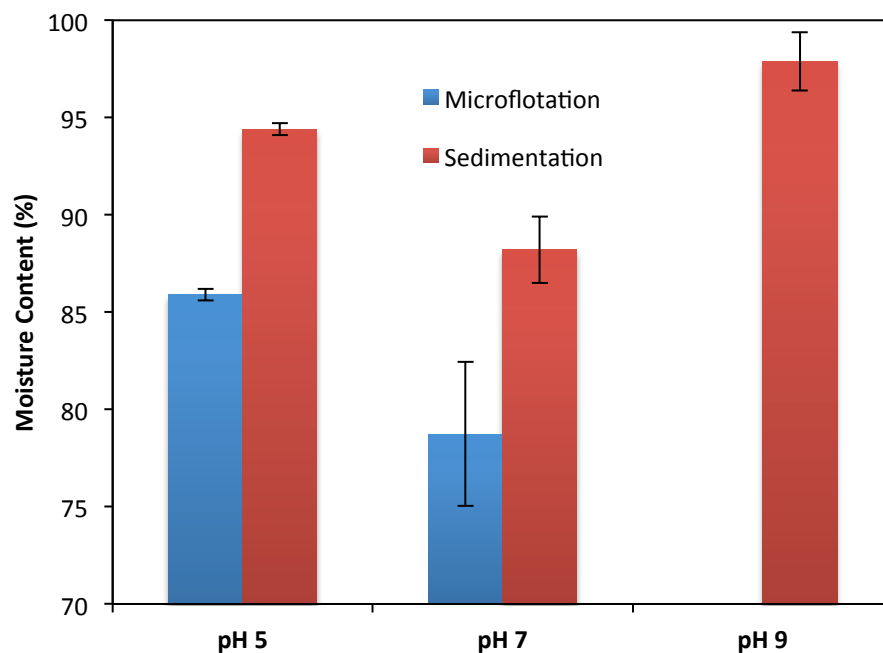
Figure 7.9: Moisture content results of harvested cells for two recovery techniques: microflotation and sedimentation. Neutral pH condition yielded lower moisture content than acidic conditions due to the relatively larger and coarser flocs formed under neutral pH. Under alkaline condition, highest cell moisture content was obtained because the gelatinous nature of flocculated cells. For each pH condition however, higher moisture content was measured for cells allowed to separate by sedimentation. Note that only results under pH 5 and 7 for cell recovery with microbubbles are shown here as no significant cell recovery with bubbles was achieved under pH 9.

7.8   Summary

The recovery of yeast from growth medium has been investigated using Microflotation. Microbubbles generated with the fluidic oscillator increased as diffuser mesh pore size increased. The effect of pH, Chitosan concentration on the recovery efficiency of yeast has been reported as well as the effect of bubble size and the comparison between microflotation and sedimentation as separation techniques.

Size, density and hydrophobicity of flocs are all characteristics that can be affected by both the medium pH and the flocculant concentration. The medium pH is an essential parameter in cell flocculation. Acidic and neutral conditions are favourable for flotation but alkaline conditions are less so due to the nature of flocs generated. Use of chitosan as a flocculant proved effective. Recovery efficiency is a function of chitosan concentration and varies directly with increased dosage until a critical concentration is attained before decrease in efficiency occurs.

Bubble size affect recovery efficiency in a different way. For smaller particles, separation efficiency is more effective with small bubbles because of the increased collision probability. As particle size increases, the tangential stress imposed by the particle on the bubble increases, consequently bringing about a decrease in the terminal rise velocity of the bubble as well as a corresponding increase in its residence time. Therefore, recovery efficiency becomes low. As the bubble size increases, their buoyant force balances out the tangential stress for the given particle size, and as such, optimum recovery efficiency is obtained. Further increase in bubble size results in reduced collision efficiency with particles and as such, low recovery efficiency. Thus, below or beyond the critical bubble-particle ratio, efficiency becomes less optimal.

Bubble based techniques facilitates recovery of cells from solution compared to non-bubble based systems because sedimentation velocity of particles is lower than the rise velocity of the particle-bubble aggregate. Another advantage with bubble based separation technique is the decrease in cell moisture content after recovery, which could significantly cut down cost of drying.

The selection of a suitable harvesting and dewatering method is critical to the economic production of yeast for various applications. It is expedient to have a concentrated and uncontaminated yeast biomass after harvesting. The non-intrusive approach of the fluidic oscillator mediated microflotation is essential and could be employed to achieve both desired end products. And in the event of medium reuse, recycling can be done to save cost. Apart from the low pressure usage of this technology relative to DAF, the system can process high culture volumes in a continuous state operation, which makes it conveniently suitable to scale-up if large commercialisation is sought. Although the study conducted here was of lab bench scale in the bubble column, large lab bench studies on using fluidic oscillator microbubbles with off-the-shelf diffusers have shown similar bubble size distributions and much higher bubble flux rates, indicative that microflotation will scale up industrially.

Chapter 8

CONCLUSIONS AND FUTURE PERSPECTIVES

This chapter presents the main findings and conclusions of this research study and also the future perspectives for further research works. The main findings are chapter specific and are therefore found in their respective chapters. Here, an attempt is made to synthesize these findings to address/answer the research questions.

8.1   General Conclusions

The study was set out to design a microporous diffuser system to be equipped with a fluidic oscillator for microbubble generation and also, apply the microbubble unit in the flotation separation of particles or oil. The conventional (non-bubble based) separation techniques in general are only suitable for solids separation and relatively inefficient with finer particles. In addition to that, they are limited to batch-scale production and unable to scale to industrial requirements for continuous production. Flotation (bubble based) separation systems were developed as solutions to these disadvantages but their methods of bubble generation where efficient, are unfortunately energy intensive, accounting for ~90% of the total operating cost in a flotation plant. The study therefore sought to address the challenges associated with conventional flotation systems by designing and developing a Microflotation unit that features a microporous diffuser in a flotation column powered by a fluidic oscillator. The study also sought to know whether the Microflotation system can meet the required bubble size target for flotation as well as achieve the separation of both colloidally dispersed oil or particles from a liquid medium. Therefore a substantial amount of information/data from both published literatures and laboratory tests were gathered culminating in the development of the Microflotation system.

The literature review in *Chapter 2* starts with a detailed analysis of colloidal particles and their physical characteristics in liquid media. Subsequently, the zeta potential was mentioned, as its role in particle charge is critical for particle-particle and particle-bubble agglomeration is essential. A review of the separation techniques showed that two groups of separation approaches exist for particle or oil removal. The first excludes the use of bubbles, hence the name – non-bubble based techniques. On the

other hand, the bubble based techniques support the application of bubbles. From the review, key examples of non-bubble based separation techniques were outlined, viz: centrifugation, filtration and sedimentation and subsequently reviewed in detail. Of key importance however, are the disadvantages mentioned of these separation techniques. Some of the main examples include: large footprint; relatively low recovery efficiency, increased recovery time, unsuitability for continuous large-scale production. Owing to these shortcomings the review revealed an industrial shift from non-bubble based systems to focus on their bubble-based counterparts as a solution.

Following the assessment of microbubbles and their general behavior in liquid, which is central to flotation practices, a critical review of the fundamentals of flotation was undertaken highlighting the relevant and most applied models. Each model focused on a different pertinent issue governing flotation, which generally underpinned the importance of bubble-particle collision, attachment and stability for successful collection. In addition, the models emphasized the importance of both bubble and particle size recovery and concluded that for a given mean particle size, separation efficiency is indirectly proportionate to bubble size.

The chapter further presented the different methods of bubble generation as well as the different flotation types. From the reviews, it was apparent that the success of flotation is intrinsically linked with the system efficacy to generate bubbles. Thus, the flotation systems were classified into two groups based on their bubble generation methods -high power and low power consumption systems. Both the advantages and the disadvantages of these systems were expounded. Regarding the disadvantages in particular, two problems were identified in relation to bubble formation: firstly, the high power consumption of existing flotation techniques and secondly, the inefficiency of the low power consumption systems to generate the target bubble size. It was reported that DAF uses ~6 bars to pressures air in water, which is a substantially high amount of energy. But another disadvantage less reported is the operation of the variable speed pumps in a DAF unit. Contrastingly, the low power consumption systems are inherently inefficient in generating microbubbles largely owing to three main problems, namely: wetting force, parallel percolation and diffuser surface characteristics.

The chapter finalizes by introducing the fluidic oscillator, an alternative bubble-generating device with the promise of energy efficiency. A review of its main features was presented, as was its mode of operation and previous applications. Importantly, the study highlights the potential of the fluidic oscillator system to meet the challenges of traditional flotation systems and argued for its inclusion as part of a flotation system.

The experimental materials and methods were presented in *Chapter 3*. Given the importance of size in separation, it was essential to characterize both the bubble and particle sizes. Therefore, the chapter was structured into three key parts. The first section dealt with the characterization of bubbles. Two different methods - optical and acoustic method - were employed for bubble size measurement but the optical method was mainly used due to some technical issues with the acoustic method in course of the study period. The performance of several microporous diffusers both bespoke and off-the-shelf was evaluated with and without the fluidic oscillator. The other aspect mentioned in this section is the frequency of oscillation measurement with the aid of an accelerometer. In the second section, the methodologies for particle analysis were presented. Particles/oil samples were analyzed for size under varying pre-treatment conditions such as coagulant concentrations, pH using the Mastersizer. Zeta potential an essential parameter influencing particle agglomeration was assayed using the ZetaPALS under varying experimental conditions, namely pH and growth phase.

The chapter concluded with the protocol for Microflotation separation for all three applications (Oil, Algae and Yeast). The steps taken in estimating the recovery efficiency were clearly outlined. Also important was the comparison in recovery efficiency and moisture content for samples separated by sedimentation and microflotation.

The first experimental results were presented in *Chapter 4*. The chapter explored the effectiveness of both off-the-shelf and bespoke diffusers in the generation of microbubbles. Generating ~ 100 μm bubbles is not without difficulty and one main reason for this is attributed to the diffuser membrane surface properties. The second is the coalescence of bubble as a result of the diffuser pitch size. Low pitches resulted in

increased bubble-bubble interaction. Another reason for generating coarse bubbles is that conventional diffusers are susceptible to maldistribution and subsequently, increased coalescence due mainly to the nature of the diffuser plenum chamber. While the first problem was solved by simply oscillating the air supply, the others required a different approach. Thus, the solution was to design a diffuser, to address the problem due to maldistribution whilst also achieving the target bubble size range. This was done by fitting the plenum chamber with internal distributor vanes along which are orifices from where the airflow emerges. Given this condition, improved air supply across the diffuser surface was achieved. It was found that compared to traditional bubble generation techniques, diffusers equipped with the fluidic oscillator generated relatively smaller bubbles of the scale of the exit pore. Furthermore, the frequency of oscillation was found to vary directly proportionate to air supply flow rate and inversely with feedback loop length. Bubble size varied proportionate to diffuser membrane pore size and the supply flowrate.

Having generated microbubbles and obtained the optimum operating conditions, microbubbles by fluidic oscillation, the result from the previous chapter on bubbles was chosen for application in separation.

In *Chapter 5*, the study explored the feasibility of fluidic oscillator powered flotation column (Microflotation) for the treatment of oil-contaminated water. It was found that the application of microbubbles is a separation intensification process over sedimentation and the use of coarse bubbles. Results showed separation efficiency of 91%, 77% and 14% with microbubbles, sedimentation (no-bubble) and fine bubbles respectively. Furthermore, the presence and concentration of surface-active agents was found to influence the size distribution of oil droplets in the emulsion and consequently, the separation efficiency. Increase in surfactant concentration resulted in decrease in oil droplet size, thereby leading to a decrease in separation efficiency. Highest oil separation result was recorded at lowest (0.3 wt%) surfactant concentration whilst the least result was obtained at highest (10 wt%) surfactant concentration.

The results of the investigations on the performance of Microflotation for algal recovery were presented and discussed in *Chapter 6*. The performance of samples

treated under different metallic coagulant types were evaluated in terms of recovery efficiency, optimum coagulant dosage and pH effect followed by a comparison of the cost of coagulant. The pH influence on separation was investigated by varying solution pH. The result showed highest recovery efficiency under acidic conditions for all three metallic coagulants tested. Optimum recovery efficiency was obtained at pH 5 whilst the lowest was obtained at pH 7, 8 and 9 for Aluminum, Ferric sulphate and Ferric chloride respectively. Basically, Aluminum sulphate exhibited a non-monotonic trend across the pH levels tested. Ferric sulphate also revealed a similar outcome. However, the recovery efficiency trend with Ferric chloride showed a rather monotonic response across pH.

Another factor that influenced algae separation from the liquid medium is the concentration of the coagulant. Different coagulant dosage levels were tested for all three coagulants and pH regimes. It was observed that at low coagulant dose, separation efficiency was lowest. The justification provided for this outcome is that charge neutralization of particles requires substantial amount of counter ions without which, particle charge will only be partially neutralized, and hence particle agglomeration is low. Given this condition, particle-bubble attachment will be low. Conversely, as coagulant dose increased, separation increased consequently due to the presence of sufficient counter ions, giving rise to larger, denser flocs. Overall, the result from chapter 6 highlighted that separation of microalgae is dependent on both medium pH and coagulant concentration but more importantly, Microflotation proved effective in the separation of algae from an aqueous solution.

In *Chapter 7*, the result of the performance of Microflotation for yeast harvest was reported. Particle size measured under cells inoculated at pH 5 and 7 showed an increase in mean particle size for cells at pH 7 than pH 5. It was also found that increase in chitosan concentration resulted to an increase in particle size until a critical concentration was reached before a decrease in particle agglomeration was observed. This behavior was also reflected in the recovery efficiency. Recovery efficiency increased with increasing particle size until the critical flocculant concentration before a decrease was eventually recorded.

Then, microbubbles generated by fluidic oscillation was applied in the recovery of yeast from culture medium. It was found that recovery efficiency is a function of both the bubble size and particle size. For small particles, recovery efficiency favored relatively smaller bubbles otherwise, efficiency increased with bubble size. Particle-bubble interaction is dependent on the nature of the particles. Hydrophobic particles were more likely to adhere to bubbles than hydrophilic particles. Under acidic pH, particles were found to be hydrophobic and as such, bubble-particle collection was unity. The same was true for recovery under neutral conditions. Thus recovery efficiency result recorded under both medium pH conditions reached 99%. But under pH 9, particles exhibited hydrophilic tendencies and consequently, recovery efficiency with bubbles was decreased.

Finally, a comparison of recovery efficiency between bubbles and sedimentation was made and the result showed a slight increase in recovery efficiency with bubbles over sedimentation. This slight increase was attributed to the size of the yeast cells (~20 μm), which favored sedimentation. Moisture content results revealed however, a decrease in moisture content of the harvested cells (~ 7 %) less moisture for cells harvested by Microflotation than sedimentation.

8.2:   Future Works and Perspectives

Results from this study have shown the efficiency of the fluidic oscillator driven flotation system in the production of microbubbles of the size range of the exit pore and its effectiveness in the recovery of colloidal oil/particles with significant improvement over steady flow bubble generation method. Following the findings from this work, there are a several areas requiring further investigations.

Owing to the fact that this research work was limited to oil and cell recovery from the liquid medium, it is recommended for future study, to investigate the application of Microflotation on the recovery of minerals such as quartz, clay e.t.c to improve our understanding of the system robustness and versatility. It is also important to conduct comprehensive study on the energy consumption aspect of the fluidic oscillator and draw comparisons with the energy requirements of a DAF unit. The application of Microflotation for the removal of pigments, ink, fibers and heavy metals from water

should be explored in future works. Given the large effluent generated from restaurants and the paper industry, the treatment of restaurant wastewater and also treatment of wastewater from paper industry using Microflotation is worth exploring.

Investigating the performance of Microflotation for various species of algae, yeast, bacteria cells and other marine organisms of high economic value would make a valuable contribution to the energy sector and other industries. Thus effect of varying flowrate, cell growth phase should be investigated to obtain best recipe for cell harvest. Furthermore, selective harvesting should be attempted with Microflotation for conditions where heterogeneous cell communities exist in a medium. Also, more investigation should be aimed at exploring the use of other flocculating and coagulating agents. Development into the use of high performance polymers and bioflocculants could prove useful in flotation. More work is needed to improve our understanding of the best operating conditions such as flocculating time, flocculant concentration, pH effect and effect of medium composition on the recovery efficiency of particles.

Owing to the role bubble size plays in flotation, future works should explore the generation of microbubbles with more membrane types and pores sizes. Also, it would be interesting to study the effect of varying membrane properties such as varying the membrane hydrophobic and hydrophilic levels. The other aspect worth considering is to explore the different configurations of the fluidic oscillator. Altering the volume of the fluidic oscillator attachment wall, as well as varying the length of the feedback loop lengths are all essential options that would improve our understanding of bubble generation by oscillation. Another option worth investigating is to explore bubble generation using different oscillator design.

Diffuser design is an important aspect in microbubble production. One of the challenges encountered in this study is the low volumetric flowrate through the diffuser. Given that bubble flux and size are key rate limiting parameters, it would be beneficial and essential to explore efficient diffuser designs to achieve high bubble flux without compromising the desired bubble size. Another option is to test and analyze the performance of more off-the-shelf diffusers.

Ultimately, the aim of an engineering project is continuous large-scale production. Following the results of this study, subsequent works should be carried out on pilot scale with the aim of eventually scaling up to industrial requirements.

REFERENCES

ABRAHAMSON, J. 1975. Collision rates of small particles in a vigorously turbulent fluid. *Chemical Engineering Science,* 30**,** 1371-1379.

AHMED, N. & JAMESON, G. 1985. The effect of bubble size on the rate of flotation of fine particles. *International journal of mineral processing,* 14**,** 195-215.

AKAGI, Y., OKADA, K., KOSAKA, K. & TAKAHASHI, T. 1987. Liquid weeping accompanied by bubble formation at submerged orifices. *Industrial & Engineering Chemistry Research,* 26**,** 1546-1550.

AL-SHAMRANI, A. A., JAMES, A. & XIAO, H. 2002. Destabilisation of oil‚Äìwater emulsions and separation by dissolved air flotation. *Water Research,* 36**,** 1503-1512.

AL-SHAMRANI, A. A., JAMES, A. & XIAO, H. 2002. Separation of oil from water by dissolved air flotation. *Colloids and Surfaces A: Physicochemical and Engineering Aspects,* 209**,** 15-26.

AMRI, M. A., BONALY, R., DUTEURTRE, B. & MOLL, M. 1979. Interrelation between Ca2+ and K+ ions in the flocculation of two Brewers yeast strains. *European journal of applied microbiology and biotechnology,* 7**,** 235-240.

ANFRUNS, J. & KITCHENER, J. 1977. Rate of capture of small particles in flotation. *Trans. Inst. Min. Metal,* 86**,** C9-c15.

ARMENANTE, P. M. 2012. *Coagulation and Flocculation,* New Jersey, Accessed.

BEN-AMOTZ, A., GRESSEL, J. & AVRON, M. 1987. Massive Accumulation of Phytoene Induced by Norflurazon in Dunaliella Bardawil (Chlorophyceae) Prevents Recovery from Photoinhibition 1. *Journal of Phycology,* 23**,** 176-181.

BOLTO, B. & GREGORY, J. 2007. Organic polyelectrolytes in water treatment. *Water Research,* 41**,** 2301-2324.

BOUSSINESQ, V. 1885. Sur la resistance qu'oppose un liquide indefini en repos. *Acad Sci,* 100**,** 935-7.

CHEN, Y. L. 2008. *Preparation and Characterization of Water-Soluble Chitosan Gel for Skin Hydration.* Universiti Sains Malaysia.

CHENG, W. P., CHI, F. H., YU, R. F. & LEE, Y. C. 2005. Using chitosan as a coagulant in recovery of organic matters from the mash and lauter wastewater of brewery. *Journal of Polymers and the Environment,* 13**,** 383-388.

CHI, F. & CHENG, W. 2006. Use of Chitosan as Coagulant to Treat Wastewater from Milk Processing Plant. *Journal of Polymers and the Environment,* 14**,** 411-417.

CHLUP, P. H., BERNARD, D. & STEWART, G. G. 2008. Disc Stack Centrifuge Operating Parameters and Their Impact on Yeast Physiology. *Journal of the Institute of Brewing,* 114**,** 45-61.

CHOW, C., HOUSE, J., VELZEBOER, R., DRIKAS, M., BURCH, M. & STEFFENSEN, D. 1998. The effect of ferric chloride flocculation on cyanobacterial cells. *Water Research,* 32**,** 808-814.

CHOW, L. S. 2007. *Performance study on dissolved air flotation (DAF) unit and process performance improvement study in the physiochemical treatment of wastewater.* M.Eng, Universiti Teknologi Malaysia.

CLIFT, R., GRACE, J. R. & M.E.WEBER 1978. Bubbles, Drops and Particles. *Academic Press,London***,** 380.

COLLINS, G. L. 1975. *Dispersed air flotation of fine particles.* PhD, University of London.

CRINI, G. 2005. Recent developments in polysaccharide-based materials used as adsorbents in wastewater treatment. *Progress in polymer science,* 30**,** 38-70.

CRINI, G. & BADOT, P.-M. 2008. Application of chitosan, a natural aminopolysaccharide, for dye removal from aqueous solutions by adsorption processes using batch studies: A review of recent literature. *Progress in Polymer Science,* 33**,** 399-447.

CRITTENDEN, J. & HARZA, M. W. 2005. *Water treatment: principles and design*, John Wiley & Sons.

DAI, Z., FORNASIERO, D. & RALSTON, J. 2000. Particle-bubble collision models - a review. *Advances in Colloid and Interface Science,* 85**,** 231-256.

DAUER, R. R. & DUNLOP, E. H. 1991. High gradient magnetic separation of yeast. *Biotechnology and Bioengineering,* 37**,** 1021-1028.

DENGIS, P. B., NÉLISSEN, L. R. & ROUXHET, P. G. 1995. Mechanisms of yeast flocculation: comparison of top- and bottom-fermenting strains. *Applied and environmental microbiology,* 61**,** 718-728.

DERJAGUIN, B. V., DUKHIN, S. S. & RULEV, N. N. 1982. Kinetic Theory of the Flotation of Small Particles. *Russian Chemical Reviews,* 51**,** 51.

DERJAGUIN, B. V. 1993. Main factors affecting the stability of colloids. *Progress in Surface Science,* 43**,** 109-114.

DERJAGUIN, B. V. & DUKHIN, S. S. 1993. Theory of flotation of small and medium-size particles. *Progress in Surface Science,* 43**,** 241-266.

DESHPANDE, K. B. & ZIMMERMAN, W. B. 2005. Experimental study of mass transfer limited reaction,Part II: Existence of cross-over phenomenon. *Chemical Engineering Science,* 60**,** 4147-4156.

DESHPANDE, K. B. & ZIMMERMAN, W. B. 2005. Experimental study of mass transfer limited reaction,Part I: Use of fibre optic spectrometry to infer asymmetric mass transfer coefficients. *Chemical Engineering Science,* 60**,** 2879-2893.

DIVAKARAN, R. & SIVASANKARA PILLAI, V. 2001. Flocculation of kaolinite suspensions in water by chitosan. *Water Research,* 35**,** 3904-3908.

DIVAKARAN, R. & SIVASANKARA PILLAI, V. 2002. Flocculation of river silt using chitosan. *Water Research,* 36**,** 2414-2418.

DOBBY, G. & FINCH, J. 1987. Particle size dependence in flotation derived from a fundamental model of the capture process. *International journal of mineral processing,* 21**,** 241-260.

DUINEVELD, P. C. 1995. The rise velocity and shape of bubbles in pure water at high Reynolds number. *Journal of Fluid Mechanics,* 292**,** 325-332.

EDZWALD, J. K. 2010. Dissolved air flotation and me. *Water Research,* 44**,** 2077-2106.

ENGLERT, A. H., RODRIGUES, R. T. & RUBIO, J. 2009. Dissolved air flotation (DAF) of fine quartz particles using an amine as collector. *International Journal of Mineral Processing,* 90**,** 27-34.

FRUMKIN, A. & BAGOTSKAYA, I. Descent velocity of a mercury drop in a viscous medium. Dokl. AN SSSR, 1947. 135-140.

FUERSTENAU, D. 1980. Fine particle flotation. *Fine particles processing,* 1**,** 669-705.

FUERSTENAU, D. & WAYMAN, C. 1958. Effect of chemical reagents on the motion of single air bubbles in water. *Trans. AIME,* 211**,** 694-699.

GAUDIN, A. 1957. Flotation. *McGraw-Hill Book Company, New York,* 560**,** 157-162.

GAUDIN, A. M., SCHUHMANN, R. & SCHLECHTEN, A. W. 1942. Flotation Kinetics. II. The Effect of Size on the Behavior of Galena Particles. *The Journal of Physical Chemistry,* 46**,** 902-910.

GILMOUR, D., HIPKINS, M. & BONEY, A. 1982. The effect of salt stress on the primary processes of photosynthesis in Dunaliella tertiolecta. *Plant Science Letters,* 26**,** 325-330.

GLEMBOTSKII, A. V., EVTIKOVA, G. A., PETRUKHIN, O. M., MAROV, I. N., ZOLOTOV, Y. A., SPIVAKOV, B. Y. & SAVINTSEVA, Y. P. 1975. The reaction of chelate-forming reagents with minerals under flotation conditions. *Soviet Mining,* 11**,** 401-405.

GOCHIN, R. J. & SOLARI, J. 1983. The role of hydrophobicity in dissolved air flotation. *Water Research,* 17**,** 651-657.

GRAMMATIKA, M. & ZIMMERMAN, W. B. 2001. Microhydrodynamics of flotation processes in the sea surface layer. *Dynamics of Atmospheres and Oceans,* 34**,** 327-348.

GRATTONI, C., MOOSAI, R. & DAWE, R. A. 2003. Photographic observations showing spreading and non-spreading of oil on gas bubbles of relevance to gas flotation for oily wastewater cleanup. *Colloids and Surfaces A: Physicochemical and Engineering Aspects,* 214**,** 151-155.

GREGORY, J. 1998. The role of floc density in solid-liquid separation. *Filtration & Separation,* 35**,** 367-366.

GUDIN, C. & CHAUMONT, D. 1991. Cell fragility ‚Äî The key problem of microalgae mass production in closed photobioreactors. *Bioresource Technology,* 38**,** 145-151.

GUDIN, C. & THEPENIER, C. 1986. Bioconversion of solar energy into organic chemicals by microalgae. *Advances in biotechnological processes,* 6.

GUIBAL, E. 2004. Interactions of metal ions with chitosan-based sorbents: a review. *Separation and Purification Technology,* 38**,** 43-74.

HANLY, G., FORNASIERO, D., RALSTON, J. & SEDEV, R. 2011. Electrostatics and Metal Oxide Wettability. *The Journal of Physical Chemistry C,* 115**,** 14914-14921.

HANOTU, J., BANDULASENA, H. C. H. & ZIMMERMAN, W. B. 2012. Microflotation performance for algal separation. *Biotechnology and Bioengineering,* 109**,** 1663-1673.

HARPER, J. 1973. On bubbles with small immobile adsorbed films rising in liquids at low Reynolds numbers. *J. Fluid Mech,* 58**,** 539.

HATTI-KAUL, R. 2010. Downstream Processing in Industrial Biotechnology. *Industrial Biotechnology.* Wiley-VCH Verlag GmbH & Co. KGaA.

HERNLEM, B. & TSAI, L. S. 2000. Chlorine generation and disinfection by electroflotation. *Journal of food science,* 65**,** 834-837.

HEWITT, D., FORNASIERO, D. & RALSTON, J. 1994. Bubble particle attachment efficiency. *Minerals Engineering,* 7**,** 657-665.

HOOVER, R. & MALHOTRA, D. 1976. Emulsion flotation of molybdenite. *Flotation--A. M. Gaudin Memorial*.

HOSNY, A. Y. 1996. Separating oil from oil-water emulsions by electroflotation technique. *Separations Technology,* 6**,** 9-17.

HUANG, Z., LEGENDRE, D. & GUIRAUD, P. 2012. Effect of interface contamination on particle-bubble collision. *Chemical Engineering Science,* 68**,**

1-18.

HUNTER, R. J. 1981. *Zeta potential in colloid science: principles and applications*, Academic press London.

JAMESON, G., NAM, S. & YOUNG, M. M. 1977. Physical factors affecting recovery rates in flotation. *Minerals Science and Engineering,* 9**,** 103-118.

JIANG, L., KRASOWSKA, M., FORNASIERO, D., KOH, P. & RALSTON, J. 2010. Electrostatic attraction between a hydrophilic solid and a bubble. *Phys. Chem. Chem. Phys.,* 12**,** 14527-14533.

KELSALL, G. H., TANG, S., SMITH, A. L. & YURDAKUL, S. 1996. Measurement of rise and electrophoretic velocities of gas bubbles. *Journal of the Chemical Society, Faraday Transactions,* 92**,** 3879-3885.

KELSALL, G. H., TANG, S., YURDAKUL, S. & SMITH, A. L. 1996. Electrophoretic behaviour of bubbles in aqueous electrolytes. *Journal of the Chemical Society, Faraday Transactions,* 92**,** 3887-3893.

KIRBY, B. J. & HASSELBRINK, E. F. 2004. Zeta potential of microfluidic substrates: 1. Theory, experimental techniques, and effects on separations. *Electrophoresis,* 25**,** 187-202.

KIRBY, B. J. & HASSELBRINK, E. F. 2004. Zeta potential of microfluidic substrates: 2. Data for polymers. *Electrophoresis,* 25**,** 203-213.

KIHN, J. C., MASY, C. L. & MESTDAGH, M. M. 1988. Yeast flocculation: competition between nonspecific repulsion and specific bonding in cell adhesion. *Canadian journal of microbiology,* 34**,** 773-778.

KITCHENER, J. & GOCHIN, R. 1981. The mechanism of dissolved air flotation for potable water: basic analysis and a proposal. *Water Research,* 15**,** 585-590.

KOH, P. & WARREN, L. A pilot plant test of the shear-flocculation of ultrafine scheelite. Chemeca 80: Process Industries in the 80's; 8th Australian Chemical Engineering Conference, 1980. Institution of Chemical Engineers, Institution of Engineers, Australia and the Royal Australian Chemical Institute, 90.

KOURKOUTAS, Y., BEKATOROU, A., BANAT, I. M., MARCHANT, R. & KOUTINAS, A. A. 2004. Immobilization technologies and support materials suitable in alcohol beverages production: a review. *Food Microbiology,* 21**,** 377-397.

KURIYAMA, H., UMEDA, I. & KOBAYASHI, H. 1991. Role of cations in the flocculation of Saccharomyces cerevisiae and discrimination of the corresponding proteins. *Canadian journal of microbiology,* 37**,** 397-403.

LEVICH, V. 1962. Physicochemical Hydrodynamics, Prentice-Hall, Englewood Cliffs, NJ, 1962. *Chap. VI,* 60**,** 355.

LI, P. & TSUGE, H. 2006. Water Treatment by Induced Air Flotation Using Microbubbles. *Journal Of Chemical Engineering Of Japan,* 39**,** 896-903.

LIU, Q. & WANNAS, D. 2004. The Role of Polymeric-depressant-induced Flocculation in Fine Particle Flotation. *Particle Size Enlargement in Mineral Processing, Proceedings of the UBC-McGill Biennial International Symposium on Fundamentals of Mineral Processing 5th, Hamilton, Canada***,** 2-25.

LIU, S., WANG, Q., MA, H., HUANG, P., LI, J. & KIKUCHI, T. 2010. Effect of micro-bubbles on coagulation flotation process of dyeing wastewater. *Separation and Purification Technology,* 71**,** 337-346.

LOZANO-PARADA, J. H. & ZIMMERMAN, W. B. 2010. The role of kinetics in the design of plasma microreactors. *Chemical Engineering Science,* 65**,** 4925-4930.

LU, S. & SONG, S. 1991. Hydrophobic interaction in flocculation and flotation 1. Hydrophobic flocculation of fine mineral particles in aqueous solution. *Colloids and Surfaces,* 57**,** 49-60.

MAKUTA, T. & TAKEMURA, F. 2006. Simulation of micro gas bubble generation of uniform diameter in an ultrasonic field by a boundary element method. *Physics of Fluids,* 18**,** 108102.

MANICA, ROGERIO, PARKINSON, LUKE, RALSTON, JOHN, CHAN & C., D. Y. 2010. *Interpreting the Dynamic Interaction between a Very Small Rising Bubble and a Hydrophilic Titania Surface,* Columbus, OH, ETATS-UNIS, American Chemical Society.

MANOR, O. & CHAN, D. Y. C. 2009. Terminal Velocity and Mobile Surface Species in Rising Microbubbles. *Langmuir,* 25**,** 8899-8902.

MANOR, O., VAKARELSKI, I. U., STEVENS, G. W., GRIESER, F., DAGASTINE, R. R. & CHAN, D. Y. C. 2008. Dynamic Forces between Bubbles and Surfaces and Hydrodynamic Boundary Conditions. *Langmuir,* 24**,** 11533-11543.

MANSOUR, L. B. & CHALBI, S. 2006. Removal of oil from oil/water emulsions using electroflotation process. *Journal of applied electrochemistry,* 36**,** 577-581.

MIETTINEN, T., RALSTON, J. & FORNASIERO, D. 2010. The limits of fine particle flotation. *Minerals Engineering,* 23**,** 420-437.

MILL, P. J. 1964. The Nature of the Interactions between Flocculent Cells in the Flocculation of Saccharomyces cerevisiae. *Journal of General Microbiology,* 35**,** 61-68.

MIYAHARA, T. & HAYASHINO, T. 1995. Size of Bubbles Generated from Perforated Plates in Non-Newtonian Liquids. *Journal of Chemical Engineering of Japan,* 28**,** 596-600.

MOHN, F. 1980. Experiences and strategies in the recovery of biomass from mass cultures of microalgae. *Algae biomass***,** 547-71.

MOLINA GRIMA, E., BELARBI, E. H., ACIAN FERNANDEZ, F. G., ROBLES MEDINA, A. & CHISTI, Y. 2003. Recovery of microalgal biomass and metabolites: process options and economics. *Biotechnology Advances,* 20**,** 491-515.

MOORE, D. W. 1959. The rise of a gas bubble in a viscous liquid. *Journal of Fluid Mechanics,* 6**,** 113-130.

MOOSAI, R. & DAWE, R. A. 2003. Gas attachment of oil droplets for gas flotation for oily wastewater cleanup. *Separation and purification technology,* 33**,** 303-314.

MORTIER, A. & SOARES, E. 2007. Separation of yeasts by addition of flocculent cells of Saccharomyces cerevisiae. *World Journal of Microbiology and Biotechnology,* 23**,** 1401-1407.

MURUGANANTHAN, M., BHASKAR RAJU, G. & PRABHAKAR, S. 2004. Separation of pollutants from tannery effluents by electro flotation. *Separation and Purification technology,* 40**,** 69-75.

NGUYEN, A. V. 1998. Particle-bubble encounter probability with mobile bubble surfaces. *International journal of mineral processing,* 55**,** 73-86.

NGUYEN, A. V. & EVANS, G. M. 2004. Movement of fine particles on an air bubble surface studied using high-speed video microscopy. *Journal of Colloid and Interface Science,* 273**,** 271-277.

NGUYEN, A. V., GEORGE, P. & JAMESON, G. J. 2006. Demonstration of a minimum in the recovery of nanoparticles by flotation: Theory and experiment. *Chemical engineering science,* 61**,** 2494-2509.

NISHIHARA, H., TORAYA, T. & FUKUI, S. 1982. Flocculation of cell walls of brewer's yeast and effects of metal ions, protein-denaturants and enzyme treatments. *Archives of Microbiology,* 131**,** 112-115.

PALLAS, N. & PETHICA, B. 1983. The surface tension of water. *Colloids and Surfaces,* 6**,** 221-227.

PARKINSON, L. & RALSTON, J. 2010. The Interaction between a Very Small Rising Bubble and a Hydrophilic Titania Surface. *The Journal of Physical Chemistry C,* 114**,** 2273-2281.

PARKINSON, L., SEDEV, R., FORNASIERO, D. & RALSTON, J. 2008. The terminal rise velocity of 10,Äì100 Œºm diameter bubbles in water. *Journal of Colloid and Interface Science,* 322**,** 168-172.

PERNITSKY, J., D., EDZWALD & K., J. 2006. Selection of alum and polyaluminum coagulants : principles and applications. *Journal of Water Supply: Research and Technology*. 55**,** 21.

PILENI, M.-P. 2003. The role of soft colloidal templates in controlling the size and shape of inorganic nanocrystals. *Nature materials,* 2**,** 145-150.

PYKE, B., FORNASIERO, D. & RALSTON, J. 2003. Bubble particle heterocoagulation under turbulent conditions. *Journal of colloid and interface science,* 265**,** 141-151.

RALSTON, J. & DUKHIN, S. S. 1999. The interaction between particles and bubbles. *Colloids and Surfaces A: Physicochemical and Engineering Aspects,* 151**,** 3-14.

REAY, D. & RATCLIFF, G. A. 1973. Removal of fine particles from water by dispersed air flotation: Effects of bubble size and particle size on collection efficiency. *The Canadian Journal of Chemical Engineering,* 51**,** 178-185.

REAY, D. & RATCLIFF, G. A. 1975. Experimental testing of the hydrodynamic collision model of fine particle flotation. *The Canadian Journal of Chemical Engineering,* 53**,** 481-486.

RENAULT, F., SANCEY, B., BADOT, P. M. & CRINI, G. 2009. Chitosan for coagulation/flocculation processes, An eco-friendly approach. *European Polymer Journal,* 45**,** 1337-1348.

RODRIGUES, R. & RUBIO, J. 2003. New basis for measuring the size distribution of bubbles. *Minerals Engineering,* 16**,** 757-765.

RODRIGUES, R. T. & RUBIO, J. 2007. DAF - dissolved air flotation: Potential applications in the mining and mineral processing industry. *International Journal of Mineral Processing,* 82**,** 1-13.

RUBIO, J., SOUZA, M. L. & SMITH, R. W. 2002. Overview of flotation as a wastewater treatment technique. *Minerals Engineering,* 15**,** 139-155.

RULYOV, N. 1989. Colloidal-hydrodynamic flotation theory. *Khimiya i Teknologiya Vody,* 11**,** 195-216.

RULYOV, N. 2001. Turbulent microflotation: theory and experiment. *Colloids and Surfaces A: Physicochemical and Engineering Aspects,* 192**,** 73-91.

SAM, A., GOMEZ, C. O. & FINCH, J. A. 1996. Axial velocity profiles of single bubbles in water/frother solutions. *International Journal of Mineral Processing,* 47**,** 177-196.

SCHELUDKO, A., TOSHEV, B. & BOJADJIEV, D. 1976. Attachment of particles to a liquid surface (capillary theory of flotation). *J. Chem. Soc., Faraday Trans. 1,* 72**,** 2815-2828.

SCHULZE, H. & GOTTSCHALK, G. 1981. Preliminary experimental investigations of hydrodynamic interaction between particles and a gas bubble. *Aufbereitungs-technik,* 22**,** 254-263.

SCHULZE, H. J. 1992. Probability of particle attachment on gas bubbles by sliding. *Advances in Colloid and Interface Science,* 40**,** 283-305.

SCHWARZ, S., GRANO, S. R., FORNASIERO, D. & RALSTON, J. 2002. Froth behaviour in the presence and absence of model quartz particles. *Proceedings of WCPT4, World Congress on Particle Technology*, Sydney, Paper.

SHEN, H.-Y., MOONJAI, N., VERSTREPEN, J., K., DELVAUX & R., F. 2003. *Impact of attachment immobilization on yeast physiology and fermentation performance,* St. Paul, MN, ETATS-UNIS, American Society of Brewing Chemists.

SHULER, M. L. & KARGI, F. 2002. Recovery and purification of products: Bioprocess Engineering. *In:* AMUNDSON, N. R. (ed.). Prentice Hall New Jersey.

SOARES, E. V. & SEYNAEVE, J. 2000. Induction of flocculation of brewer's yeast strains of Saccharomyces cerevisiae by changing the calcium concentration and pH of culture medium. *Biotechnology Letters,* 22**,** 1827-1832.

SOARES, E. V. & SEYNAEVE, J. 2000. The use of succinic acid, as a pH buffer, expands the potentialities of utilisation of a chemically defined medium in Saccharomyces cerevisiae flocculation studies. *Biotechnology Letters,* 22**,** 859-863.

SPEERS, ALEX, R., WAN, YONG-QUAN, JIN, YU-LAI, STEWART & J., R. 2006. *Effects of fermentation parameters and cell wall properties on yeast flocculation,* London, ROYAUME-UNI, Institute of Brewing.

STEWART, G. & GORING, T. 1976. Effect of some monovalent and divalent metal ions on the flocculation of brewer's yeast strains. *Journal of the Institute of Brewing,* 82**,** 341-342.

STRATFORD, M. 1989. Yeast flocculation: Calcium specificity. *Yeast,* 5**,** 487-496.

STRATFORD, M. 1992. Yeast flocculation: Receptor definition by mnn mutants and concanavalin A. *Yeast,* 8**,** 635-645.

STRATFORD, M. & BOND, C. J. 1992. Selective separation of microorganisms by lectins: Yeast and concanavalin A as a model system. *Biotechnology and Bioengineering,* 40**,** 835-843.

STRATFORD, M. & BRUNDISH, H. M. 1990. Yeast flocculation: Cationic inhibition. *Yeast,* 6**,** 77-86.

STREHAIANO, P., RAMON-PORTUGAL, F. & TAILLANDIER, P. 2006. Yeasts as Biocatalysts. Yeast in Food and Beverages. *In*: QUEROL, A. & FLEET, G. (eds.) *Yeast Handbook*. Springer Berlin Heidelberg.

STUMM, W. & MORGAN, J. 1996. Aquatic chemistry: chemical equilibrium and rates in natural waters. *John Wiley, New York*.

SUBRAHMANYAM, T. V. & FORSSBERG, K. S. E. 1990. Fine particles processing: shear-flocculation and carrier flotation - A review. *International Journal of Mineral Processing,* 30**,** 265-286.

SUTHERLAND, K. L. 1948. Physical Chemistry of Flotation. XI. Kinetics of the Flotation Process. *The Journal of Physical and Colloid Chemistry,* 52**,** 394-425.

SUTHERLAND, K. L. & WARK, I. W. Principles of flotation. 1955. Australasian Institute of Mining and Metallurgy.

TAKAHASHI, M. 2005. Zeta Potential of Microbubbles in Aqueous Solutions: Electrical Properties of the Gas-Water Interface. *The Journal of Physical Chemistry B,* 109**,** 21858-21864.

TAO, D. 2005. Role of bubble size in flotation of coarse and fine particles- A review. *Separation science and technology,* 39**,** 741-760.

TEIXEIRA, M. R. & ROSA, M. J. 2006. Comparing dissolved air flotation and conventional sedimentation to remove cyanobacterial cells of Microcystis aeruginosa: Part I: The key operating conditions. *Separation and Purification Technology,* 52**,** 84-94.

TEIXEIRA, M. R. & ROSA, M. J. 2007. Comparing dissolved air flotation and conventional sedimentation to remove cyanobacterial cells of Microcystis aeruginosa: Part II. The effect of water background organics. *Separation and Purification Technology,* 53**,** 126-134.

TEIXEIRA, M. R., SOUSA, V. & ROSA, M. J. 2010. Investigating dissolved air flotation performance with cyanobacterial cells and filaments. *Water research,* 44**,** 3337-3344.

TESAŘ, V. & BANDALUSENA, H. 2011. Bistable diverter valve in microfluidics. *Experiments in Fluids,* 50**,** 1225-1233.

TESAŘ, V. & TRÁVNÍČEK, Z. 2005. Pulsating and Synthetic Impinging Jets. *Journal of Visualization,* 8**,** 201-208.

TESAŘ, V. C., HUNG, C.-H. & ZIMMERMAN, W. B. 2006. No-moving-part hybrid-synthetic jet actuator. *Sensors and Actuators A: Physical,* 125**,** 159-169.

TESSELE, F., MISRA, M. & RUBIO, J. 1998. Removal of Hg, As and Se ions from gold cyanide leach solutions by dissolved air flotation. *Minerals Engineering,* 11**,** 535-543.

TRAHAR, W. & WARREN, L. 1976. The flotability of very fine particles-A review. *International Journal of Mineral Processing,* 3**,** 103-131.

VARMA, A. J., DESHPANDE, S. V. & KENNEDY, J. F. 2004. Metal complexation by chitosan and its derivatives: a review. *Carbohydrate Polymers,* 55**,** 77-93.

VINOGRADOVA, O. I. 1995. Drainage of a thin liquid film confined between hydrophobic surfaces. *Langmuir,* 11**,** 2213-2220.

WARREN, L. J. 1982. Flocculation of stirred suspensions of cassiterite and tourmaline. *Colloids and Surfaces,* 5**,** 301-319.

WATERS, K. E., HADLER, K. & CILLIERS, J. J. 2008. The flotation of fine particles using charged microbubbles. *Minerals Engineering,* 21**,** 918-923.

WEEKS, M., MUNRO, P. & SPEDDING, P. 1983. New concepts for rapid yeast settling. II. pH switching with an inert powder. *Biotechnology and bioengineering,* 25**,** 699-711.

WILLIAMS, D. J. A. & WILLIAMS, K. P. 1978. Electrophoresis and zeta potential of kaolinite. *Journal of Colloid and Interface Science,* 65**,** 79-87.

WU, X.-J. & CHAHINE, G. L. 2010. Development of an acoustic instrument for bubble size distribution measurement. *Journal of Hydrodynamics, Ser. B,* 22**,**

330-336.

WYATT, N. B., GLOE, L. M., BRADY, P. V., HEWSON, J. C., GRILLET, A. M., HANKINS, M. G. & POHL, P. I. 2012. Critical conditions for ferric chloride-induced flocculation of freshwater algae. *Biotechnology and Bioengineering,* 109**,** 493-501.

XU, T. J., ZHAO, X. Q. & BAI, F. W. 2005. Continuous ethanol production using self-flocculating yeast in a cascade of fermentors. *Enzyme and Microbial Technology,* 37**,** 634-640.

YAN, Y.-D. & JAMESON, G. J. 2004. Application of the Jameson Cell technology for algae and phosphorus removal from maturation ponds. *International Journal of Mineral Processing,* 73**,** 23-28.

YANG, G. Q., DU, B. & FAN, L. S. 2007. Bubble formation and dynamics in gas-liquid-solid fluidization-A review. *Chemical Engineering Science,* 62**,** 2-27.

YANG, S. M., HAN, S. P. & HONG, J. J. 1995. Capture of small particles on a bubble collector by Brownian diffusion and interception. *Journal of colloid and interface science,* 169**,** 125-134.

YE, Y. & MILLER, J. D. 1989. The significance of bubble/particle contact time during collision in the analysis of flotation phenomena. *International Journal of Mineral Processing,* 25**,** 199-219.

YOON, R. & LUTTRELL, G. 1989. The effect of bubble size on fine particle flotation. *Mineral Processing and Extractive Metallurgy Review,* 5**,** 101-122.

YOON, R. H. 2000. The role of hydrodynamic and surface forces in bubble-particle interaction. *International Journal of Mineral Processing,* 58**,** 129-143.

YOON, R. H. & MAO, L. 1996. Application of extended DLVO theory, IV: derivation of flotation rate equation from first principles. *Journal of Colloid*

and Interface Science, 181**,** 613-626.

ZANGI, R. & BERNE, B. 2006. Aggregation and dispersion of small hydrophobic particles in aqueous electrolyte solutions. *The Journal of Physical Chemistry B,* 110**,** 22736-22741.

ZHENG, Y. Y. & ZHAO, C. C. 1993. A Study of kinetics on induced-air flotation for oil-water separation. *Separation science and technology,* 28**,** 1233-1240.

ZIMMERMAN, B., W., TESAŘ, VACLAV, BUTLER, SIMON, BANDULASENA & H., H. C. 2008. Microbubble Generation. 2**,** 8.

ZIMMERMAN, W. B., HEWAKANDAMBY, B. N., TESAŘ, V., BANDULASENA, H. C. H. & OMOTOWA, O. A. 2009. On the design and simulation of an airlift loop bioreactor with microbubble generation by fluidic oscillation. *Food and Bioproducts Processing,* 87**,** 215-227.

ZIMMERMAN, W. B., TESAŘ, V. & BANDULASENA, H. C. H. 2011. Towards energy efficient nanobubble generation with fluidic oscillation. *Current Opinion in Colloid & Interface Science,* 16**,** 350-356.

ZIMMERMAN, W. B., ZANDI, M., HEMAKA BANDULASENA, H. C., TESAŘ, V., JAMES GILMOUR, D. & YING, K. 2011. Design of an airlift loop bioreactor and pilot scales studies with fluidic oscillator induced microbubbles for growth of a microalgae Dunaliella salina. *Applied Energy,* 88**,** 3357-3369.

ZOUBOULIS, A. I. & AVRANAS, A. 2000. Treatment of oil-in-water emulsions by coagulation and dissolved-air flotation. *Colloids and Surfaces A: Physicochemical and Engineering Aspects,* 172**,** 153-161.

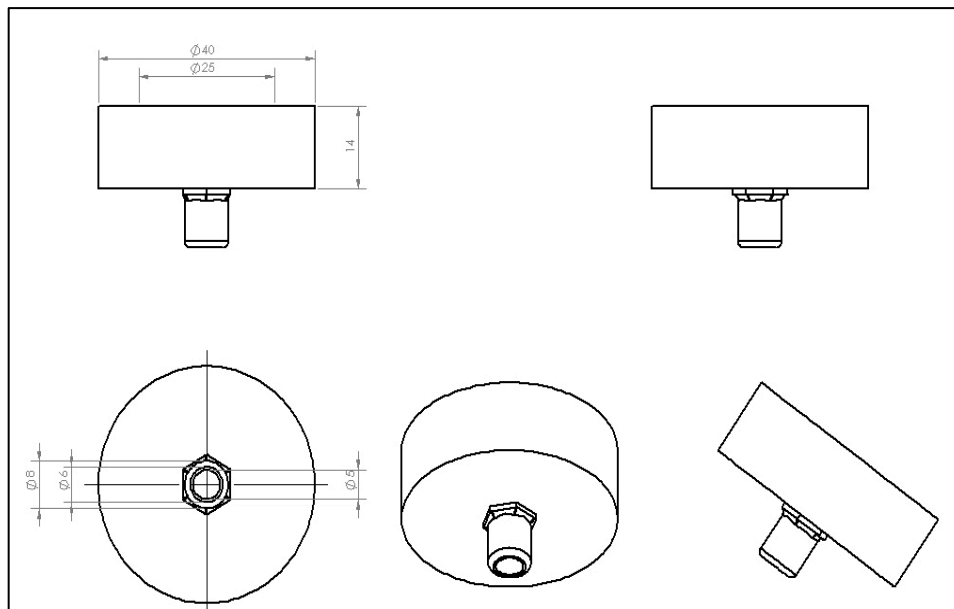# Appendix I
Design of the Distributer-Vane Microbubble Diffuser

(a)
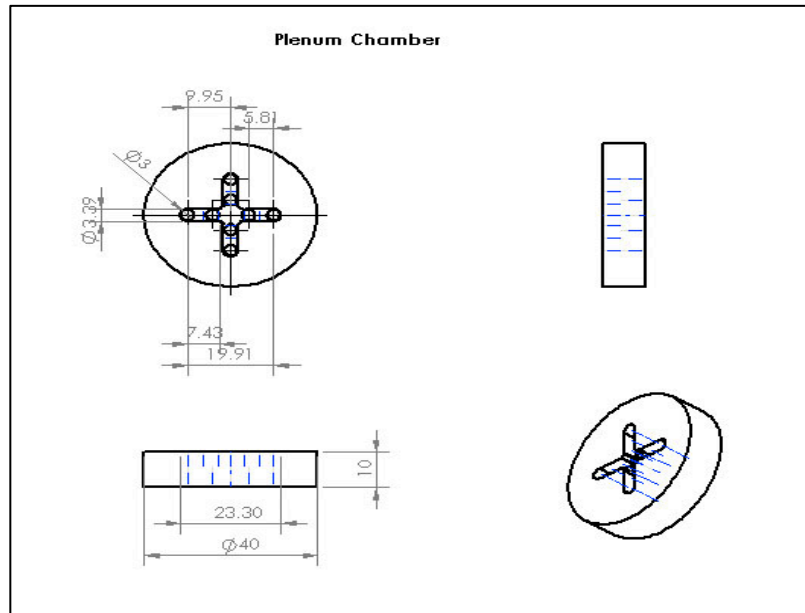
(b)

Figure 1: Design of the bespoke distributor vane diffuser. (a) Detailed representation of the diffuser internal (plenum chamber), showing the structure of the distributor vanes. (b) The diffuser lower part on which the plenum chamber is mounted.

Appendix II
Instruments used to Assay Samples

Figure 1: Photograph of the multi-system acoustic bubble sizer. The set consists of an interface were hydrophones (Transmitting and Receiving) are connected. Signals at set frequencies are sent via the transmitting hydrophones with the receiving hydrophone positioned directly opposite the transmitting hydrophone but across the rising bubble cloud, to collect the attenuating signals from where bubble size can be estimated.

Figure 2: Picture of the Mastersizer used for particle size measurements. Incident laser beam is scattered as it passes through a dispersed sample containing particles. Small particles scatter light at higher angles while larger particles at smaller angles relative to the incident laser beam. The instrument collects the scattered light at different angles and based on the Mie theory of light scattering, an estimation of the particle size is made.
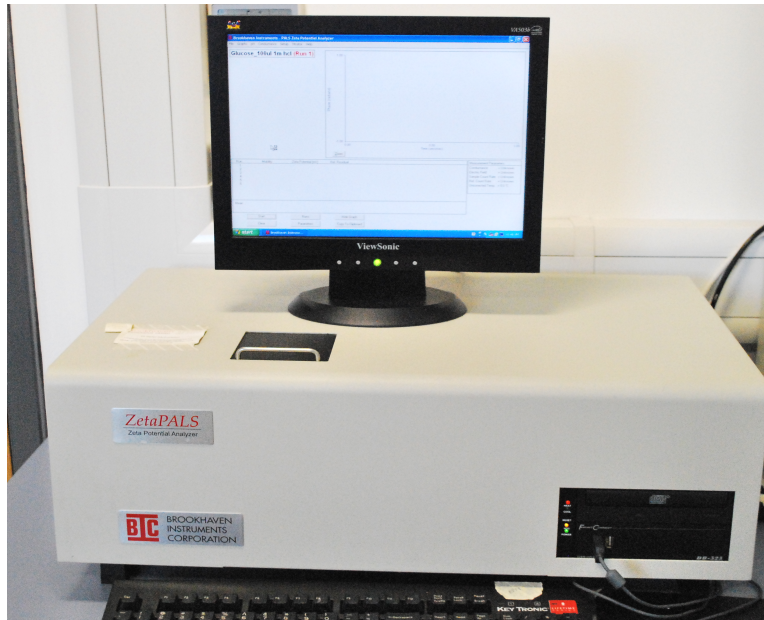
Figure 3: Picture of the ZetaPALS used for particle zetapotential measurements. Using the phase analysis light scattering, the ZetaPALS determines the electrophoretic mobility of charged, colloidal suspensions from where the zetapotential is deduced.

Figure 4: Picture of the oven used for sample heating for moisture content analyses. Samples were collected after harvest and heated for one hour until the moisture was completely driven off.

Figure 5: Photograph of the Scanning Electron Micrograph (SEM).

LIST OF PUBLICATIONS

JOURNAL PAPERS

HANOTU, J., KARUNAKARAN, E., BANDULASENA, H., BIGGS, C. & ZIMMERMAN, W. B. 2013. Harvesting and Dewatering Yeast by Microflotation. *Biochemical Engineering Journal, Submitted*.

HANOTU, J., BANDULASENA, H. C. H., CHIU, T. Y. & ZIMMERMAN, W. B. 2013. Oil emulsion separation with fluidic oscillator generated microbubbles. *International Journal of Multiphase Flow,* 56**,** 119-125.

HANOTU, J., YING, K., SHADA, O. I., BANDULASENA, H. & ZIMMERMAN, W. B. 2013. Microalgae recovery by microflotation for biofuel production using metallic coagulants. *Biofuels,* 4**,** 363-369.

HANOTU, J., BANDULASENA, H. C. H. & ZIMMERMAN, W. B. 2012. Microflotation performance for algal separation. *Biotechnology and Bioengineering,* 109**,** 1663-1673.

YING, K., AL-MASHHADANI, K.H., HANOTU, J., ZIMMERMAN, W. 2013. Mass Transfer in Microbubble Driven Airlift Bioreactor for Microalgal Culture. *International Journal of Engineering Research and Technology*. 1, 2.

CONFERENCE

ZANDI, M., ZIMMERMAN, W., GILMOUR, J., WOOLASS, S., ADDERLEY, B., YING, K., BANDULASENA, H., SCHOFIELD, N. & HANOTU, J. Steel plant CO_2 sequestration using high efficiency micro-algal bioreactor.

MAGAZINE

PANDHAL, J., HANOTU, J., ZIMMERMAN, W. 2013. Algae-The Next Biofuel. *China Water Risk*, 11 July. Available online at: http://chinawaterrisk.org/opinions/algae-the-next-biofuel/

HANOTU, J., ZIMMERMAN, W., MURPHY, K. 2012. Bubbles for Biofuels. *The Chemical Engineer (tce)*, April. p.34-37.